ELECTROCHEMICAL SUPERCAPACITORS

NANOSTRUCTURED MANGANESE OXIDE AND COMPOSITE ELECTRODES FOR ELECTROCHEMICAL SUPERCAPACITORS

By

MARCO CHEONG, B. Sc.

A Thesis

Submitted to the School of Graduate Studies

in Partial Fulfillment of the Requirements

for the Degree

Master of Applied Science

McMaster University

MASTER OF APPLIED SCIENCE (2008).....McMaster University

(Materials Science & Engineering).....Hamilton, Ontario

TITLE: Nanostructured Manganese Oxide and Composite Electrodes for Electrochemical Supercapacitors

AUTHOR: Marco Cheong, B. Sc. (McMaster University)

SUPERVISOR: Professor I. Zhitomirsky

NUMBER OF PAGES: vii, 113

Abstract

Electrochemical supercapacitors (ES) are urgently needed as components in many advanced power systems. The development of advanced ES is expected to enable radical innovation in the area of hybrid vehicles and electronic devices. Nanostructured manganese oxides in amorphous or various crystalline forms have been found to be promising electrode materials for ES. The use of composite electrodes of manganese oxide with carbon nanotubes is being proposed to improve the overall electrochemical performance of the ES.

Electrodeposition methods have been developed for the fabrication of manganese oxide films with/without carbon nanotubes for applications in ES. Electrolytic deposition of manganese oxides was found to be possible using Mn^{2+} and Mn^{7+} species, co-deposition of multiwall carbon nanotubes (MWNT) and manganese oxide using cathodic electrosynthesis was successfully achieved.

Novel chemical process has been developed for the synthesis of nano-size manganese oxide particles. Electrophoretic deposition of the nano-size manganese oxide particles was able to be performed in both aqueous and non-aqueous solutions. Electrophoretic co-deposition of the nano-size manganese oxide particles with carbon nanotubes was successfully achieved.

The mechanisms and kinetics of all the deposition methods are discussed. Charge storage properties of the films prepared by different deposition methods are investigated and compared.

Acknowledgement

I would like to express my sincere appreciation to my supervisor, Professor Igor Zhitomirsky, his wide knowledge and guidance have been of great value for me. Throughout my thesis-writing period, he provided encouragement, sound advice and lots of good ideas.

I would like to thank Nanda Nagarajan, who introduce me to electrochemical supercapacitors and gave me countless lectures in electrochemistry, which made my beginning in the project much easier.

I am very grateful to Janice Wei for her friendship and assistance in the laboratory, who made it actually fun to work in the laboratory.

Many thanks to all members of Dr. Zhitomirsky's team, Xin Pang, Jun Cao, Travis Casagrande, Jun Li, Feng Sun and Gideon Moses Jacob for their kind help and friendship.

Last but not the least; special gratitude goes to my parents. Their love and encouragement greatly support my life and study.

Table of Contents

Table of Figures

1. Introduction

Energy is central to our present and future economic prosperity, therefore improving and strengthening our energy system can clearly provide significant economic benefits for our society. Electrochemical supercapacitors (ES) are urgently needed as critical components in many advanced power systems requiring high power density and high energy density. Considering the batteries, fuel cells and solar cells, the energy density is high, but with low power density. ES improve their performance in terms of power density.

The development of electrochemical supercapacitors (ES) is the subject of intense experimental and theoretical work. This research focuses on advanced materials, new fabrication technologies, design and modeling. Three types of materials have been mostly used for electrochemical capacitors: including high surface area carbon, metal oxides or hydroxides and conducting polymers.

Much effort has been focused on the development of electrode materials, which have high specific capacitance in various electrolytes. To realize a high capacitance, electrode materials are fabricated in three-dimensional matrix form to achieve a high surface area. There is an increasing interest in the development of advanced composite electrode materials. The composite electrode will combine two or more different materials to enhance the electrochemical performance of the electrode.

Nanostructured oxide and hydroxides of ruthenium, manganese, nickel, iron exhibit significantly higher specific capacitance (SC) compared to other materials.

Manganese oxides in their various forms have received significant attention due to the low cost, environmentally friendly character and high SC, but they generally have the problem of high resistance value. It will be beneficial to study novel methods for the fabrication of nanostructured manganese oxides and manganese oxide-carbon nanotubes composites for the use in electrochemical supercapacitors.

2. Literature Review

2.1. Energy Generation and Storage Devices

Capacitors, electrochemical supercapacitors (ES), batteries and fuel cells are important devices for energy storage. Each of the energy devices has its specific energy storage mechanism. Charge storage in capacitors is based on the charge separation and the double layer formation[1]. ES are based on the Faradic electrosorption or redox processes occurring at the electrodes[2]. Batteries are based on the reversible net chemical reaction of the electrode and electrolyte[3]. Fuel cells are based on the oxidation reaction at the catalytic electrodes[4]. The difference in the energy storage mechanism between each of the energy devices results in their different charge-discharge behavior and performance.

Two main parameters are used fundamentally for describing the performance of energy devices: the energy density and the power density. Maximum power density is the maximum power output per unit mass, and energy density is the amount of energy stored per unit mass. An ideal energy system should provide both a high energy density and high power density.

Due to the fundamental differences between capacitors, ES, batteries and fuel cells, each of the energy devices has their own methodology in calculating the maximum power density and energy density. For ES, the power density can be calculated by:

$$P_{max} = V^2 / 4R \quad \textbf{(2.1)}$$

where V is the voltage, and R is the equivalent series resistance (ESR). The energy density can be calculated by:

$$W = CV^2/2 \quad \textbf{(2.2)}$$

where C is the capacitance.

As seen in the equations above, an ideal ES should have a high capacitance value, high voltage window and low resistance. It should also have high surface area (usually about 2000 m^2 g^{-1}), good corrosion resistance, controlled pore structure, processability and compatibility in composite materials and relatively low cost[4].

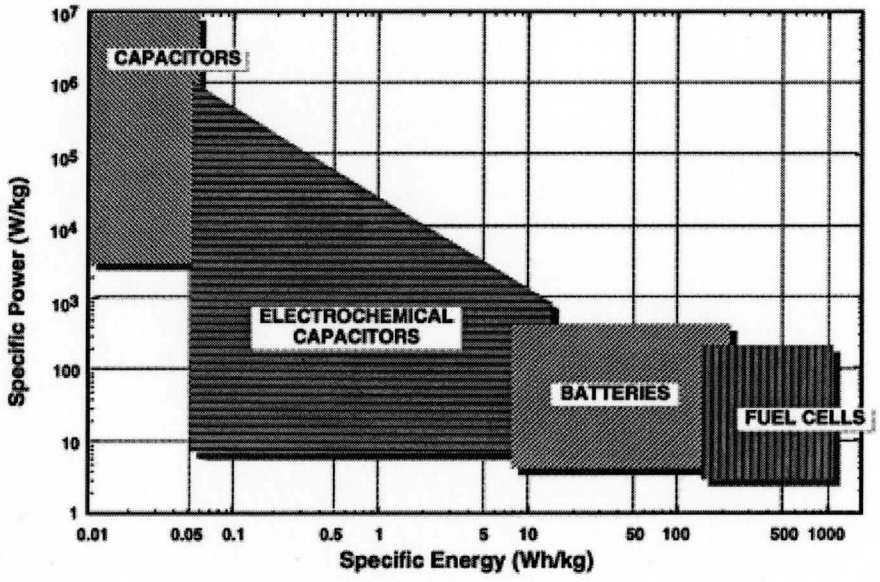

Figure 2-1 Ragone plot of current energy devices[1].

The ragone plot is always used for the comparison between different energy storage devices. In Figure 2-1, it is shown that batteries and fuel cells have very high energy density, but they have low power density. On the other hand, capacitors and ES have very high power density, but they have low energy density[5].

It is important to combine batteries/fuel cells with ES in an energy system, where the ES can act as a power reserve to deliver peak power during a limited time. With the advantage of having power density two to three orders of magnitude better than batteries and fuel cells, ES are important for the future development of energy systems[5].

2.2. Applications of Supercapacitors

The development of hybrid and electric vehicles requires the use of efficient ES, which provide load-levelling for batteries and fuel cells during starting, acceleration and breaking. ES are important for storage of the energy obtained from braking for use in acceleration and hill-climbing[6]. Therefore, ES allow significant energy savings and optimized operation for engines, fuel cells and batteries. The reduction in vehicle fuel consumption offers energy economy and important environmental benefits[7, 8].

Dedicated for energy storage, ES offer new solutions for many other applications. Significant interest has been generated in high power ES for railway and subway type applications. ES have been utilized for door actuation applications in new aircraft. ES are important for the development of photovoltaic generation systems, which need to be connected to the grid that acts as a pool of energy. In such systems, ES can be used to store energy, which can be delivered with high power efficiency[5].

ES have also gained significant attention in consumer electronics due to the ability of fast recharging, large cycling capability and longer lifetime when compared to batteries. ES have been utilized for cell phones, portable media players, cameras and

computers. It is believed that the development of ES is expected to enable radical innovation in the consumer electronics area[6].

2.3. Different Types of Supercapacitors

2.3.1. Electrochemical Double Layer Supercapacitors (EDLC)

The history of electrochemical double layer supercapacitors (EDLC) started at 1957 when Becker invented the first high surface area carbon based capacitor[9]. The energy storage mechanism of double layer supercapacitors is very similar to the traditional capacitors. Traditional capacitors consist of two conducting electrodes separated by a dielectric material. For the case of parallel plate capacitors, the capacitance value can be calculated by:

$$C = k\frac{\varepsilon_o A}{d} \quad \textbf{(2.3)}$$

where k is the dielectric constant of the dielectric material, ε_o is the permittivity of free space, A is the area of the electrode and d is the separation distance between the electrodes.

The energy storage mechanism of the EDLCs is based on the electric double layer formed at the electrodes-electrolyte interface. The equation in calculating the capacitance value is

$$C_{dl} = {}^{\varepsilon\varepsilon_O A}\!/_{d} \quad \textbf{(2.4)}$$

where ε is the dielectric constant of the electrical double-layer region, ε_O is the permittivity of free space, A is the surface area of the electrode, and d is the electrical double-layer thickness.

The separation distance for double layer supercapacitors is usually in the angstrom range when compared to the micro-meter range for traditional capacitors. Taking into account the high surface area of active materials (typically > 1500 m^2g^{-1}), the capacitance value of double layer supercapacitors is by several orders of magnitude higher than the capacitance of traditional capacitors[10, 11].

2.3.2. Pseudo-Supercapacitors

Pseudo-supercapacitors are the latest development in the ES research. The energy storage mechanism of ES arises from the reversible Faradaic reactions or from the absorption of potential determining ions at the available surface of active material. It is important to note that the Faradaic reaction is not electrostatic in nature, thus distinguishing the difference between double layer supercapacitors and pseudo-supercapacitors.

Shukla et al.[11] performed a study by comparing carbon double-layer supercapacitors with pseudo-supercapacitors with similar surface area. They concluded that the pseudo-supercapacitors have a capacitance value 70 times higher than that for the carbon double-layer supercapacitors.

Pseudo-supercapacitors demonstrate a much more complex charge storage mechanism when compared to the double layer supercapacitors, where the capacitance

value only depends on the surface area of the electrode and the electrical double layer thickness. In pseudo-capacitors, the capacitance value depends on the number of adsorbed species, potential window, charge storage mechanism and other factors.

2.4. Electrode Materials for Supercapacitors

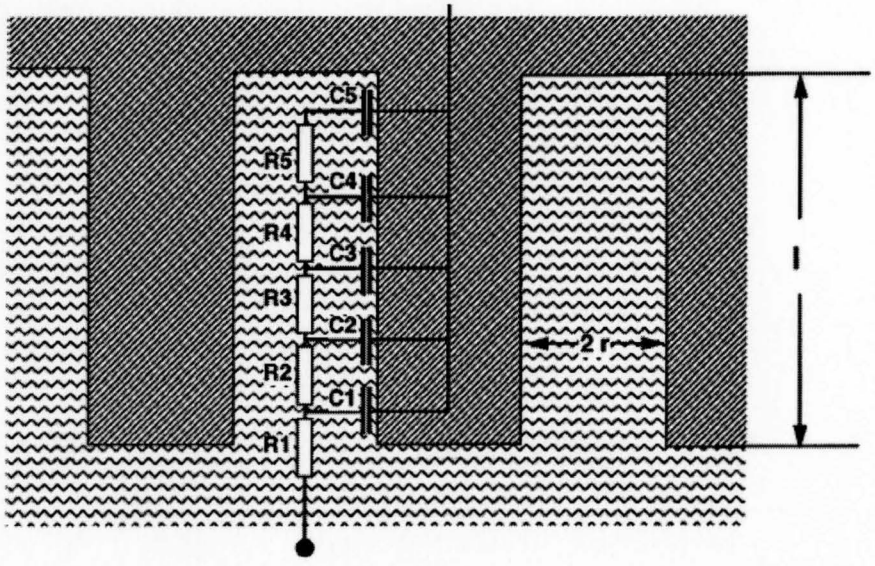

Figure 2-2 Equivalent circuit representation of the distributed resistance and capacitance within a pore[1].

The charge storage mechanism of both EDLC and pseudo-supercapacitors involves surface reactions. Therefore, the use of porous nanostructured materials with high surface area for electrodes is essential for the development of ES. However, porous electrode materials can give raise to equivalent series resistance (ESR) and reduce the power density of the capacitors. Figure 2-2 is the equivalent circuit of the pore of a porous electrode, the resistance (R) and capacitance (C) elements representing the

elemental double layer capacitance or pseudo-capacitance and the respective electrolyte resistance at a particular depth of the pore[1].

The impedance of the capacitors can be expressed as:

$$Z(\omega) = 1/j\omega C \quad \textbf{(2.5)}$$

where j is the $\sqrt{-1}$, ω is the frequency and C is the capacitance. Due to the diffusion limitation in pores, at high frequencies the current flows predominantly along R1 to C1 and almost no current flows deep into the pore[1]. As a result, the capacitance of C2, C3, C4 and C5 in the system cannot be utilized completely.

The optimum porosity of the electrodes is different in EDLC and pseudo-capacitors due to the difference in charge storage mechanism. The general studies are showing that pore > 0.5nm are available for the electro-adsorption of simple hydrated ions[12]. There is a considerable debate over the lower size limit of pores that can be accessed by organic electrolytes, but it is generally believed that pores<2nm are accessible by the organic electrolytes[13].

2.4.1. Carbon Materials

Carbons can be used as: electro-conductive additives, supports for active materials, intercalation hosts, substrates for current leads, an as agents for the control of heat transfer, porosity, surface-area and capacitance.

Carbon has crystalline allotropes: diamond, graphite and fullerenes. The crystalline allotropes are different from each other due to the bonding formed between the carbon atoms[3]. Not all forms of carbon are suitable for being used as ES due to

practical reasons. Currently only graphite and fullerenes are being used widely in the ES applications. Each of the two forms of carbon has various subcategories due to the different fabrication processes.

Graphite materials also include amorphous carbons with sections of hexagonal carbon layers with very little order parallel to the layers. Carbonization is referred as the process in converting carbon rich organic precursors into various forms of carbon material[14]. In the carbonization process, the carbon precursor is heat treated at high temperature at a specific atmosphere. Carbon blacks, carbon fibres and other form of carbon materials can be prepared and tailored for specific applications by controlling the carbonization process as listed in Table 1[15], the factors that control the properties of the final product are the carbon precursor and processing conditions.

Table 1 Common precursors and controlling production factors for various classes of carbon materials[15].

Carbon material	Common precursors	Controlling production factor	Structural/textural feature
Carbon blacks	Hydrocarbon gas or liquid	Precursor concentration	Colloidal/nanosized
Vapour-grown carbon fibres	Hydrocarbon gas	Presence of a catalyst	Catalyst particle size/shape
Fullerene	Graphite rod	Condensation of carbon vapour	Nanosize molecule
Nanotubes	Hydrocarbon vapour	Condensation of carbon vapour	Single wall, multi-wall, chiral
Pitch derived carbon fibres	Coal pitch, petroleum pitch	Spinning	Mesophase formation and growth
Activated carbons	Biomass, coals, petroleum coke, selected polymers	Carbonization/activation	Nanosize pores

After the formation of carbon materials, activation technique can be used to further increase the surface area/porosity of the carbon materials. The carbon materials can be activated thermally or chemically. Thermal activation and chemical activation can be employed to control the porosity, pore-size distribution and the nature of the internal surfaces of the carbon materials[16, 17].

It is also important to note that carbon surface functionalities can affect the performance of the electrochemical double-layer capacitors. Properties such as wettability, point of zero charge, electrical contact resistance, adsoption of ions (capacitance) and self-discharges characteristics are affected by the carbon surface functional groups[18]. Graphitic carbon surfaces are made up of two chemically different kinds of sites: basal and edge carbon sites. Edge sites are generally more electrochemically active than basal sites as they are associated with unpaired electrons[19]. The surface of porous carbons is usually associated with atoms such as oxygen, hydrogen, and even nitrogen, sulphur and halogens depending on the carbonization process and the activation process[20]. Oxygen can be physisorbed (reversibly adsorbed) and chemisorpted (irreversibly adsorbed) by carbons upon exposure to air. Carbon-oxygen complexes that formed from the chemisorption are the most important surface group for capacitors applications of carbons[21]. Three types of surface oxides have been proposed to form on carbon surfaces; acidic, basic and neutral [22, 23]. Functional groups that are electrochemically inert in the potential range of operation can enhance the wettability of carbon electrodes, improve pore access and allow greater surface utilization. As a result, the functional groups increase the specific capacitance of the carbon electrodes[24].

Three types of carbon forms are commonly used as electrode materials in electrochemical double layer capacitors. They are carbon blacks, carbon fibres and carbon nanotubes.

2.4.1.1.Carbon Blacks

Carbon blacks are often referred as the class of carbon materials prepared by partial combustion or thermal decomposition of hydrocarbons in the gas phase. The carbon blacks are often near spherical particles of colloidal size[25, 26]. Carbon blacks are used commonly as the filling materials in battery and supercapacitors electrodes[27]. High quality carbon blacks have the advantages of high conductivity, high porosity, small particle size and a chemically clean (oxygen free) surface[3].

With optimum carbon black loading, the performance of the electrochemical double layer capacitors can be enhanced significantly by the increase in conductivity and increase of surface area. However, if the carbon black loading is too low, the carbon black will not have significant effect on the composite conductivity, on the other hand, if the loading of carbon black is too high, the conductivity of the composite will increase rapidly to a limiting value[3].

Carbon blacks have more accessible surface when compared to other forms of high surface area carbons[28]. The specific capacitance of the electrochemical double layer capacitors, containing carbon blacks, can reach up to 250 F/g[29]; the CV window of carbon blacks electrochemical double layer capacitors can be seen in Figure 2-3. The disadvantages of carbon blacks are: (1) The low compacted density, (2) The increase in

electrical resistance due to the high concentrations of binder needed in the formation of the mechanically stable electrode[3].

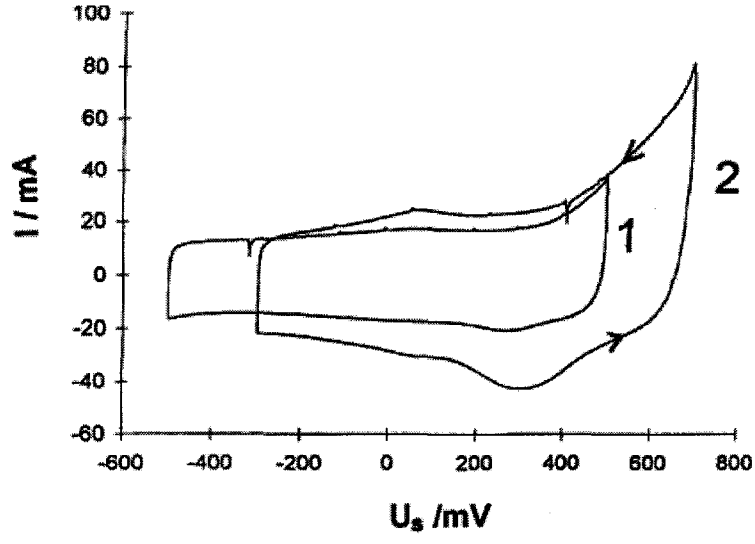

Figure 2-3 The CV window of carbon blacks as electrode materials for EDLC at different potential ranges: (1) from -0.5V to +0.5V, (2) from -0.3V to + 0.7V[29].

2.4.1.2. Carbon Fibres

Carbon fibres can be formed by thermosetting organic materials such as cellulose, phenolic resins, polyacrylonitrile and pitch-based materials, and then extraction of the precursor solution through a die or spinnerette, following by the drawing of the extrudant into a thin fibre[30]. After the fibres are formed, they need to be carbonized and activated before they can be used as electrode materials for electrochemical double layer capacitors. The control of the activation parameters such as temperature and pH of the activation solution allows the control of the pore diameter and pore length of the carbon fibres.

Activated carbon fibres have a typical diameter of 10 μm with micropores of less than 2 nm on the surface of the fibres. Due to the simple structure, electrolyte accessibility of activated carbon fibres is very good. As a result, the use of activated carbon fibres as electrode materials for ES tends to have a high adsorption capacities and adsorption rates[31].

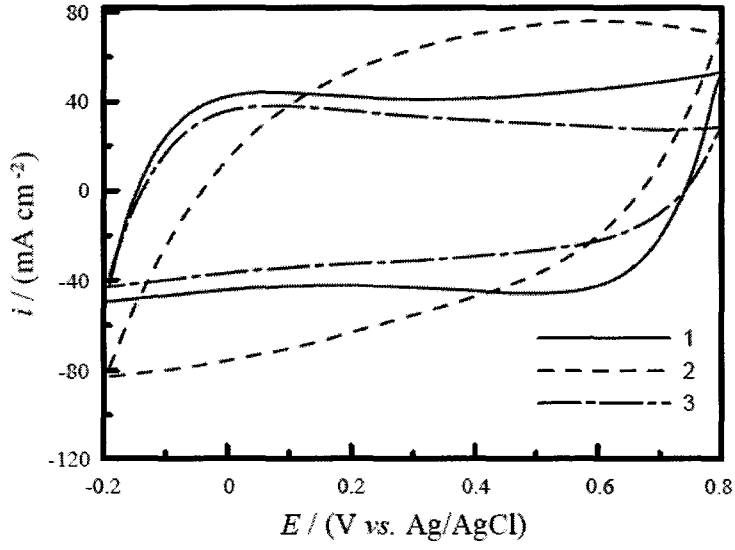

Figure 2-4 CV curves for activated carbon fibers electrode in different electrolytes: (1) 1M $NaNO_3$, (2) 0.5M H_2SO_4 and (3) 0.5M Na_2SO_4[32]

Carbon fibres can be woven into carbon clothes and used as electrode materials. The carbon clothes have the advantage of high surface area, as a result, high capacitance value of 153 F/g has been observed[32]. The activated carbon fibres have excellent electrical conductivity and demonstrate ideal charge-discharge behaviour as shown in Figure 2-4; however, in the forms of carbon clothes, there is significant contact resistance between the carbon fibres. Therefore, it is necessary to keep the carbon fibres inside the

carbon clothes in close contact with each other to minimize the problem. Also, the high cost of the carbon fibres and carbon clothes limit the use of them in the ES applications.

2.4.1.3. Carbon Nanotubes

Carbon nanotubes (CNT) can be produced by: arc-discharge method, laser-furnace method and chemical vapour deposition. The commercial production of carbon nanotubes is generally limited to the catalytic decomposition of certain hydrocarbons[33]. There are two types of carbon nanotubes: single-walled (SWNT) and multi-walled nanotubes (MWNT). SWNT is described as rolling of a single graphene layer into cylinder with a typical diameter of 1 nm and a length of up to 5 μm. MWNT can be: (a) multiple co-centric SWNT with different diameter, (b) multiple SWNT inside a large SWNT, or (c) the combination of both (a) and (b). The size of MWNT varies from diameter of 1 to 50 nm and length of 10 μm.

The high surface-volume ratio, electric conductivity, chemical and mechanical stability made CNT as ideal material to be used for supercapacitors and other energy storage devices[34].

Unlike other forms of carbon materials, CNT naturally show capacitive behaviour and ideal charge-discharge behaviour (Figure 2-5) in their pure form. They have a specific capacitance in the range from 15 to 80 F/g depending on the surface-volume ratio[35]. For some CNT, the capacitance can be up to 130 F/g if the central canal is opened enough for the assessment of electrolyte[36]. The capacitance of CNT can be increased by the attachment of functional groups on the surface. Frackowiak et al.[35]

successfully increased the surface area of the CNT by two to three times by attaching OH functional groups to the CNT and demonstrated significance increase in the capacitance value. Merino et al.[37] recorded an increase of capacitance from 1 F/g to 60 F/g between an as-prepared CNT and an activated CNT.

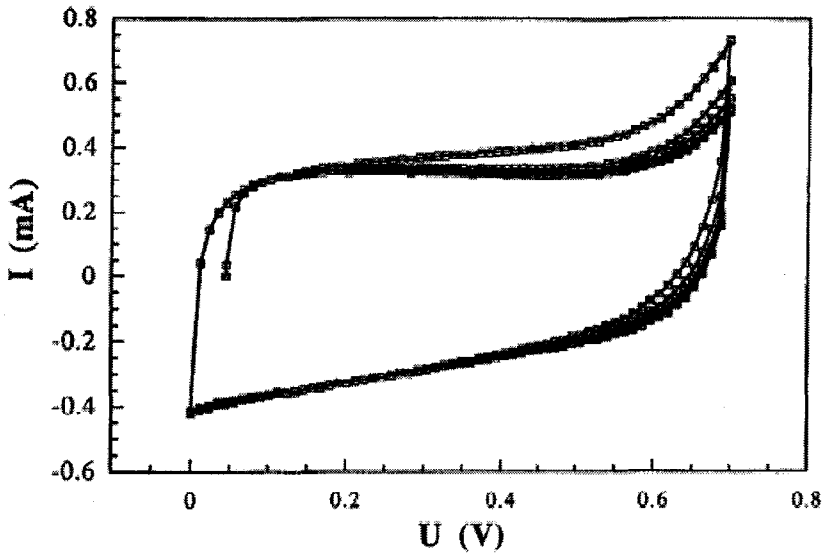

Figure 2-5 CV characteristics of a capacitor built from CNT[35].

The use of CNT as electrode materials in ES is limited by the low production rate of CNT and high cost, therefore, CNT is usually used in conjunction with other electrochemically active materials in the form of composite materials in ES applications. Most of the research have been focused on the use of CNT in conducing polymers, where CNT have increased capacitance value, improved charge-discharge behaviour, and give rise to the high power-energy density of the composite electrodes by reducing the internal resistance[38, 39].

2.4.2. Oxide Materials

Oxide materials generally demonstrate pseudo-capacitive behaviour. Out of all the oxide materials, transitional metal oxides demonstrate superior pseudo-capacitive behaviour. Materials such as ruthenium oxide, nickel oxide, iron oxide and manganese oxide are being studied extensively for their pseudo-capacitive behaviour.

2.4.2.1.Ruthenium Oxide

Ruthenium oxide is the first material that has been studied for the metal oxide pseudo-capacitive behaviour[40]. The charge storage mechanism of ruthenium oxide is based on the reversible oxidation and reduction of ruthenium oxide involving proton exchange described by[41]:

$$RuO_x(OH)_y + \delta H^+ + \delta e^- \leftrightarrow RuO_{x-\delta}(OH)_{y+\delta} \quad (2.6)$$

The hydrous form of ruthenium oxide with disordered structure allows electric charge to be stored in bulk oxides in addition to the electrode-electrolyte interface[42]. The small crystal size of ruthenium oxide also helps to enhance the conductivity of the bulk material.

Ruthenium oxide also has the advantages of having a high ionic conductivity, stability in acidic solution, large voltage window of about 1 V and ideal charge-discharge behavior (Figure 2-6). Ruthenium oxide shows a very high capacitance value of 720 F/g (at 2 mV/s)[43], therefore, ruthenium oxide and ruthenium hydroxide are considered to be the best material for pseudo-supercapacitors. However, the only problem related to the use of ruthenium oxide-based materials is the cost and relative scarcity of ruthenium.

The environmental problems associated with the use of strong acidic electrolytes have limited its commercial use.

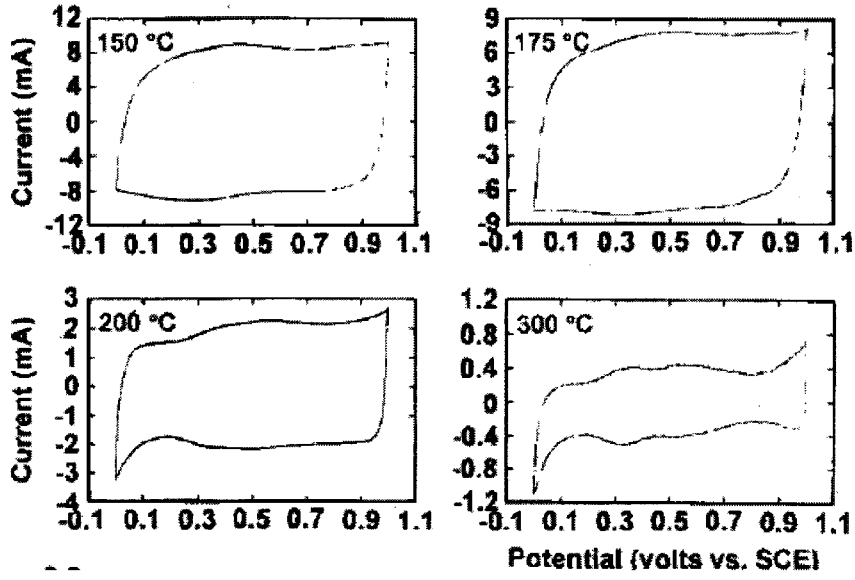

Figure 2-6 Change of CV windows of ruthenium oxide electrode after heat treatment at different temperatures[41].

2.4.2.2.Nickel Oxide

The high cost and scarcity of ruthenium promotes the search of alternative material for pseudo-supercapacitors. Nickel oxide is another promising electrode material for pseudo-supercapacitors. Nickel oxide shows stability in basic solutions and the charge storage mechanism was suggested to be[44]:

$$NiO + OH^- \leftrightarrow NiOOH + e^- \quad (2.7)$$

The charge storage mechanism of nickel oxide is based on the predominant H^+ desorption in the initial stage (E < ~0.3V vs. SCE) of oxidation and predominant OH^- adsorption in the latter stage (E > ~0.3V vs. SCE) of oxidation and versa during reduction[45].

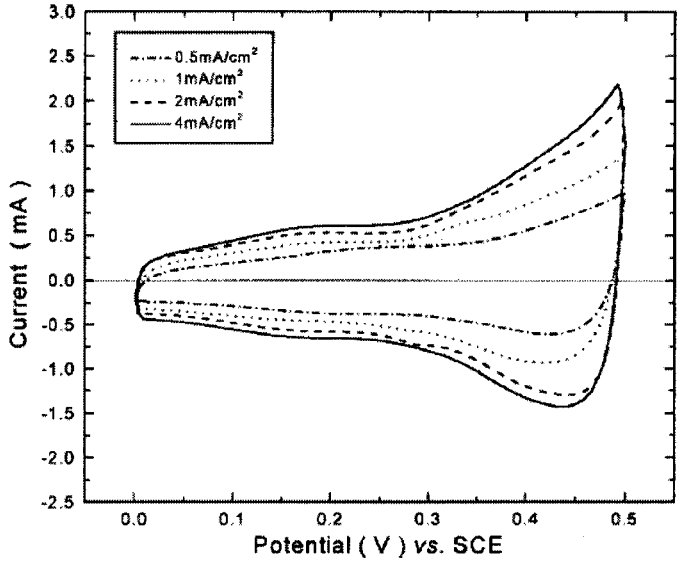

Figure 2-7 CV window of electrochemically deposited NiO_x electrodes deposited at different current densities[45].

The generally low capacitance value of nickel oxide (278 F/g at 2 mV/s)[45] can be explained by: (1) The two steps charge storage mechanism limits the reaction rate of charge/discharge of the supercapacitors. (2) The fact that the reaction only takes place at the electrode-electrolyte interface limits the amount of charge that can be stored in the supercapacitors.

The disadvantage of nickel oxide as electrode materials for pseudo–supercapacitors includes: (1) the relatively low capacitance value of the materials. (2) The small voltage window (0.0 V to 0.5V vs. SCE) greatly reduced the energy/power characteristic of the pseudo-supercapacitors. (3) The non-symmetrical shape of the cyclic voltammetry results in the different behaviour of the supercapacitors during charge and discharge as shown in Figure 2-7.

2.4.2.3.Cobalt Oxide

Other than nickel oxide, cobalt oxide is also considered as a promising electrode material for pseudo-supercapacitors. The heat treatment of the cobalt oxide changes the phases of the cobalt oxide, and different phases of cobalt oxide have different charge storage mechanism and demonstrated different charge-discharge behaviour[46]

Cobalt hydroxide produced by electrochemical precipitation and heat treated at temperature less than 200 °C has the following charge storage mechanism[47, 48]:

$$Co(OH)_2 + OH^- \leftrightarrow CoOOH + H_2O + e^- \quad (2.8)$$

For the cobalt oxide produced by the same method but with heat treatment above 200°C, it has a different charge storage mechanism:

$$Co_3O_4 + H_2O + OH^- \leftrightarrow 3CoOOH + e^- \quad (2.9)$$

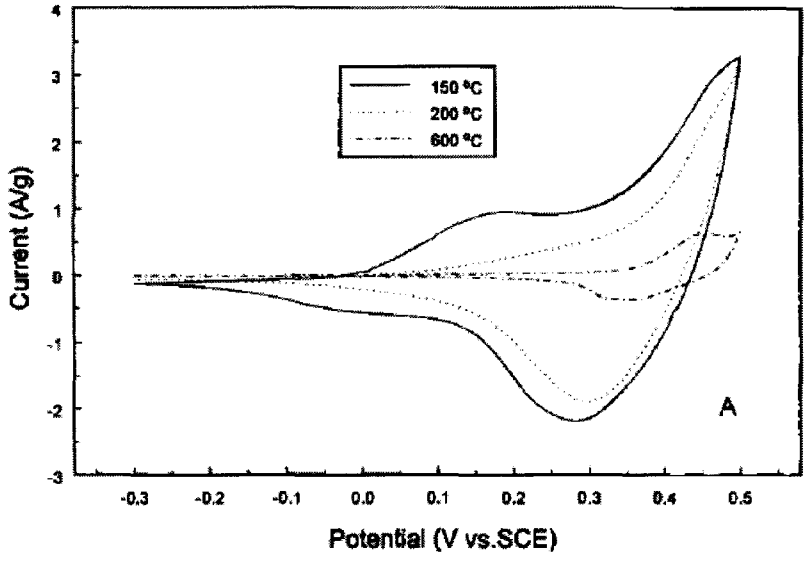

Figure 2-8 CV of the cobalt oxide electrodes after heat treatment at different temperatures in 1 M KOH at a scan rate of 5 mV/s.

Similar to the nickel oxide, the charge storage mechanism is limited to the electrode-electrolyte interface. The limitation greatly affects the amount of charge that can be stored in the pseudo-supercapacitors. As a result, it has an even lower capacitance value of 164 F/g when compared to the 278 F/g of nickel oxide.

However, despite the low capacitance value, the advantage of using cobalt oxide as the electrode material is due to its negative potential voltage window (from -0.15 V to 0.35V vs. SCE as shown in Figure 2-8).

Cobalt oxide is one of the few materials that demonstrate capacitive behaviour at the negative voltage range. The combine use of cobalt oxide as negative electrode and other oxide (i.e. ruthenium oxide or nickel oxide) as positive electrode in a device is known to be asymmetric design. The advantage of the asymmetric device can help to increase the overall potential window of the pseudo-supercapacitors.

2.4.2.4.Manganese Oxide

The use of manganese oxide as an electrode material for ES was proposed in 1999 by Lee and Goodenough[38, 49]. They prepared amorphous manganese dioxide by solution based chemical route and the manganese dioxide powder was then rolled into thin sheet. The resulting film was reported to have a SC of 200F/g with excellent cyclability, the energy density and power density was comparable to ruthenium oxide/hydroxide.

Shortly after the report, different groups around the world started studying manganese dioxide and various forms of manganese oxide as electrode materials for ES. Close to 70 papers were being published on the use of manganese oxide in ES since

1999[50]. Pang et al.[51, 52], Chin et al.[53] and Broughton et al.[54, 55], reported SC of 698 F/g, 720 F/g and 700 F/g, respectively. The theoretical SC of manganese oxide was calculated to be close to 1370 F/g[56], a lot of improvement in the fabrication process can be done at current stage in achieving a higher SC value.

The charge storage mechanism of manganese oxide was generally believed to involve electron transfer at manganese sites; the interfacial reaction mechanism that balances the charge transfer remains unclear[57]. Lee et al.[49] suggested that for both $MnO_2.nH_2O$ and $K_xMnO_2.nH_2O$ supercapacitors with aqueous KCl electrolyte solution, charge transfer at Mn sites is balanced by the chemisorption/desorption of K^+ ions. Pang et al.[52] proposed that the pseudo-capacitance of manganese oxide/hydroxide involve insertion of protons within the near-surface region, which generally can be expressed as:

$$\mathbf{MnOOH_{\delta} + \lambda H^+ + \lambda e^- \leftrightarrow MnO_{2-\lambda}(OH)_{\delta+\lambda}} \quad \mathbf{(2.10)}$$

Manganese oxides in their various forms have received significant attention due to the low cost. Manganese is one of the most abundant materials in the world, and the synthesis of manganese oxides have been studied extensively due to their applications in batteries. Fabrication techniques such as materials synthesis and packaging can be employed from the battery technology. This will significantly reduce the research and development cost of the electrochemical supercapacitors.

Environmentally friendly character is also another major advantage when comparing manganese oxide with other transitional metal oxide electrodes. Unlike other metal oxide electrodes, which show capacitive behaviour only in acidic electrolytes, manganese oxides perform equally well in both neutral electrolytes and acidic

electrolytes, due to their unique charge storage mechanism. The use of acidic electrolyte generally causes environmental problem related to the disposal of the devices or even post hazard in the case of electrolyte leakage. With the use of manganese oxide as electrode materials, all these problems can be prevented.

Excellent electrochemical performance is the major advantage of manganese oxide when compare to other materials. Manganese oxide has a theoretical SC value of 1370 F/g and an experimental SC value of 720 F/g have been achieved in literature. It is comparable to ruthenium oxide electrodes, and much better than other metal oxide electrodes such as nickel oxide and cobalt oxide. The large voltage window of manganese oxide electrodes (Figure 2-9) can increase the energy and power characteristic of the capacitor. The ideal charge-discharge behaviour and excellent cyclability made manganese oxide as one of the best electrode materials for ES applications.

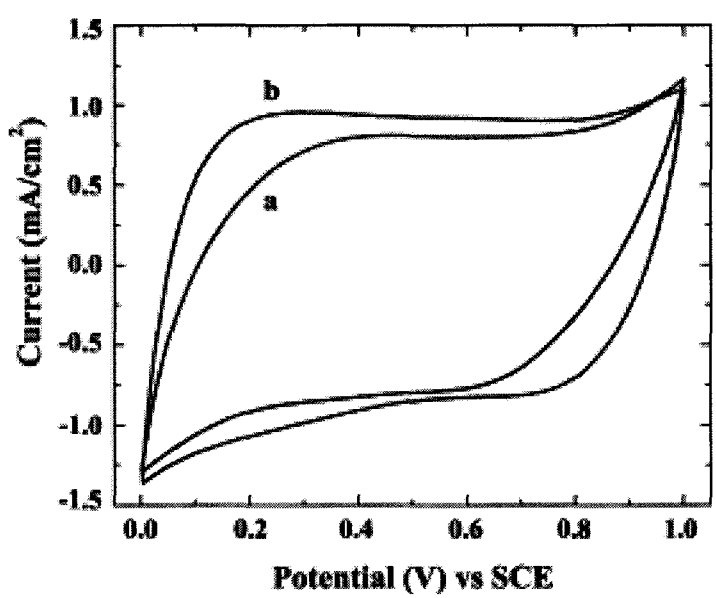

Figure 2-9 CV of the manganese oxide electrode (a) before and (b) after heat treatment at 200 °C.

2.4.3. Polymer Materials

Polymer materials have been regarded as promising electrochemical active material for ES applications. The capacitive behaviour of the polymer materials is based on the Faradic charge transferred, or pseudo-capacitive behaviour. The charge storage mechanism of polymer materials can be explained by Figure 2-10. The electronic charge is injected into the polymer chains, and ionic charge is transferred into the polymer matrix to maintain charge neutrality[58].

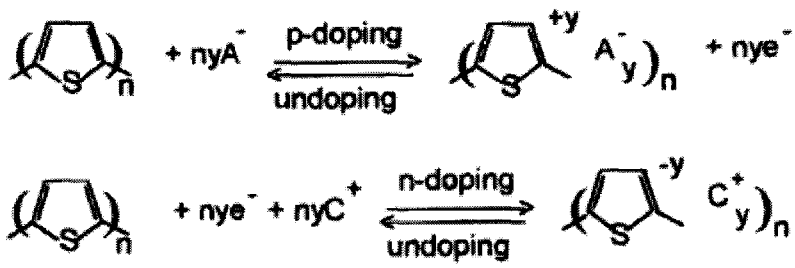

Figure 2-10 Charge storage mechanism of polymer materials in ES (with polythiophene as an example)[58].

When compared with other forms of electrochemical active electrode materials, polymer materials have advantages such as fast charge-discharge kinetics, low cost, suitable morphology, fast doping-undoping process and ease of synthesis[58]. With proper cell design, polymer materials can be used in non-aqueous electrolytes, where the polymer materials demonstrate a much larger voltage window of 3.0V to 3.2V. Aqueous electrolytes generally have a maximum voltage window of 1.4V due to the electrolysis of water[59].

Polymers such as polymethyl methacrylate (PMMA, p-phenylenevinylene (PPV), polypyrrole (PPy) and polyaniline (PANI) are used as the electrode materials in ES applications[60].

The versatility of ECP makes possible different types of polymer supercapacitors, the devices with p-doped polymer as positive electrode and n-doped as negative electrode are the only ones having advantage of high operating potentials[60].

Polymer materials generally have lower conductivity when compared with carbon materials. Polymer materials are often use in the form of composite with carbon to increase the conductivity and overall performance. Jurewicz et al.[61] demonstrated an increase of capacitance from 50F/g to 163 F/g after depositing a thin film of PPy by electropolymerization on MWCT.

2.5. Fabrication of Supercapacitors

Many physical and engineering aspects of the technology of electrochemical capacitor development are similar to those for battery production, e.g., packaging, electrode sealing, bipolar embodiments, use of separators, and accommodation of the electrolyte solution[4]. The long history of the batteries development enables the rapid development and commercialization of ES, and the research of ES is primary focus on the electrodes materials development[62].

2.5.1. Design of Supercapacitors

ES can be classified into the following types[10]:

- Aqueous electrolyte, carbon double-layer types;

- Nonaqueous electrolyte, carbon double-layer types;
- Aqueous, mixed oxide, redox pseudo-capacitance, and double layer types;
- Aqueous or nonaqueous, redox conducting-polymer types;

The common requirements for all types of ES are[10]: (a) small ESR of the electrodes and the electrolyte to maximize the power performance, (b) optimal pore size distribution to enhance to energy-power characteristic, (c) purity of the electrodes and the electrolytes to prevent the self-discharge, (d) stability of the electrode materials in the electrolyte to minimize the self-discharge behaviour.

The requirements for the cell design are different for different types of ES[2]. In the case of EDLC, the design of the cell is limited to the engineering of the pore size distributions of the carbon electrodes to give optimized power performance, and the attachment of different surface functional group to enhance the energy performance.

The design of pseudo-capacitors has a much wider choice of design parameters because of the large choice of electrochemical active materials and their corresponding fabrication methods. Nanostructured porous metal oxide thin film electrodes give maximum surface area for the surface absorption of charged ions; as a result, the electrochemical active materials are generally used in the form of thin films.

2.5.2. Fabrications of Electrode Materials

Thin films can be fabricated in various ways, but for ES applications, the thin film fabrication methods are quite limited, due to the film thickness and the materials

requirements. Only a few methods are generally used in the electrode materials fabrication.

2.5.2.1.Sol-Gel Method

Sol-gel is a wet-chemical technique for material fabrication. The process starts with a chemical solution that reacts to produce colloidal particles of metal oxide. The reaction is generally hydrolysis and condensation of metal ions resulting in the formation of inorganic network of oxo (M-O-M), similar to that of polymeric materials.

The materials can be deposited directly on a substrate by dip-coating or spin-coating to form a highly porous structure after drying. If direct deposition is impossible, the materials can be dried and fine powders of metal oxide will form. The fine powders can be used for thin film deposition by using tradition casting technique[63]. The advantages of the sol-gel methods are in the homogeneity of the particles composition and the submicron particle size. However, the potential use of sol-gel derived metal oxide is limited to the dilute concentration of stable metal oxide suspension[53].

Pang et al.[51, 52] studied the manganese oxide films prepared by direct deposition from the sol-gel suspensions. Obtained very thin films (~ 4 $\mu g/cm^2$) showed a specific capacitance value of 700 F/g. It was mentioned that the fabrication of deposition suspensions with a concentration above 10^{-3} M presents difficulties. Reddy et al.[63, 64] investigated the manganese oxide films by pressing the manganese oxide particles prepared by sol-gel method. The manganese oxide film with 66 wt% of active material showed a capacitance value of 130 F/g.

The use of dilute suspensions of manganese oxide colloidal particles resulted in the low deposition yield. On the other hand, the manganese oxide films prepared by pressing of the sol-gel derived manganese oxide powder have a much lower capacitance value due to the loss of the porous microstructure.

2.5.2.2. Electrostatic Spray Deposition

The electrostatic spray deposition (ESD) was developed by Schoonman et al.[65]. ESD method uses a very fine aerosol of a precursor solution, which is electrohydrodynamically generated, to deposit a film on a heated electrode substrate. The ESD method offers many advantages over conventional deposition techniques, such as simple and low cost set-up, high deposition efficiency, low temperature synthesis, and easy control of the composition and surface morphology of the deposited films[66].

Nam et al.[67] studied the films of manganese oxide deposited by the ESD, and reported a capacitance value of 330 to 150 F/g as the mass of the manganese oxide increased from 18 to 116 $\mu g/cm^2$.

2.5.2.3. Sputter deposition

Sputter deposition is usually used for the deposition of pure metals. Broughton and Brett have developed the procedure for the deposition of manganese metal layer, and then electrochemically oxidized the manganese layer into manganese oxide[54, 55].

2.5.3. Electrodeposition

Electrodeposition is generally referred to the techniques of thin films fabrication with the use of electricity in an electrolyte solution. There are two electrodeposition methods: electrolytic deposition (ELD) and electrophoretic deposition (EPD). The difference in ELD and EPD mechanisms can be seen in Figure 2-11. ELD starts from solutions of metal salts, and EPD is based on the use of suspensions of ceramic particles[68].

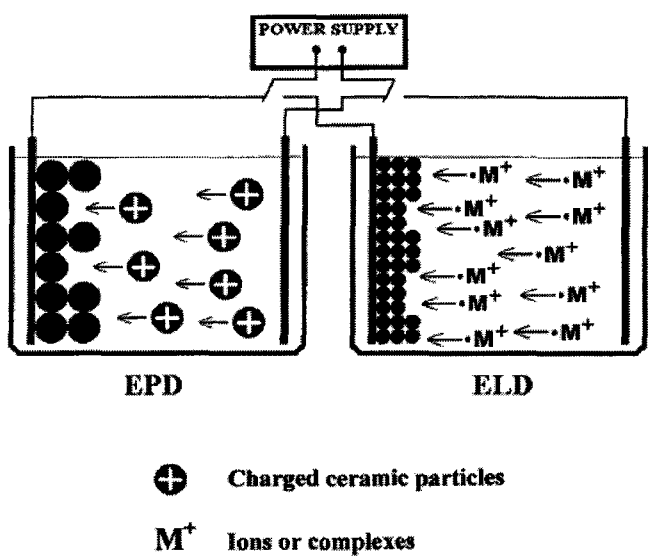

Figure 2-11 Schematic of cathodic electrophoretic deposition (EPD) and electrolytic deposition (ELD), showing electrophoretic motion of positively charged ceramic particles and ions (M^+)[68].

Electrophoretic deposition is a process in which charged ceramic particles, suspended in a liquid medium, migrate and deposit on an electrode under the influence of electric field. Electrolytic deposition is a process in which particles are produced in electrochemical reactions from solutions of metal salts and precipitate at the electrode surface to form a deposit. It is important to note that both ELD and EPD involved

accumulation of ceramic particles at the electrode and deposit is formed via particle coagulation.

The fundamental deposition mechanisms of ELD and EPD are related to the particle interactions and the classical DVLO (Derjaguin, Landau, Verwey and Overbeek) theory[69,70] gives a fundamental description of the colloids stability through particle interactions consideration.

2.5.3.1. The DLVO Theory

DLVO theory[69, 70] states that the major interaction forces between colloidal particles are the columbic double-layer repulsion and van der Waals' attraction.

The total energy V_T of interaction of two isolated and identically charged particles can be defined as:

$$V_T = V_A + V_R \quad \textbf{(2.11)}$$

The attractive energy V_A is the London-van der Waals' interaction between two spherical particles. The attractive energy can be expressed as:

$$V_A = -\frac{A}{6}\left(\frac{2}{s^2-4}+\frac{2}{s^2}+\ln\frac{s^2-4}{s^2}\right) \quad \textbf{(2.12)}$$

where A is the Hamaker constant and $s = 2 + H/a$, with H the shortest distance between the two spheres and a the particle radius. If $H \langle\langle a$, Eq. (2.12) can be simplified to:

$$V_A = -A\frac{a}{12H} \quad \textbf{(2.13)}$$

The repulsive energy V_R is the columbic double layer repulsion between two spherical particles. The repulsive energy can be expressed as:

$$V_R = 2\pi\varepsilon\varepsilon_o a\psi^2 \ln\left(1+e^{-\kappa H}\right) \quad \textbf{(2.14)}$$

where ε is the dielectric constant of the solvent, ε_o is the vacuum dielectric permittivity, a is the particle radius, ψ is the surface potential, $1/\kappa$ is the Debye length:

$$\kappa = \left(\frac{e_o^2 \sum n_i z_i^2}{\varepsilon\varepsilon_o kT}\right)^{1/2} \quad \textbf{(2.15)}$$

where e_o is the electron charge, k is the Boltzmann constant, T is the absolute temperature, n_i is the concentration of ions with valence z_i. Repulsion between colloidal particles is directly related to the diffuse layer charge on the particles.

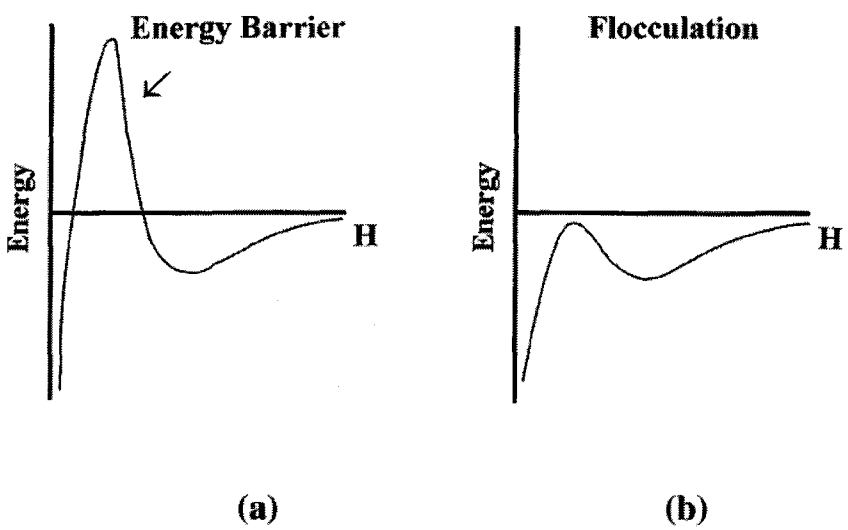

Figure 2-12 Total interaction energy between spherical particles as a function of interparticle separation according to the DLVO theory[68].

The DLVO theory describes the potential energy curve for pair interaction, as shown in Figure 2-12 (a). When the diffuse-layer repulsion is sufficiently high compared to the van der Waals' attraction, the total energy of particle interaction exhibits a maximum. This is the energy barrier to particle coagulation.

The thickness of the double layer (characterized by the Debye length, $1/\kappa$) is very sensitive to the electrolyte concentration[69, 70]. The DLVO theory explains the existence of a critical electrolyte concentration (flocculation value) for coagulation, decreasing with the valence of the electrolyte ions of a charge opposite to that of the colloidal particles (rule of Schulze and Hardey[69, 70]). It was demonstrated that the potential energy peak decreases as the electrolyte concentration increases. As the energy barrier disappears, coagulation becomes possible (Figure 2-12 (b)).

A negatively charged sol is flocculated by large cations at a smaller concentration than by small cations of the same valency. Flocculation values are affected by sol concentration, temperature, particle size of the colloid, and chemical nature of the sol.

2.5.3.2.Solvents

Solvents act as vehicles that carry the ceramic particles in suspensions (EPD) or ions in solution (ELD). The solvent used in electrodeposition must dissolve inorganic salts and organic additives. The two principle types of solvent used for electrodeposition are water and organic liquids[71, 72, 73, 74, 75].

ELD needs a sufficient amount of water for base generation in cathodic reactions[76]. However, adsorbed water in green deposits leads to shrinkage and cracking during drying, non-aqueous solvents prevent the deposit from hydrating. Mixed methyl alcohol-water and ethyl alcohol-water solutions were fond to be preferable in order to reduce cracking and porosity in the electrolytic deposits[68].

Solvents used in EPD should be inert with respect to the powder. The use of water-based suspension causes gas formation from the hydrolysis of water, the gas formation prevents the deposition of a uniform adherent layer and yielding pinholes. Organic liquids are superior to water as a suspension medium for EPD.

2.5.3.3.Binders

Binders are usually added to suspensions or solutions in order to increase the adherence and strength of the deposited material and prevent cracking. The optimal amount of binder depends on the particle size and particle surface area[68].

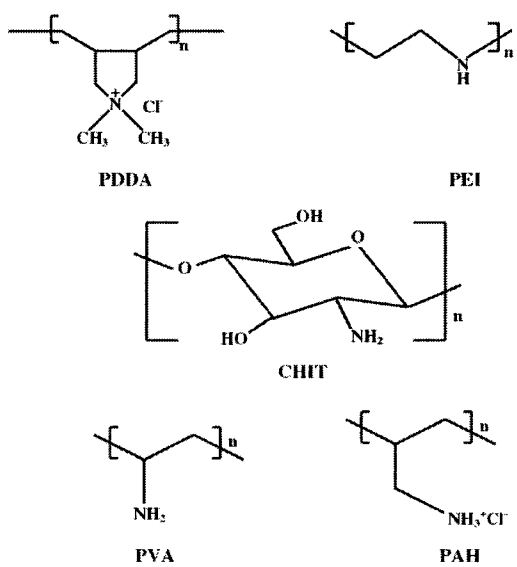

Figure 2-13 Cationic polyelectrolytes: poly (diallyldimethylammonium chloride) (PDDA), poly(ethylene imine) (PEI), chitosan (CHIT), poly(vinylamine) (PVA), and poly(allylamine hydrochloride) (PAH)[77].

The commonly used binders in EPD are non-ionic-type polymers such as polyvinyl alcohol, polyvinyl butyral, ethyl cellulose, polyacrylamide, etc [78]. The polymeric molecules adsorb onto the surfaces of ceramic particles. Charged ceramic

particles provide electrophoretic transport of the polymeric molecules to form deposits on the substrates. Cationic polyelectrolytes with inherent binding properties, such as poly(dimethyldiallylammonium chloride) (PDDA), polyethylenimine (PEI), chitosan (CHIT), poly(vinylamine) (PVA) or poly(allylamine hydro-chloride) (PAH) (Figure 2-13)[77] could be used for particle charging and electrophoretic deposition.

The use of neutral polymers for electrolytic deposition presents difficulties, as the formation of ceramic particles is achieved near the electrode surface. It is feasible to include charged polyelectrolytes into electrolytic deposits by electrochemical intercalation[68]. Using cationic polyelectrolytes (Figure 2-13) with inherent binding properties, problems related to cracking in electrolytic deposits could be diminished[68]. The intercalation of polymer particles is achieved by their adsorption on the surface of colloidal particles, which are produced near the cathode and form a cathodic deposit.

2.5.3.4.Suspension Stability and Particle Charging

A suspension for EPD is a complex system, each component has a substantial effect on deposition efficiency, and it is important to obtain well dispersed and stable suspensions. Suspensions can be dispersed by electrostatic, steric or electrosteric stabilization mechanisms. Ceramic particles must be electrically charged to permit forming by EPD[68].

In aqueous media, the charge at the particle-solvent interface could originate from adsorption or desorption of ions, or dissociation of surface groups. Surfaces of oxide particles dispersed in water tend to coordinate water molecules to form hydroxylated

surface and the hydroxylated surface can be positively or negatively charged depending on pH[68]:

$M\text{-}OH + H^+ \leftrightarrow M\text{-}OH_2^+$ (2.16)

$M\text{-}OH + OH^- \leftrightarrow M\text{-}O^- + H_2O$ (2.17)

DLVO theory stated that the colloidal stability is related to the ξ potential of the colloidal particles. As seen in Figure 2-14[68], ξ potential is positive for low pH values and negative at high pH.

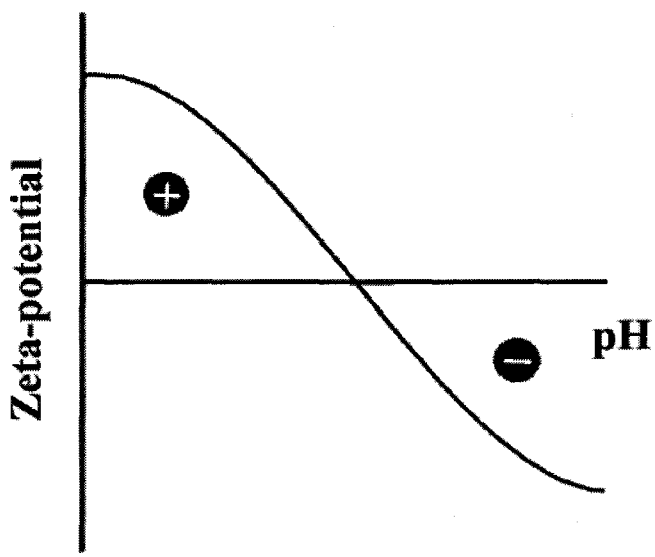

Figure 2-14 Zeta potential of ceramic particles versus pH of suspension[68].

Alcohols are proton donors[79], and pure alcohol can ionize in the following way:

$RCH_2OH + RCH_2O\text{-}H \rightarrow RCH_2O^- + RCH_2OH_2^+$ (2.18)

and an aqueous alcohol ionizes as follows:

$RCH_2O\text{-}H + H_2O \rightarrow RCH_2O^- + H_3O^+$ (2.19)

Damodaran and Moudgil[79] proposed a mechanism of particle charging. The adsorbed alcohol ionizes into a protonated alcohol and an alkoxide ion, following by the

dissociation of the protonated alcohol. The alkoxide ion then desorbs into the solution, leaving the proton on the particle surface.

A variety of additives can be used to control particle charge, in the same time producing well dispersed suspension. The addition of acid[79] can help to disperse the colloidal particles and result in surface charging. The charging of ceramic particles could be achieved by the adsorption of inorganic cations of Mg^{2+}, Ca^{2+}, Al^{3+}, etc[80]. Organic macromolecules can also be used to induce steric stabilization where the macromolecules are attached to the particles surface. The charge on a colloidal particle could also be caused by the dispersants[81].

It is concluded that the most important factors when selecting a binder-dispersant-solvent system are: chemical compatibility of components; solubility of binder and additives; particle charge; viscosity and electric resistivity of the suspension[68].

2.5.3.5.Cathodic Reactions

Various reactions can take place at the cathode and result in a local pH increase at the cathode surface[76]. The chemical reactions consume H^+ are discussed in[82, 83] and they are listed as:

$H^+ + e^- \rightarrow H_{ad}$ or H_{ab} (2.20)

$2H^+ + 2e^- \rightarrow H_2$ (2.21)

$NO_3^- + 2H^+ + 2e^- \rightarrow NO_2^- + H_2O$ (2.22)

$NO_3^- + 10H^+ + 8e^- \rightarrow NH_4^+ + 3H_2O$ (2.23)

The chemical reactions generate OH^- are discussed in[84, 85] and they are listed as:

$2H_2O + 2e^- \rightarrow H_2 + 2OH^-$ (2.24)

$O_2 + 2H_2O + 4e^- \rightarrow 4OH^-$ (2.25)

$NO_3^- + H_2O + 2e^- \rightarrow NO_2^- + 2OH^-$ (2.26)

$ClO_4^- + H_2O + 2e^- \rightarrow ClO_3^- + 2OH^-$ (2.27)

$ClO_4^- + 4H_2O + 8e^- \rightarrow Cl^- + 8OH^-$ (2.28)

The difference between the solution pH and that in the layer adjacent to the electrode increases with increasing current density and decreases with increasing temperature[86, 87]. It was reported that the cathodic surface pH in acidic electrolyte could be up to 11-12 and remained constant over the first 100-200 μm from the cathode surface[86].

2.5.3.6.Electrolytic Deposition

Electrosynthesis has a lot of distinguishing features that made it as one of the most popular techniques in thin film fabrication[84]:

- Electrochemical synthesis takes place close to the electrode within the electric double layer, which has a very high potential gradient of 10^5 V/cm. The reactions often lead to products which cannot be obtained in a regular chemical synthesis.
- The product is deposited on the electrode in the form of a thin film; uniform film can be achieved if a suitable shaped counter electrode is employed to provide uniform polarization.
- Kinetic control can be adjusted by controlling the current passed through the cell, and thermodynamic control can be adjusted by choosing the applied cell potential.

- Electrochemical synthesis can be an oxidation or a reduction reaction by controlling of the applied cell potential.
- The film composition can be controlled by varying the bath composition.
- The experiments can be performed by simple and inexpensive instruments.

The techniques in electrochemical synthesis can generally be divided into two categories: (a) cathodic reactions and (b) anodic reaction. The schematic comparison of the cathodic reaction and anodic reaction can be seen as Figure 2-15[88].

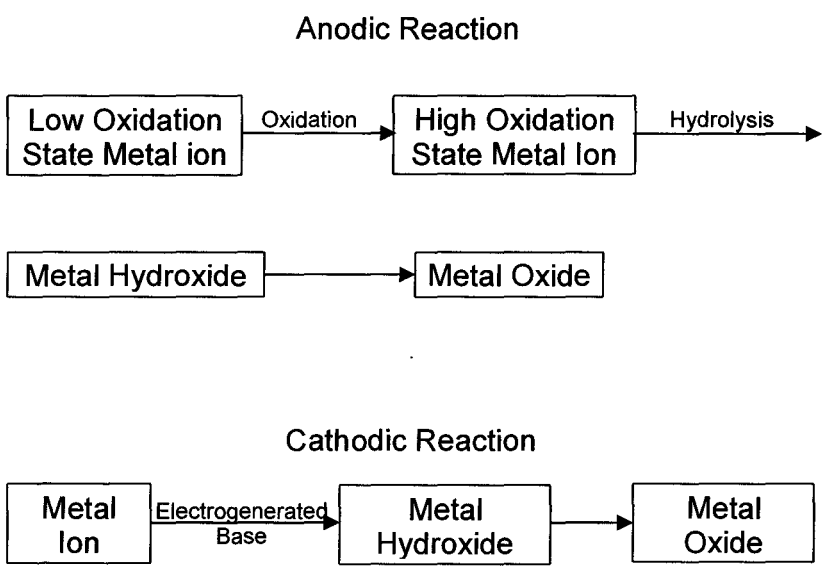

Figure 2-15 Anodic and cathodic electrolytic deposition mechanisms[88].

2.5.3.6.1.Anodic Electrolytic Deposition

Anodic reactions are generally referred as anodic oxidation. The deposition mechanism is based on the oxidation of metal ions in lower oxidation state to a higher oxidation state[88]. The pH of the electrolyte is crucial in controlling the final outcome of the film. The pH is usually chosen in a way that the metal ions in lower oxidation state is

stable while the metal ions in higher oxidation state go through hydrolysis to form metal oxide or hydroxide.

$$M^{z+} \rightarrow M^{(z+\Delta)+} + \Delta e^- \quad (2.29)$$

$$M^{(z+\Delta)+} + (z+\Delta)OH^- \rightarrow M(OH)_{z+\Delta} \rightarrow MO_{(z+\Delta)/2} + (z+\Delta)/2H_2O \quad (2.30)$$

Anodic oxidation is commonly used in battery technologies in fabricating PbO_2 and MnO_2 electrodes. It is best suited for the synthesis of compounds with metal ions in unusual high oxidation states. However, care must be taken to prevent or reduce the problems related to anodic dissolution of the depositing electrode.

2.5.3.6.2. Cathodic Electrolytic Deposition

In cathodic electrolytic deposition process, the pH in the bulk of solutions is low, whereas the cathodic reactions in Eqs. (2.20 to 2.28) result in an increase in pH value near the cathode. The cationic species could be hydrolyzed by an electrogenerated base to form colloidal particles of oxides, hydroxides or peroxides[89, 90, 91]. This method is similar to the wet chemical methods of powder processing and makes use of electrogenerated base instead of alkali[92]. Hydrolysis reactions result in the accumulation of colloidal particles near the electrode.

The colloidal particles will then be deposited onto the cathode, as it can be expected from the DLVO theory of colloidal stability. It was shown[92] that the formation of deposit is caused by flocculation introduced by the electrolyte.

2.5.3.7.Electrophoretic Deposition

The electrophoretic motion of ceramic particles results in accumulation of the particles at the electrode. The basic mechanisms of particle coagulation in the formation of electrophoretic deposits can be distinguished: electrocoagulation, accumulation and electrochemical coagulation[69, 70, 86]. Colloidal stability could be influenced by non-uniformity of the zeta potential on colloidal particles[93]. It is reasonable to expect that when ceramic particles come into contact with particles already deposited, the local lyosphere distortion and thinning mechanism proposed by Sarkar and Nicholson[94] could contribute to particle coagulation. Another important phenomenon to be considered in connection with the alternative mechanism proposed by De and Nicholson[95] is a local pH increase in non-aqueous solutions, it was found that the pH of the local area near the electrode surface increased towards to isoelectric point and facilitates particle coagulation.

3. Objective

The objective of this work is to develop advanced electrochemical supercapacitors through different engineering aspects:

- Materials: Development of nanostructured materials for ES, containing nanoparticles of manganese oxide and MWNT.
- Processing techniques: The development of electrolytic deposition and electrophoretic deposition for fabrication of advance electrodes. The development of novel electrochemical methods for co-deposition of MWNT and nanostructured manganese oxide. The development of electrochemical methods for co-deposition of manganese oxide, MWNT and polymers.
- Microstructure: The fabrication of nanostructured metal oxide/hydroxide-MWNT electrodes with high surface area and porosity.
- Characterization and optimization: Characterization and optimization of microstructure, particle size, surface area, voltage window, SC, power density and energy density.
- Design: development of the advanced design of electrodes using novel electrode materials, electrochemical deposition techniques and advanced current collectors.

4. Experimental Procedures

4.1. Starting Materials

Research grade $MnCl_2.4H_2O$, $KMnO_4$, chitosan (M_w = 200,000 degree of deacetylation 85%), sodium alginate (M_w = 12 to 80 kDa) and N-(3-Dimethylaminopropyl)-N-(ethylcarbodiimide hydrochloride) were purchased from Aldrich. Commercial purity multiwall carbon nanotubes were purchased from Arkema.

4.2. Electrochemical Cell and Equipment for Electrodeposition

The electrochemical cell for deposition included a cathodic substrate and a platinum counter-electrode. The distance between the cathode and anode was 15 mm. The volume of the cell was 300 mL. Constant voltage and constant current power supplies (EPS 2A200, Amersham Biosciences) were used for electrodeposition. The deposition current and voltage were monitored during electrodeposition.

4.3. ELD of Manganese Oxide from Mn^{2+} Solutions

4.3.1. ELD of Manganese Oxide from Mn^{2+} Solutions with Chitosan

Chitosan was dissolved in a 1% acetic acid solution. Electrodeposition was performed from 5 mM $MnCl_2$ solutions in a mixed ethanol–water (20 vol. % water) solvent, containing 0.0–0.2 g/L chitosan. Cathodic deposits were obtained on nickel foils by the galvanostatic method at a current density of 3 mA/cm^2. The deposition time was varied in the range of up to 9 minutes. Deposited films were dried at room temperature

for 24 hours. Heat treatment of the deposited films was performed at different temperatures in air during 1 hour.

4.3.2. ELD of Manganese Oxide from Mn^{2+} Solutions with Chitosan and Carbon Nanotubes

The manganese oxide with chitosan and carbon nanotubes electrodes were fabricated by alternate electrodeposition of manganese oxide-chitosan layers and carbon nanotubes-chitosan layers. Cathodic deposits were obtained on nickel foils at a constant voltage ranged from 20 V to 50 V. The deposition time was varied from 20 seconds to 1 minute.

The concentration of multiwall carbon nanotubes was varied from 0.004 g/L to 0.04 g/L in a mixed ethanol-water (20 vol. % water) solvent containing 0.2-0.5 g/L chitosan. Manganese oxide was deposited from $MnCl_2.4H_2O$ dissolved in a mixed ethanol-water (20 vol. % water) solvent, containing 0.2 g/L chitosan.

Deposited films were dried at room temperature for 24 hours. Heat treatment of the deposited films was performed at different temperatures in air during 1 hour.

4.4. ELD of Manganese Oxide from Mn^{7+} Solutions

Electrodeposition was performed from 0.02 M $KMnO_4$ aqueous solutions at ambient temperature. Cathodic deposits were obtained on stainless steel foils by the galvanostatic method at current densities of 2-10 mA/cm^2. The deposition time was varied in the range of up to 9 min. Deposited films were dried at room temperature for 24 hours.

4.5. EPD of Manganese Oxide in Ethanol Solutions

Electrophoretic deposition of manganese oxide film was performed from the 1 g/L suspensions of manganese oxide nanoparticles in ethanol at constant voltages of 50-100 V. Manganese oxide powders for electrophoretic deposition were prepared by reduction of $KMnO_4$ aqueous solutions with ethanol. The obtained precipitate was washed repeatedly in ethanol and dried under ambient temperature for 72 hours.

4.6. EPD of Manganese Oxide in Aqueous Solutions

4.6.1. EPD of Manganese Oxide in Aqueous Solutions with Sodium Alginate

Electrophoretic deposition was performed from aqueous suspensions containing 0-10 g/L manganese oxide and 0-2 g/L sodium alginate. The pH of the suspensions was adjusted to pH=9 using 0.1 M NaOH solution. After deposition, the coatings containing alginate were cross-linked in 0.1M N-(3-Dimethylaminopropyl)-N-(ethylcarbodiimide hydrochloride) solutions for 30 minutes. Electrophoretic deposits were obtained at constant voltages of 3-20 V or galvanostatically at current densities of 1-3 mA/cm^2 on stainless steel, nickel, platinum foils and graphite plate substrates. The deposition time was varied in the range of 1-10 minutes.

4.6.2. EPD of Manganese Oxide in Aqueous Solutions with Sodium Alginate and Carbon Nanotubes

Electrophoretic deposition was performed from aqueous suspensions containing 10 g/L manganese oxide, 0.2 g/L sodium alginate and 0.04 g/L carbon nanotubes. After deposition, the coatings containing alginate were cross-linked in 0.1 M N-(3-Dimethylaminopropyl)-N-(ethylcarbodiimide hydrochloride) solutions for 30 minutes. Electrophoretic deposits were obtained at a constant voltage of 10-20V on stainless steel and graphite plate substrates. The deposition time was varied in the range of 1-10 minutes.

4.7. Deposition Rate

The substrate weight was measured before and after the deposition to establish the relationship between the deposit weight and deposition time. The deposition rate was also studied in-situ using electrochemical quartz crystal microbalance (QCM922, Princeton Applied Research) controlled by a computer using a WinEchem software. Quartz crystals coated with gold or platinum with an area of 0.196 cm^2 were used as substrates for deposition. The distance between the substrate and the platinum counter electrode was 15 mm. The EQCM measured the frequency change associated with the increase in deposit weight on the substrate during deposition. The relationship between frequency change and mass change is described by the Sauerbrey equation[96]:

$$\Delta f = \frac{-2f_O^2}{A\sqrt{\rho_Q \mu_Q}} \Delta m \quad \textbf{(4.1)}$$

where Δf is the change of frequency, f_O is the resonant frequency of the unloaded resonator (9.00 MHz), A is the area of the electrode (0.196 cm^2), ρ_Q is the density of the quartz crystal (2.648 g/cm^3), μ_Q is the elastic shear modulus of the quartz crystal (2.947 x 10^{11} $g/cm.s^2$) and Δm is the change in mass.

4.8. Materials Characterization

The electrolytic deposits were scraped from the electrodes for X-ray diffraction (XRD) study, thermogravimetric analysis (TGA) and differential thermal analysis (DTA). The phase content of the deposits was determined by XRD with a diffractometer (Nicolet I2) using monochromatic Cu Kα radiation at a scanning speed of 0.5^o min^{-1}. Studies of TGA and DTA were carried out in air at a heating rate of 5 ^oC min^{-1} using a thermoanalyzer (Netzsch STA-409). The microstructures of the deposited coatings were studied using a JEOL JSM-700F scanning electron microscope (SEM). The X-ray photoelectron spectroscopy (XPS) analysis was carried out with a Kratos Axis Ultra spectrometer, using a monochromatic A1 Kα X-ray source. The mean oxidation state (MS) was investigated using the iodometric method[97].

4.9. Electrochemical Characterization

The deposited films were studied using a potentiostat (PARSTAT 2273, Princeton Applied Research) controlled by a computer using a PowerSuite electrochemical software. Electrochemical characterization of the films was performed using a standard three-electrode cell configuration with various concentration of Na_2SO_4 and K_2SO_4 aqueous

solution as the electrolyte. The electrolyte solutions were purged with purified nitrogen gas before the electrochemical measurements. The surface area of the working electrode was 1 cm^2. The counter electrode was a platinum gauze, and the reference electrode was a standard calomel reference electrode (SCE). Cyclic voltammetry (CV) studies were performed within a potential range of 0.0-1.0V versus SCE at scan rates of 2-100 mV/s. The SC was calculated using half the integrated area of the CV curve to obtain the charge Q, and subsequently dividing the charge by the mass of the electrode m and the width of the potential window ΔV:

$$C = \frac{Q}{m\Delta V} \quad \textbf{(4.2)}$$

Galvanostatic charge/discharge cycling was performed at constant current densities of 0.1-5.0 mA/cm^2. The obtained chronopotentiograms were used for the calculation of SC from the equation:

$$C = \frac{I}{(\Delta E/\Delta t)m} \quad \textbf{(4.3)}$$

where $\Delta E/\Delta t$ is the average slope of the discharge curve in the potential range ΔE, Δt the discharge time and I is the current. The specific power density (S_P) and specific energy density (S_E) were calculated from the chronopotentiograms using the following equations:

$$S_P = \frac{I\,\Delta E}{2m} \quad \textbf{(4.4)}$$

$$S_E = \frac{I\,\Delta E\,\Delta t}{2m} \quad \textbf{(4.5)}$$

4.10. Charge Storage Mechanism Characterization

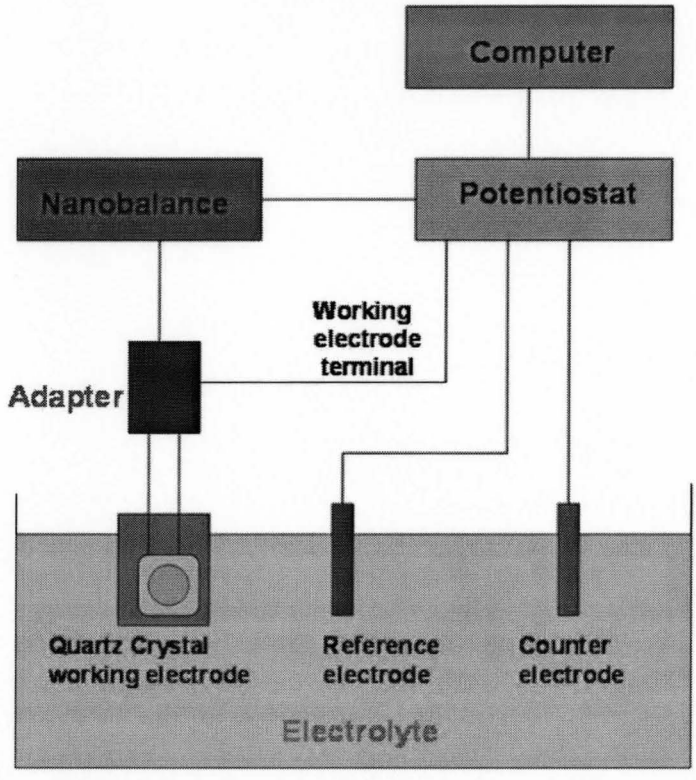

Figure 4-1 Schematic of the equipments setup of potentiostat and quartz crystal microbalance in the charge storage mechanism investigation.

The charge storage mechanism was studied by the combine use of potentiostat (PARSTAT 2273, Princeton Applied Research) and electrochemical quartz crystal microbalance (QCM922, Princeton Applied Research) controlled by a computer using a PowerSuite electrochemical software, as shown in Figure 4-1.

5. Experiment Results

5.1. ELD of Manganese Oxide from Mn^{2+} Solutions

5.1.1. ELD of Manganese Oxide from Mn^{2+} Solutions with Chitosan

Cathodic deposits were obtained from 5 mM $MnCl_2$ solutions containing 0.0-0.2 g/L chitosan. The deposits prepared without chitosan showed low adhesion and cracking, which can be attributed to drying shrinkage. The addition of chitosan to the $MnCl_2$ solutions resulted in improved adhesion and reduced cracking. These results indicate that chitosan can be used as a binder. Therefore, further experiments were performed from $MnCl_2$ solutions containing chitosan.

The TGA studies of the deposit prepared without chitosan (Figure 5-1) showed the weight loss of 7.4 wt. % below 420 °C, small weight gain in the range of 450-500 °C and additional weight loss of 3 wt. % in the range of 925-975 °C. The total weight loss in the temperature range up to 1200 °C was 10.6 wt. %. The corresponding DTA data showed a broad endotherm around 100 °C, exotherm at 500 °C and an endotherm at ~950 °C.

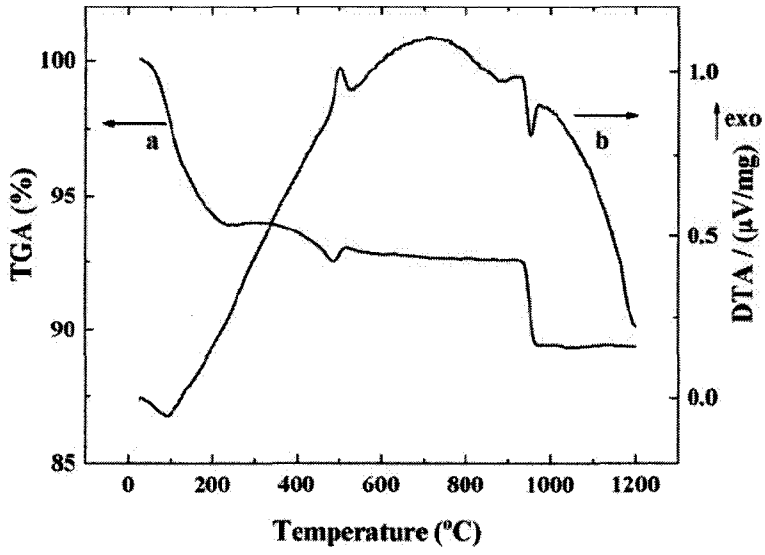

Figure 5-1 (a) TGA and (b) DTA data for the manganese oxide deposit prepared from the 5 mM $MnCl_2$ solution.

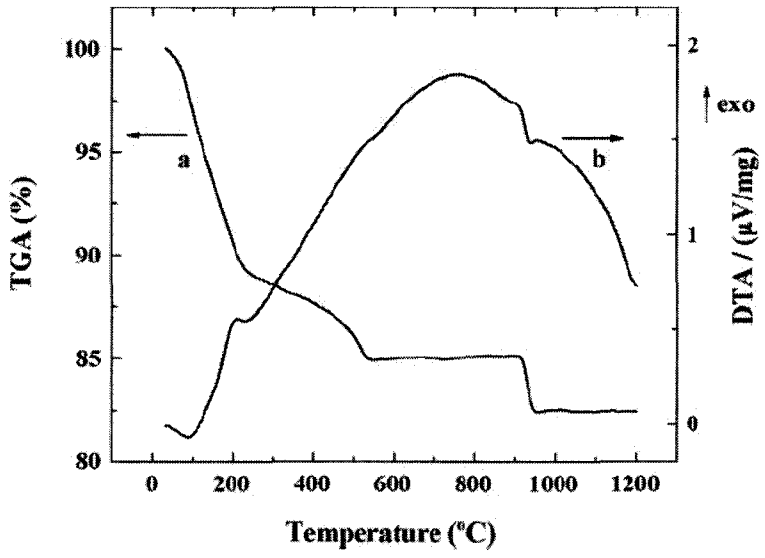

Figure 5-2 (a) TGA and (b) DTA data for the manganese oxide deposit prepared from $MnCl_2$ solution containing 0.2 g/L chitosan.

TGA studies of the deposits prepared from the 5 mM $MnCl_2$ solutions containing 0.2 g/L chitosan (Figure 5-2) showed total weight loss of 17.5% in the temperature range

up to 1200 °C. The total weight loss shown in Figure 5-2 exceeds the weight loss obtained for pure manganese oxide (Figure 5-1). The additional weight loss is attributed to burning out of co-deposited chitosan. The experimental data presented in Figure 5-2 indicates that essentially most of the weight loss (~14 wt. %) occurred below ~500 °C. An additional step in weight loss (2 wt. %) was seen in the range of 925-975 °C. The corresponding DTA data showed a broad endotherm around 100 °C, and exotherms at 200 °C and ~940 °C.

The weight loss below 500 °C in Figure 5-2 can be attributed to the dehydration of the deposit and to the burning out of chitosan. The observed endothermic effect at ~100 °C in Figure 5-1 and Figure 5-2 can be attributed to the libration of the adsorbed water while the exotherm at 200 °C seen only in Figure 5-2 can be related to the burning out of chitosan. The exotherm at ~500 °C, seen in Figure 5-1 can be attributed to the oxidative transformation of the initial Mn_3O_4 phase to the Mn_2O_3 phase, which was confirmed by XRD. The weight gain in the temperature range of 450-500 °C in the pure MnO_x sample (Figure 5-1) can be attributed to the oxygen uptake due to the oxidation. This effect was not observed for the sample with chitosan (Figure 5-2) probably due to the larger weight loss related to the burning out of the polymer. Finally the endotherms observed at 940-950 °C in Figure 5-1 and Figure 5-2 are related to transformation of Mn_2O_3 to Mn_3O_4[98].

The mechanism of chitosan electrodeposition was studied by Pang[99]. Chitosan is soluble in water only when protonated in acidic solutions. At low pH, chitosan becomes a cationic polyelectrolyte:

$Chit\text{-}NH_2 + H_3O^+ \rightarrow Chit\text{-}NH_3 + H_2O$ (5.1)

Under the action of an electric field, the charged chitosan macro-molecules move towards the cathode surface. At the cathode, the reduction of water causes the local pH increase according to the reaction:

$2H_2O + 2e^- \rightarrow H_2 + 2OH^-$ (5.2)

It is suggested that the chitosan loses its charge and forms an insoluble deposit on the cathode surface:

$Chit\text{-}NH_3^+ + OH^- \rightarrow Chit\text{-}NH_2 + H_2O$ (5.3)

X-ray studies of the deposits prepared from the 5 mM $MnCl_2$ solutions containing 0.2 g/L chitosan showed the crystalline nature of the deposit. The X-ray diffraction pattern of the deposits dried at room temperature showed peaks which were attributed to Mn_3O_4. It is suggested that the Mn^{2+} species are partially oxidized in air to form Mn_3O_4. The oxidation of Mn^{2+} species to form Mn_3O_4 was also reported for the powders prepared by chemical precipitation methods[98]. However, it is difficult to distinguish between peaks of Mn_3O_4 (JCPDS file 24-734) and γ-Mn_2O_3 (JCPDS file 18-803) due to the peak broadening.

The XRD spectra taken from the sample annealed at 300 °C displayed broad reflections of Mn_3O_4. On exposure of the deposits to the temperature of 500 °C, X-ray diffraction pattern exhibits peaks of Mn_2O_3 as shown in Figure 5-3. This data, indicating the transformation Mn_3O_4 to Mn_2O_3 is in good agreement with the results of TGA/DTA study and literature data on the investigation of Mn_3O_4 powders prepared by chemical precipitation method[98].

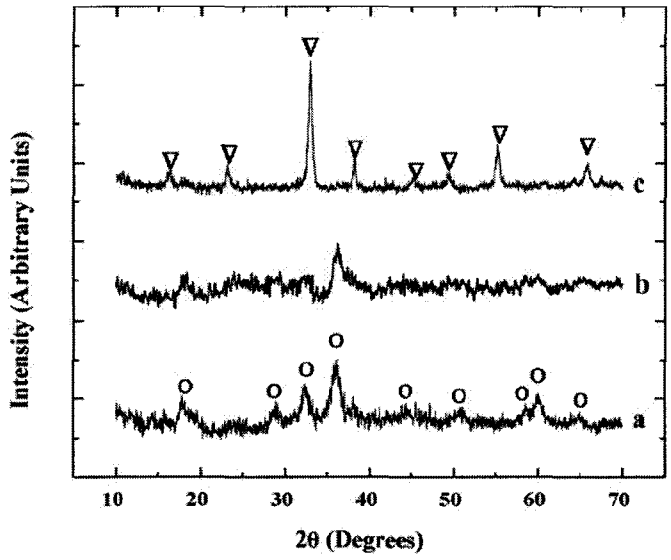

Figure 5-3 XRD data for deposits prepared from the 5 mM $MnCl_2$ solution, containing 0.2 g/L chitosan: (a) as-prepared and heat treated during 1 hour at (b) 300 °C and (c) 500 °C (○: Mn_3O_4, JCPDS file 24-734; ▽: Mn_2O_3, JCPDS file 41-1442).

SEM investigations of as-deposited MnO_x films revealed the formation of porous films with particle size on the nanometric scale, as shown in Figure 5-4a. After heat treatment at 300 °C (Figure 5-4b), the film appear to be more porous, although no noticeable change in particle size occurs. After 10 cycles of CV testing (Figure 5-4c), the films showed increasing porosity and fibrous microstructure.

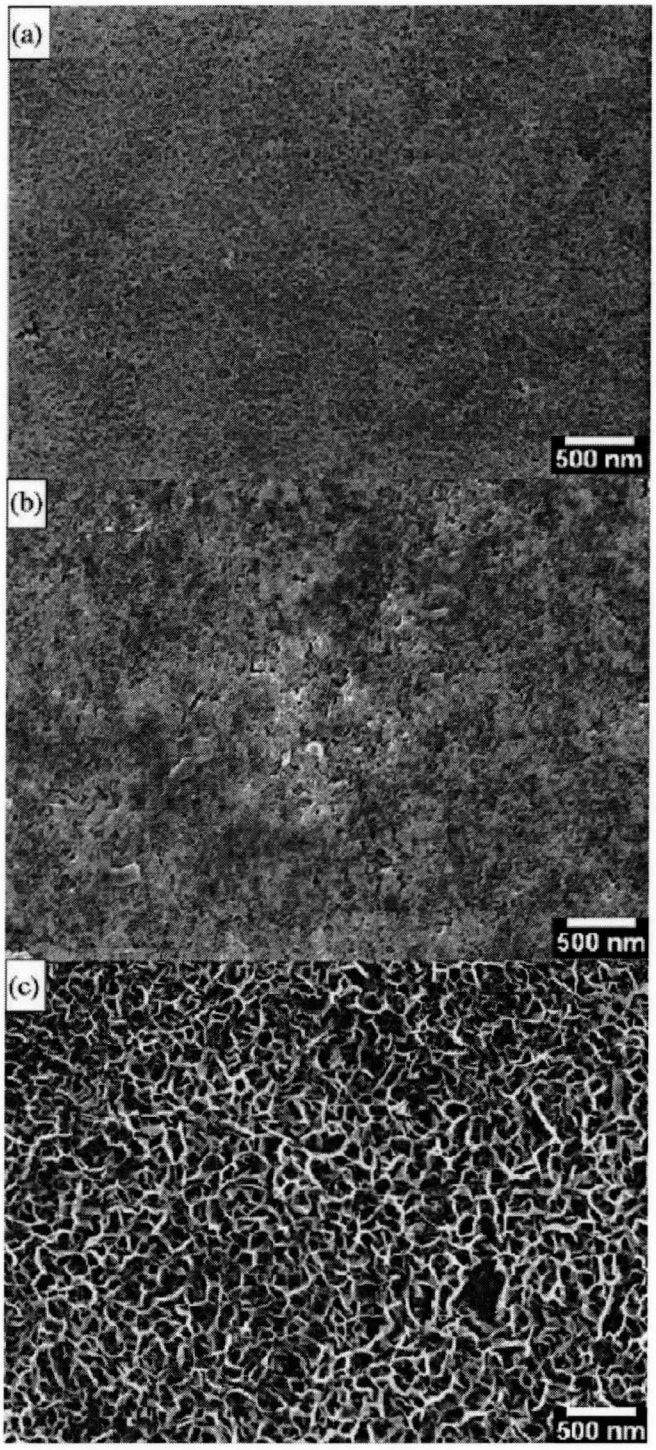

Figure 5-4 SEM micrograph showing films prepared from the 5 mM $MnCl_2$ solution containing 0.2 g/L chitosan: (a) as prepared, (b) after heat treatment at 300 °C for 1 hour and (c) after 10 cycles of CV testing of the heat-treated sample at 300 °C.

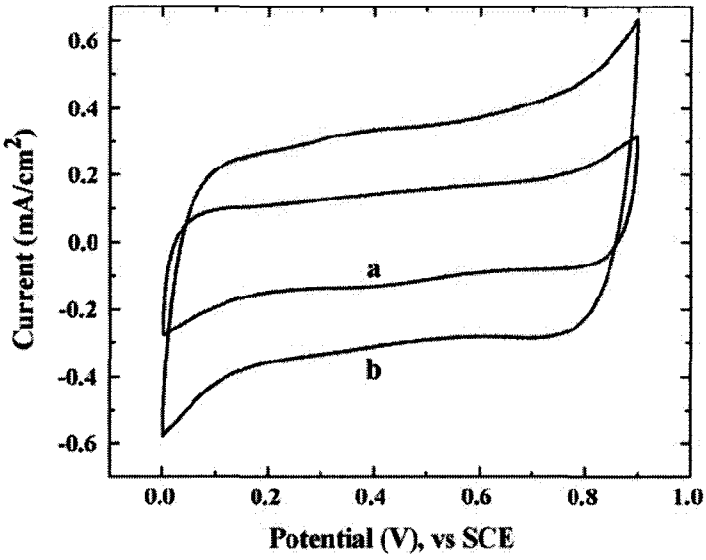

Figure 5-5 Cyclic voltammograms for the 50 μg/cm^2 MnO_x films (a) as prepared and (b) after heat treatment at 300 °C, after 10 cycles, scanned at 20 mV/s in 0.1M Na_2SO_4 solution. The calculated SC values were found to be 133 and 313 F/g, respectively.

Cyclic voltammetry has been used for the electrochemical characterization of the thin films. Figure 5-5 shows the cyclic voltammograms of the films of mass 50 μg/cm^2 before and after heat treatment scanned at 20 mV/s in 0.1M Na_2SO_4, for the 10th cycle. The heat treatment at 300 °C resulted in the SC increase from 133 F/g for the as deposited film to 313 F/g for the heat treated film. Further electrochemical characterization was done on heat-treated samples at 300 °C only.

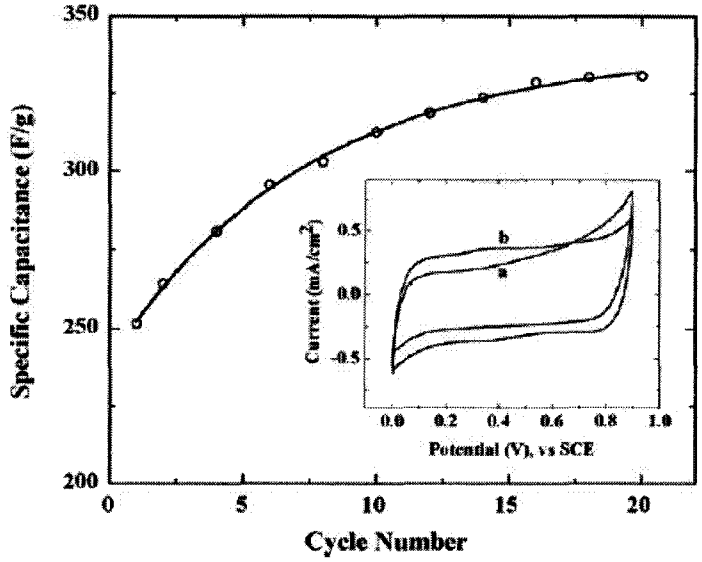

Figure 5-6 Change in the SC of the 50 μg/cm^2 MnO_x film during the first 20 cycles of CV testing, scanned at 20 mV/s. The insert figure shows the corresponding cyclic voltammograms for (a) the 1st cycle and (b) the 20th cycle.

Figure 5-6 shows that the SC of MnO_x films increases within the first 20 cycles of CV testing at a scan rate of 20 mV/s. For the 50 μg/cm^2 film, the specific capacitance increases from 251 F/g in the 1st cycle to 330 F/g in the 20th cycle. The insert in Figure 5-6 shows the corresponding cyclic voltammograms for the 1st cycle and the 20th cycle. Note that the shape of the CV is more rectangular during the 20th cycle, compared to the CV obtained in the 1st cycle. The increase in SC within the first few cycles can be attributed to the electrochemical oxidation of the MnO_x film and/or change in the morphology of the film, as evidenced by SEM observation (Figure 5-4).

The mechanism proposed by Djurfors et al.[55] can be utilized to explain the high SC of the films prepared by the cathodic electrodeposition method. Djurfors et al.[55] showed that films produced by the electrochemical oxidation of Mn/MnO in Na_2SO_4

solutions, exhibited electrochemical pseudo-capacitance. They suggested that the electrochemical oxidation of Mn/MnO films resulted in the formation of porous surface layer of hydrated MnO_x, which is solely responsible for the capacitive behavior of the films. In the present work, it is clear from the SEM pictures (Figure 5-4) that the MnO_x films show the changes in surface morphology after cycling. The resulting porous microstructure leads to enhanced capacitive behavior of these films.

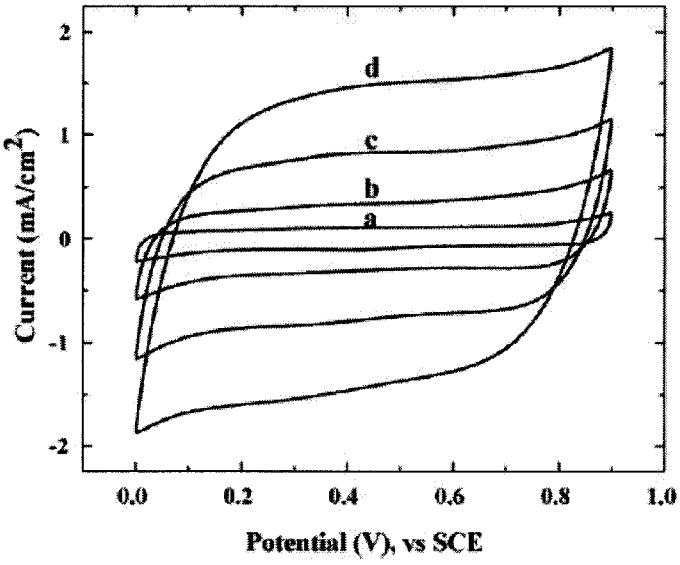

Figure 5-7 Cyclic voltammograms for the 50 μg/cm² MnO_x film at scan rates of (a) 5, (b) 20, (c) 50 and (d) 100 mV/s. The calculated SC values were found to be 400, 330, 283 and 238 F/g, respectively.

Figure 5-7 shows the effect of scan rate on the specific capacitance of the 50 μg/cm² MnO_x films. At scan rates 5 – 100 mV/s, the CV curves were nearly rectangular in the range between 0 and 0.9V versus SCE and no redox peaks were observed, indicating good capacitive behavior. The specific capacitance values calculated from the CVs are 400, 330, 283 and 238 F/g for the scan rates of 5, 20, 50 and 100 mV/s respectively. This decrease in the SC values with scan rate has been commonly

observed[100, 101, 102] and is attributed to the electrical resistance of the active material, which can be reduced by the incorporation of conductive additives[100].

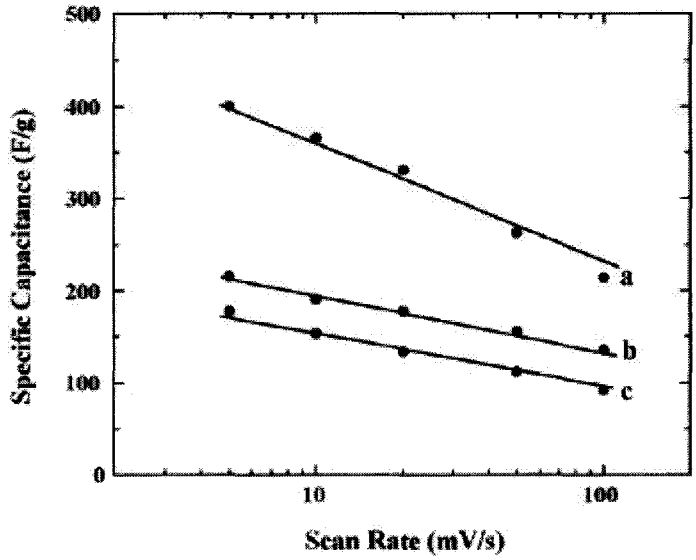

Figure 5-8 SC of the MnO_x films as a function of scan rate for deposit mass of (a) 50 μg/cm^2, (b) 75 μg/cm^2 and (c) 200 μg/cm^2.

Figure 5-8 shows the dependence of the SC on film mass, for various scan rates. At a scan rate of 5 mV/s, maximum SC of 400, 215 and 177 F/g was obtained for the 50, 75 and 200 μg/cm^2 films respectively. The experimental data presented in Figure 5-8 indicates that the SC decreases with increasing film mass. Therefore, better utilization of active material can be achieved in thin layers. An important direction for future research is the fabrication of films with greater porosity in order to achieve better electrolyte penetration and greater utilization of the active material.

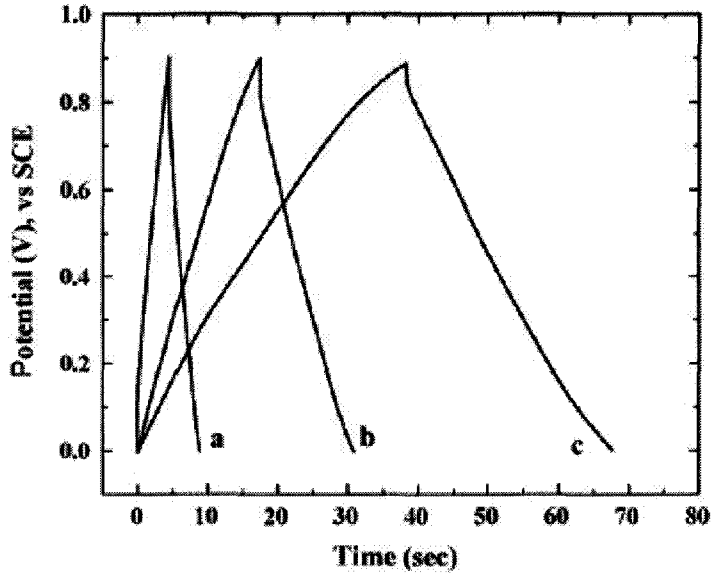

Figure 5-9 Charge-discharge curves for the 50 μg/cm^2 MnO_x film obtained at a constant current density of (a) 2, (b) 1 and (c) 0.5 mA/cm^2. The calculated SC values were found to be 201, 340 and 376 F/g respectively.

The charge-discharge behavior of the MnO_x films was examined by chronopotentiometry. Figure 5-9 shows the galvanostatic charge-discharge curves for the 50 μg/cm^2 MnO_x film. The charge-discharge curves are almost linear and indicate good capacitive behavior. The small initial potential drop observed during discharge was attributed to electrical resistance of active material. The average SC calculated from the charge-discharge curves are 376, 340 and 201 F/g for the current densities of 0.5, 1 and 2 mA/cm^2. These values are close to the SC values obtained by CV testing. The decrease in SC with increasing current density observed in the chronopotentiometry experiments is concurrent with a similar SC reduction with scan rate in the CV data (Figure 5-8).

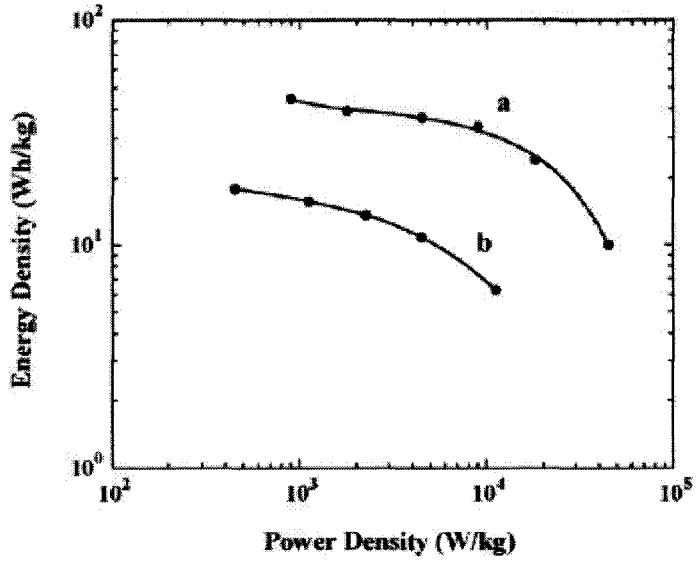

Figure 5-10 Ragone plots for the MnO_x films of mass (a) 50 μg/cm^2 and (b) 200 μg/cm^2 based on the results from chronopotentiometry.

The specific power densities and the specific energy densities were calculated for the 50 and 200 μg/cm^2 MnO_x films from their respective charge-discharge curves, using Eqs. 4.4 and 4.5. A plot of the S_P versus S_E, termed as the Ragone plot, is shown in Figure 5-10. The 50 μg/cm^2 MnO_x film showed higher S_P and S_E values, compared to the 200 μg/cm^2 film, due to the higher resistance of the thicker film. For the 50 μg/cm^2 MnO_x film, a higher power density of 45 kW/kg was obtained at an energy density of 10 Wh/kg.

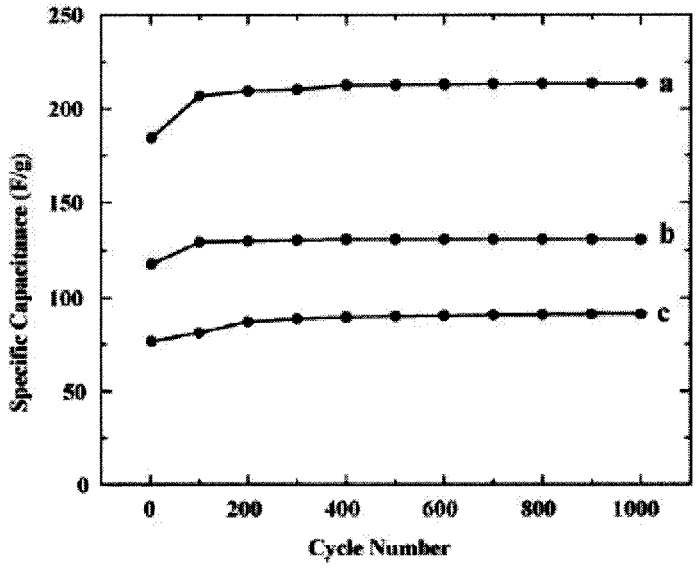

Figure 5-11 Variation of the specific capacitance with CV charge-discharge cycle number, at a scan rate of 100 mV/s, for the MnO_x films of mass (a) 50 μg/cm^2, (b) 75 μg/cm^2 and (c) 200 μg/cm^2.

Figure 5-11 shows the cycling behavior of the 50, 75 and 200 μg/cm^2 MnO_x films at a scan rate of 100 mV/s. As can be seen, all three samples show an initial increase in capacitance, in agreement with the obtained result as a scan rate of 20 mV/s (Figure 5-5). Once a maximum SC is reached, there is no drop in the SC with increasing cycles, up to 1000 cycles. Thus, the MnO_x films of this work show excellent cycling stability.

5.1.2. ELD of Manganese Oxide from Mn^{2+} Solutions with Chitosan and Carbon Nanotubes

The electrolytic co-deposition of manganese oxide with chitosan and carbon nanotubes faces significant challenge. It was found that carbon nanotubes formed relatively stable suspensions in chitosan solutions. However, carbon nanotubes showed low colloidal stability after addition of manganese salts to the solution. In this work,

alternative deposition of manganese oxide layers and carbon nanotubes layers was investigated using chitosan as a dispersant and a charging additive.

The electrosynthesis experiments described in previous section showed that manganese oxide films can be deposited cathodically. Therefore, for deposition of composite manganese oxide-carbon nanotubes films, a cathodic deposition method for the deposition of carbon nanotubes layer need to be developed.

The carbon nanotubes layers were successfully deposited by EPD from chitosan solution containing well dispersed carbon nanotubes. The TGA data shows that the CNT does not demonstrate any major weight loss during the first 450 °C. During the range of 450 to 700 °C, the CNT showed a rapid weight loss of up to 97.3 wt. %. The rapid weight loss can be explained by the oxidation of carbon nanotubes. For the pure chitosan deposit, the film shows a rapid weight loss of 46.3 wt. % below 300 °C, and additional weight loss of 52.4 wt. % in the range of 300-600 °C. The total weight loss remains unchanged after 600 °C. For the chitosan-CNT composite film, the film shows a rapid weight loss of 36.1 wt.% below 300 °C, and additional weight loss of 59.6 wt. % in the range of 300-600 °C. The total weight loss remains unchanged after 600 °C.

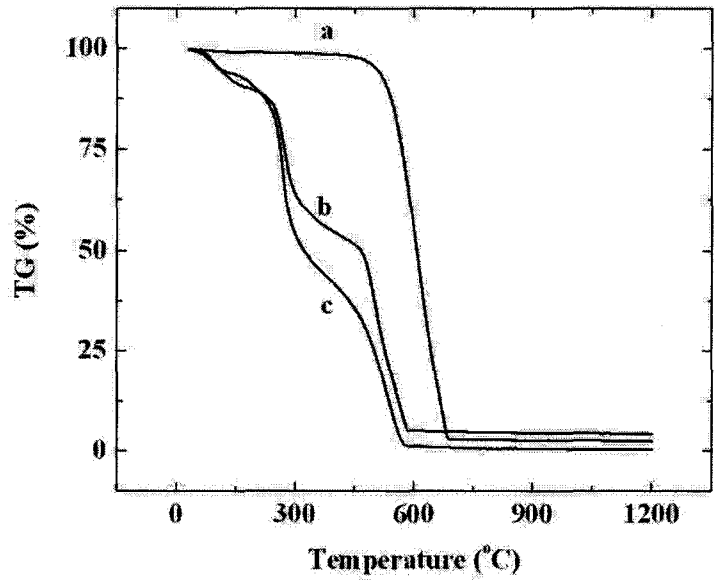

Figure 5-12 TGA data for (a) pure CNT, (b) chitosan-CNT composite film, and (c) chitosan film.

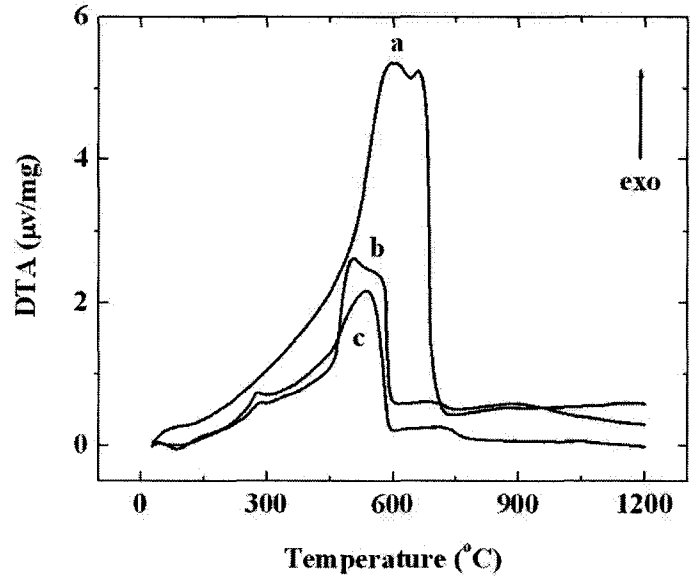

Figure 5-13 DTA data for (a) pure CNT, (b) chitosan-CNT composite film, and (c) chitosan film.

The DTA data for CNT shows a very board exotherm in the range from 450 to 700 °C, inside this board exotherm, there are two significant exotherms at 600 and 650 °C. The board exotherm indicates that the burning out of CNT happens at a wide temperature range. For the pure chitosan deposit, the film shows an endotherm at 100 °C,

corresponding to dehydration, and 2 other exotherms at 300 and 500 °C, corresponding to the burning out of the chitosan. For the chitosan-CNT composite film, it demonstrates very similar endotherm and exotherms as the pure chitosan film, however, all the peaks were intensified and observed in a broader temperature range due to the additional exothermic effect related to burning out of CNT.

The weight loss below 300 °C in Figure 5-12 corresponds to the dehydration of the deposit and to the burning out chitosan. The observed endothermic effect at 100 °C can be attributed to the liberation of the adsorbed water while the exotherm at 200 °C seen in the chitosan-CNT film and pure chitosan film can be related to the burning out of chitosan. The difference in TGA/DTA data for chitosan-CNT films and pure chitosan films indicates co-deposition of chitosan and CNT and the formation of composite chitosan-CNT films.

The successful deposition of CNT can also be seen from the SEM picture of the deposited film in Figure 5-14 where chitosan-CNT films are being deposited at different voltages. Some CNT bundles can be seen lying parallel on top of the film surface. It is important to note that SEM observation of individual CNT presents difficulties, attributed to low size of CNT.

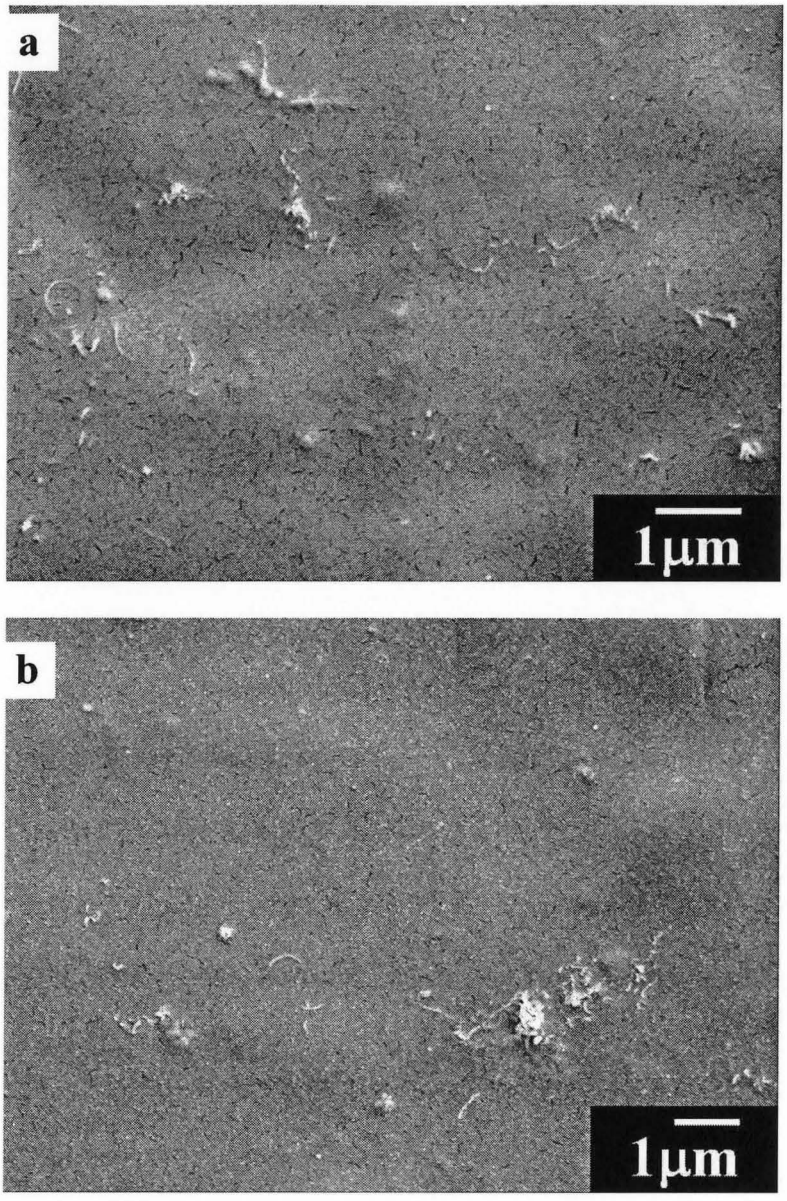
a
1μm
b
1μm

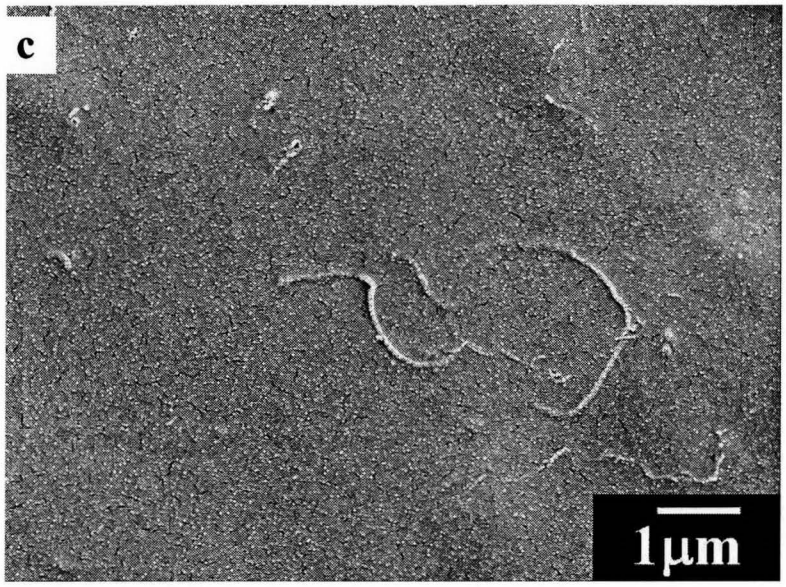

Figure 5-14 SEM pictures of the chitosan-CNT composite films deposited at (a) 20 V, (b) 30 V and (c) 50 V.

However, in a closer examination of Figure 5-14, the chitosan-CNT composite films appears to have "dots" on the film surface, and these "dots" appear more frequently when the deposition voltage is high. Moreover, the "dots" on the film surfaces generally have a diameter of 10-20 nm, which match with the diameter of the CNT. The "dots" could be the evidence of CNT being deposited perpendicular to the substrate. The investigation of such hypothesis leads to the study of the cross section of the deposited film.

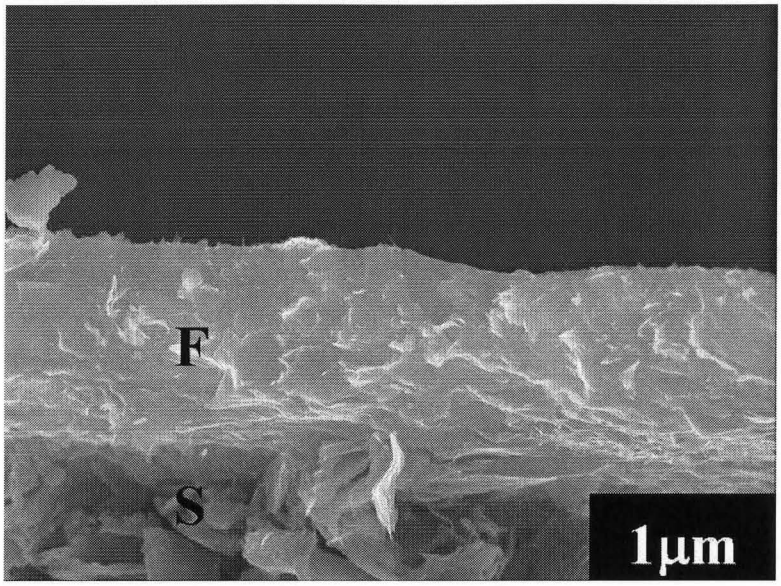

Figure 5-15 SEM picture of the cross section of the chitosan-CNT composite film on graphite substrate where (S) is the substrate and (F) is the film.

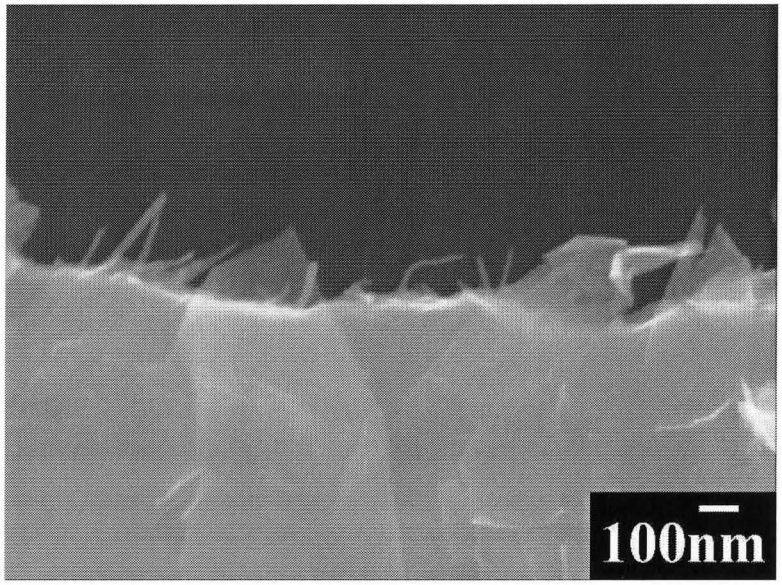

Figure 5-16 SEM picture of the cross-section of the chitosan-CNT composite film on graphite at high magnification.

Figure 5-15 shows the cross section of the film deposited on a graphite substrate at a deposition voltage of 50 V. Figure 5-16 shows a higher magnification image of the

cross section of such chitosan-CNT composite film. As seen from Figure 5-16, the CNT show a preferred orientation perpendicular to the substrate and some CNT are protruding out of the chitosan film. Such observation can explain the appearance of "dots" of the size of 10-20 nm on top of chitosan-CNT composite films. The "dots" observed on top of the deposited film are the end point of the CNT.

The deposition of the chitosan-CNT films was performed on a stainless steel plate as a cathode and platinum plate as a counter electrode. The cathode and the anode plates were parallel to each other. Such a parallel plates setting enabled a uniform electric field with electric field lines perpendicular to the cathode and anode plates. During deposition, the CNT in the suspension aligned with the electric field. The stronger the electric field, the higher degree of alignment, and that explains the observation of higher number of "dots" observed on film deposited at a higher voltage. The perpendicular orientation of CNT is beneficial for the development of ES, since such an orientation can provide direct electron/ion conducting pathway through the thin film, and it greatly enhances the performance of the electrode materials. Therefore, a high deposition voltage is beneficial in the deposition of the chitosan-CNT composite films.

After the development of the deposition technique for the chitosan-CNT films, the chitosan-CNT film was deposited onto the nickel substrate first and then the deposition of manganese oxide film was performed. However, the testing of such a film did not yield high SC due to the high concentration of chitosan inside the film. The high concentration of chitosan greatly increased the resistivity of the manganese oxide electrode, and resulting in a lower SC values.

Heat treatment was performed after the deposition of different layers in order to remove the chitosan binder and increase film porosity and ionic conductivity. TGA/DTA data (Figure 5-12 and Figure 5-13), indicates that heat-treatment at 300 °C can result in burning out of chitosan. It is important to note that TGA/DTA data were obtained at a heating rate of 5 degrees/min, where heat treatment of the films for burning out of chitosan was performed at 300 °C during 1 hour. The heat-treatment also resulted in improved adherence of the films to substrate. SEM pictures of the composition films can be seen in Figure 5-17.

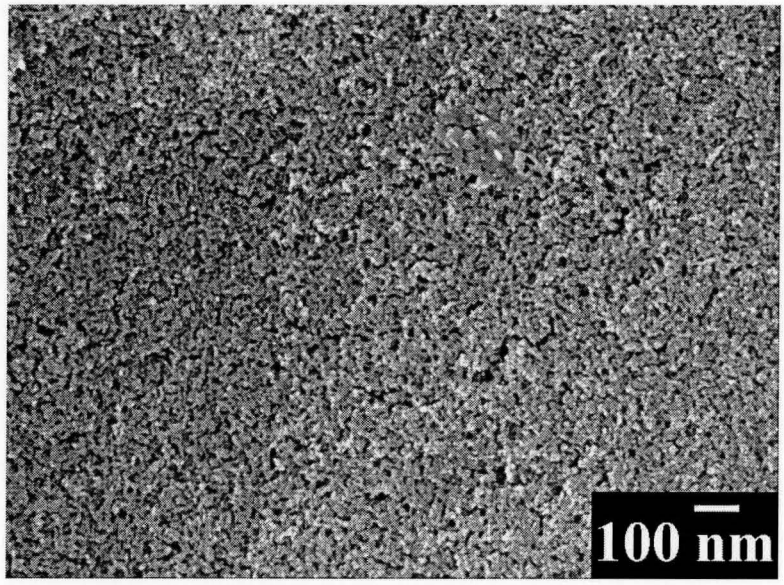

Figure 5-17 SEM picture of the CNT-MnO_x composite electrode with MnO_x layer on top after heat-treatment at 300 °C.

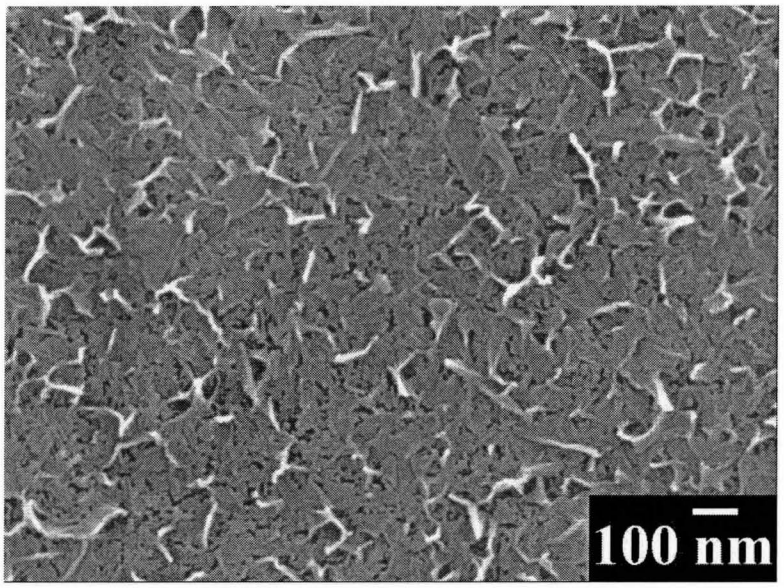

Figure 5-18 SEM picture of the CNT-MnO_x composite electrode with MnO_x layer on top after electrochemical testing.

The MnO_x film on the top layer is deposited from the $MnCl_2.4H_2O$, therefore, it demonstrated a similar morphology change from nanocrystal (spherical) to the dendrite structure as seen in Figure 5-18.

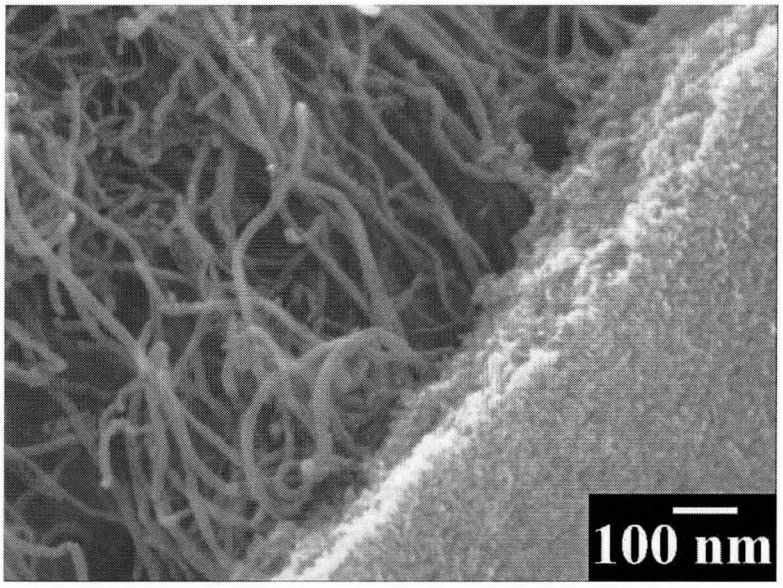

Figure 5-19 SEM picture of the CNT-MnO_x composite electrode taken from the edge of the electrode.

A better view of the multilayer structure of the composite electrode can be seen in Figure 5-19 where the edge of the electrode where the CNT is exposed.

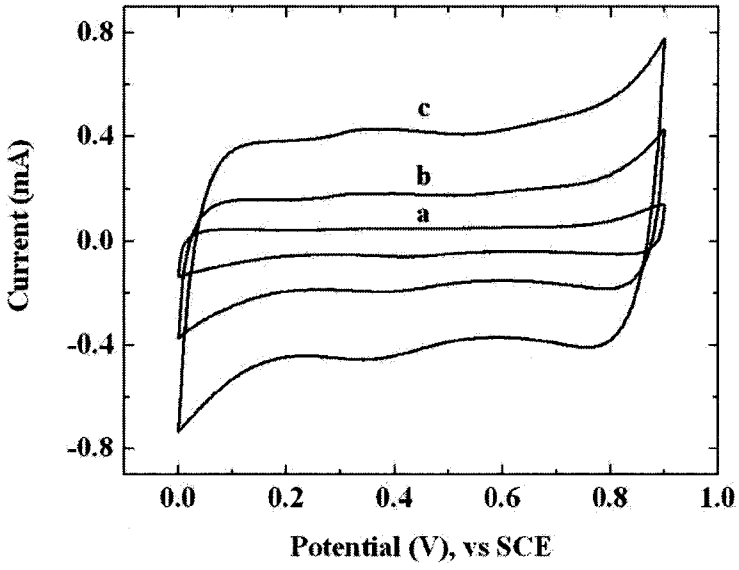

Figure 5-20 CV of CNT-MnO_x composite electrode with a mass of 37.0 µg/cm^2 tested in 0.1 M Na_2SO_4 electrolyte at a scan rate of (a) 5 mV/s, (b) 20 mV/s and (c) 50 mV/s.

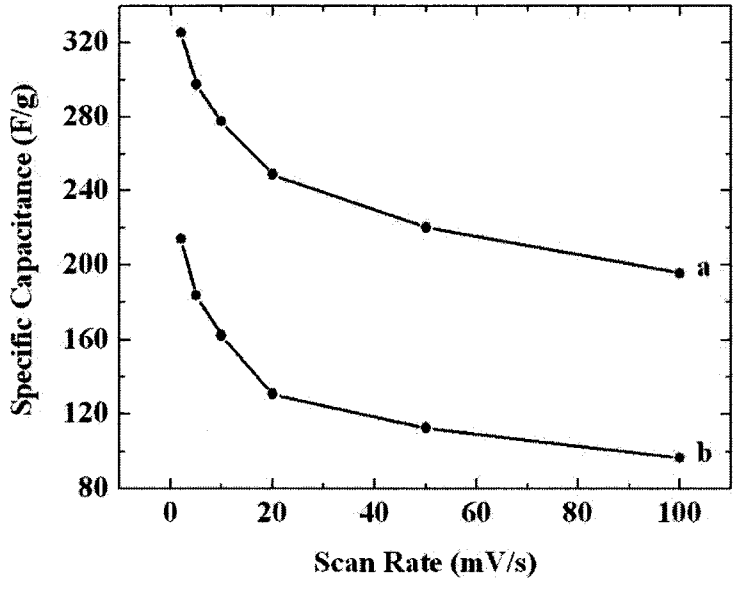

Figure 5-21 SC as a function of scan rate for (a) 37 µg/cm^2 and (b) 118.0 µg/cm^2 CNT-MnO_x composite electrode tested at 0.1 M Na_2SO_4 electrolyte.

The cyclic voltammetry testing results for the-MnO_x composite electrode is shown in Figure 5-20. Various thickness of CNT-MnO_x composite electrodes have been tested, and their SC values at different scan rate are shown at Figure 5-21.

For the CNT-MnO_x composite electrode with mass of 37.0 $\mu g/cm^2$, SC achieved a relatively high value of 325 F/g at 2 mV/s. However, the SC of 325 F/g for the composite film is smaller than the pure MnO_x film deposited from $MnCl_2.4H_2O$ without CNT. It is important to note that CNT is a capacitive material. However, its capacitive behavior is based on the formation of double layer. The charge storage mechanism is different from that of the manganese oxide. The SC of CNT is much lower than the MnO_x, therefore, the combine use of both materials may result in lowering the amount of active MnO_x in the electrode and lower the SC of composite material. It is suggested that multiple layers of lower thickness are necessary with lower CNT content in order to optimize the performance of composite electrodes.

5.2. ELD of Manganese Oxide from Mn^{7+} Solutions

Cathodic electrodeposition of manganese oxide films was performed from 20 mM $KMnO_4$ solutions on nickel substrates. The deposits prepared on the nickel plates without any surface treatment showed low adhesion, which can be attributed to the formation of nickel oxide on the nickel plate surface. Therefore, surface treatment such as chemical etching and/or electrochemical etching of the substrates must be performed before deposition to enable well adhered and uniform manganese oxide films.

The deposition mechanism can be attributed to the diffusion and cathodic reduction of anionic MnO_4^- species. The reduction of MnO_4^- species and precipitation of manganese dioxide are in agreement with the Pourbaix diagram for manganese[103]. However, only limited information is available in literature related to the complex chemistry of the reduction of MnO_4^-. The kinetic pathway of reducing Mn^{7+} to Mn^{4+} depends on electrode potential, pH, concentration of MnO_4^- and other species in the solution. It is suggested that in neutral aqueous solutions the following reaction can result in the reduction of MnO_4^- species[104]:

$MnO_4^- + 2H_2O + 3e^- \rightarrow MnO_2 + 4OH^-$ (5.4)

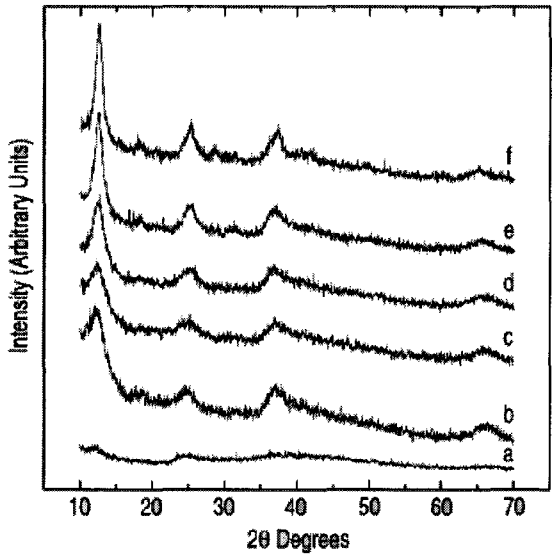

Figure 5-22 X-ray diffraction patterns for the deposits obtained from the 20 mM $KMnO_4$ aqueous solutions: (a) as prepared and after heat treatment at (b) 200 °C, (c) 300 °C, (d) 400 °C, (e) 500 °C and (f) 600 °C.

X-ray diffraction studies showed that as-prepared deposits were poorly crystallized and exhibited very small peaks (Figure 5-22). The XRD spectra taken from the sample heat treated at 200 °C for 1 hour displayed broad reflexes, which can be

attributed to rancieite structure (JCPDS file 22-0718). The peak broadening could be related to the small particle size. More distinct and sharp rancieite peaks were observed at higher temperatures in the range of up to 600 °C.

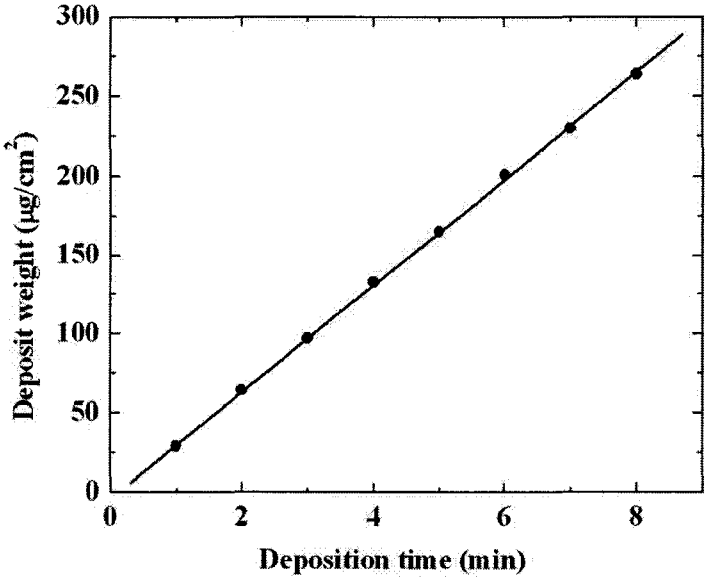

Figure 5-23 Deposit mass versus deposition time for deposits prepared from 0.1 M $KMnO_4$ solution at current density of 10 mA/cm² on nickel plate.

The deposition rate of the manganese oxide film from $KMnO_4$ solution can be seen in Figure 5-23. The deposition yield increased with increasing deposition time at a constant current density, indicating the formation of manganese oxide films of different thickness up to 250 μg/cm². The linear deposition rate relationship suggested the deposit weight of the film can be very well controlled by the deposition time.

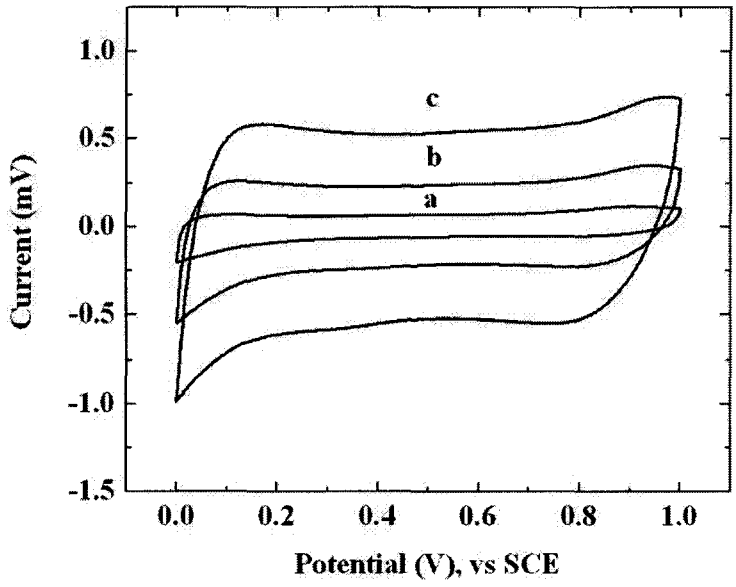

Figure 5-24 Cyclic voltammograms of manganese oxide film deposited on nickel plate after electrochemical etching, at a scan rate of (a) 5 mV/s, (b) 20 mV/s and (c) 50 mV/s for 90 μg/cm^2 film at 0.1 M Na_2SO_4 electrolyte.

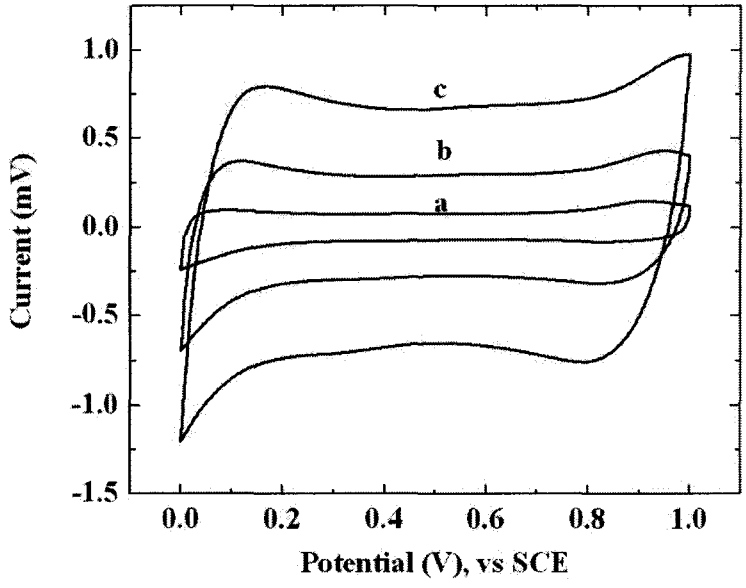

Figure 5-25 Cyclic voltammograms of manganese oxide film deposited on nickel plate after chemical etching at a scan rate of (a) 5 mV/s, (b) 20 mV/s and (c) 50 mV/s for 90 μg/cm^2 film at 0.1 M Na_2SO_4 electrolyte.

The deposited manganese oxide films are highly sensitive to different deposition conditions. The size of CV window appears differently if the deposition is performed at the same substrate but with different surface treatment of the substrates prior to the deposition as seen in Figure 5-24 and Figure 5-25. As a result, the SC values of the deposited films will be different as well (Figure 5-26).

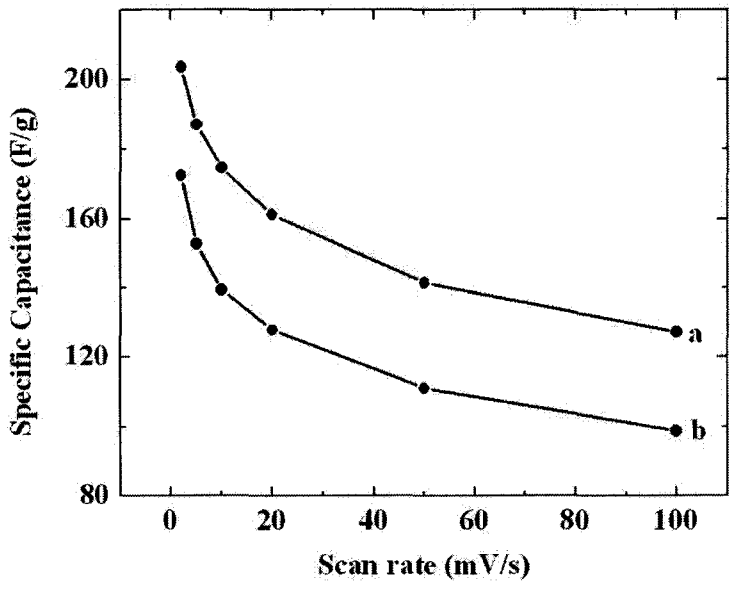

Figure 5-26 Specific capacitance versus scan rate of 90 μg/cm^2 manganese oxide film deposited from 0.1M $KMnO_4$ solution at nickel plates after (a) chemical etching and (b) electrochemical etching at 0.1 M Na_2SO_4 electrolyte.

Deposition current densities also play a critical part in affecting the SC values of the deposited manganese oxide electrodes as seen in Figure 5-27 and Figure 5-28. It is known[104] that oxide films deposited at higher current density usually exhibit a higher microporosity. The increase in porosity can result in enhanced ionic conductivity and higher SC.

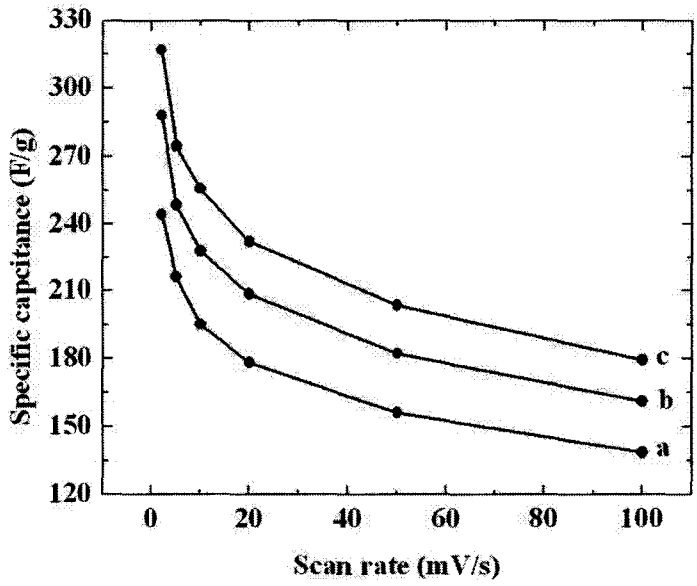

Figure 5-27 Comparison of specific capacitance of manganese oxide films with a film thickness of 50 μg/cm^2 deposited at different current densities (a) 2 mA/cm^2, (b) 5 mA/cm^2 and (d) 10 mA/cm^2 in 0.1 M Na_2SO_4 electrolyte.

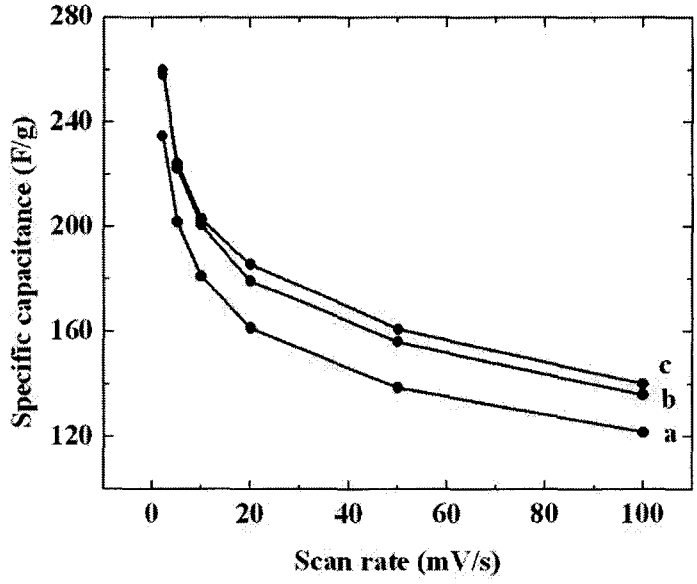

Figure 5-28 Comparison of specific capacitance of manganese oxide films with a film thickness of 100 μg/cm^2 deposited at different current densities (a) 2 mA/cm^2, (b) 5 mA/cm^2 and (c) 10 mA/cm^2 in 0.1 M Na_2SO_4 electrolyte.

The CV windows and the SC values are very sensitive to the electrolyte solutions concentration. It is found that at high electrolyte concentration, the size of the CV windows become larger. The large CV windows correspond to a larger SC values (Figure 5-29).

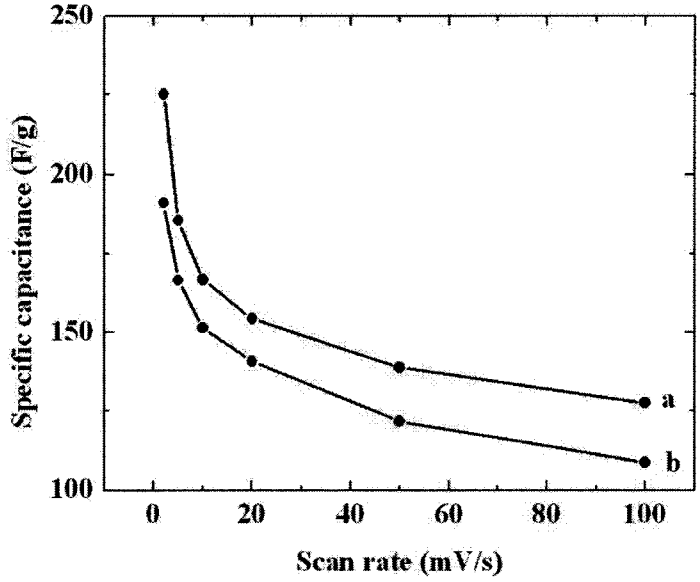

Figure 5-29 Specific capacitance versus scan rate for the 100 μg/cm^2 manganese oxide film prepared from 0.1 M $KMnO_4$ solution and tested in (a) 0.5 M Na_2SO_4 and (b) 0.1 M Na_2SO_4.

Since the charge storage mechanism of the manganese oxide film is believed to be based on the insertion of protons within the near-surface region[52], the increase in SC with the increased electrolyte concentration suggested that the cations in the electrolyte solution also contributed to the charge storage mechanism.

The manganese oxide films were also tested in K_2SO_4 aqueous electrolytes of various concentrations. At increased electrolyte concentration, the manganese oxide films demonstrated larger CV windows and high SC values (Figure 5-30).

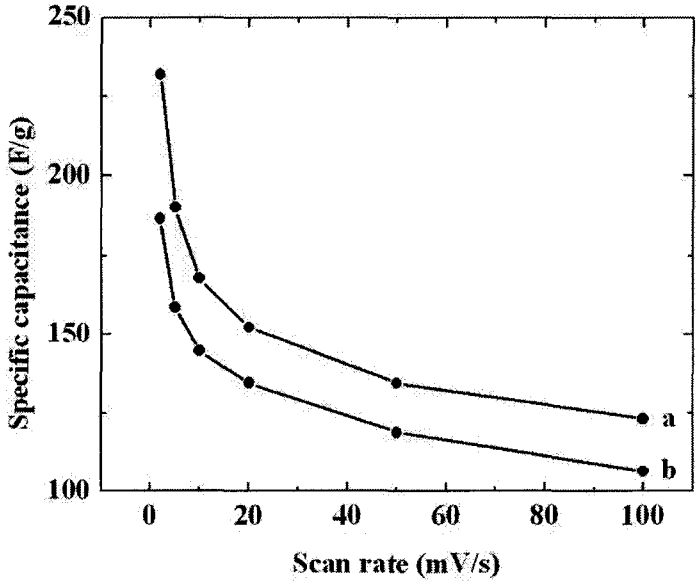

Figure 5-30 Specific capacitance versus scan rate for the 100 ug/cm^2 manganese oxide film prepared from 0.1 M $KMnO_4$ solution tested in (a) 0.5 M K_2SO_4 and (b) 0.1 M K_2SO_4.

Table 2 Specific capacitance values of the 100 ug/cm^2 manganese oxide film tested in different electrolytes of various concentrations.

Scan Rate	0.1 M Na_2SO_4	0.5 M Na_2SO_4	0.1 M K_2SO_4	0.5 M K_2SO_4
2 mV/s	192 F/g	225 F/g	187 F/g	232 F/g
5 mV/s	167 F/g	186 F/g	159 F/g	190 F/g
10 mV/s	152 F/g	167 F/g	145 F/g	168 F/g
20 mV/s	141 F/g	154 F/g	135 F/g	152 F/g
50 mV/s	122 F/g	139 F/g	119 F/g	135 F/g
100 mV/s	109 F/g	128 F/g	106 F/g	123 F/g

By comparing the SC values of the manganese oxide film tested in different electrolytes of various concentrations, it is interesting to see that the manganese oxide film demonstrated similar specific capacitance value with difference less than 10% in

both Na_2SO_4 and K_2SO_4 electrolytes of the same concentration. Electrochemical testing of the manganese oxide films at other neutral electrolytes has been done. For electrolytes such as NaCl and KCl, the films show instability in the presence of Cl^- ions, and the films disintegrate after the first cycle of charging and discharging. Neutral electrolytes such as $NaNO_3$ and KNO_3 have also been tested, but the CV windows show multiple redox peaks due to the presence of NO_3^- ions. The multiple redox peaks during the charge-discharge of the manganese oxide film suggests chemical reaction between the manganese oxide and the NO_3^- ion, and the multiple redox peaks prevent the manganese oxide to achieve an ideal box shape for ES application.

Compared to the polymer-mediated electrosynthesis, this approach offers the advantage of direct formation of electrochemically active MnO_x by the reduction of MnO_4^- species. In contrast, polymer-mediated electrosynthesis requires burning out of polymers and electrochemical oxidation of the Mn_3O_4 phase. However, polymer-mediated electrosynthesis enables co-deposition of various oxides and modification of composition and properties of the deposit. The deposit composition can be varied by the use of polychelates[77]. The co-deposition of manganese oxide and other materials from $KMnO_4$ presents difficulties, related the reduction of MnO_4^- species in the presence of other cations and organic materials.

5.3. EPD of Manganese Oxide in Ethanol Solutions

Manganese oxide nanopowders were prepared by chemical precipitation method and deposited on various substrates by EPD. The formation of manganese oxide particles can be described by the reduction reaction:

$$4MnO_4^- + 3CH_3CH_2OH + 4H^+ \rightarrow 4MnO_2 + 3CH_3COOH + 5H_2O \quad (5.5)$$

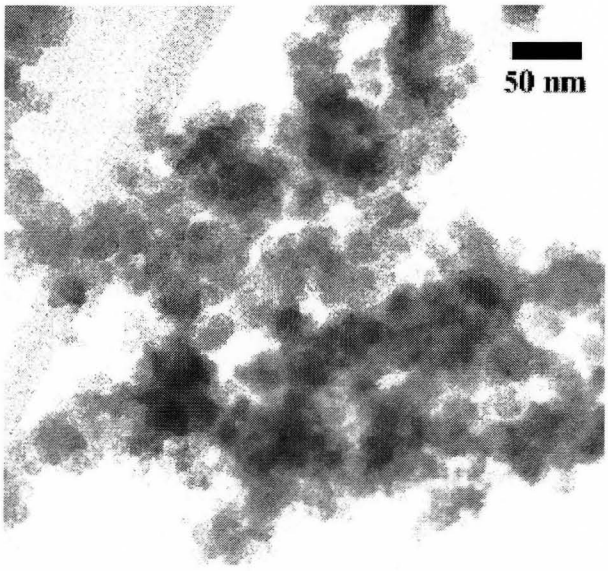

Figure 5-31 TEM micrograph of the as-prepared MnO_x nanoparticles.

Figure 5-31 shows TEM pictures of the powders prepared for EPD. The MS of manganese in the precipitated powders was found to be 3.6. XRD studies (Figure 5-32) showed that as-precipitated powders were amorphous. After heat treatment at elevated temperature, XRD structure of birnessite phase (JCPDS file 87-1497). The particles were nearly spherical, with the size of ~ 30 nm, while some agglomerated particles of ~ 100 nm are also seen.

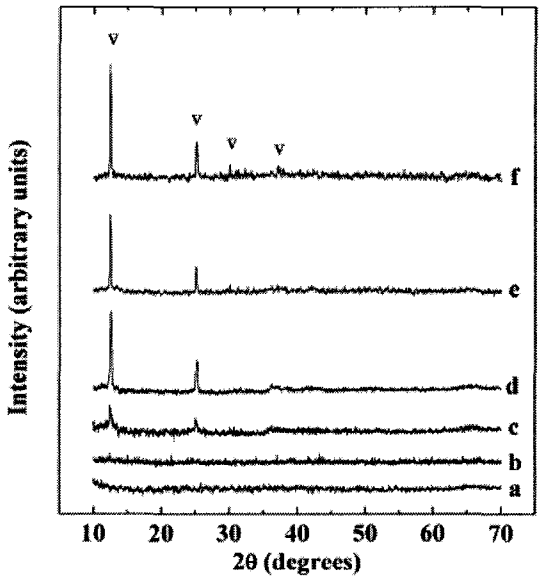

Figure 5-32 X-ray diffraction patters for manganese oxide prepared by chemical precipitation method: (a) as prepared sample and after heat treatment at (b) 300 °C, (c) 400 °C, (d) 500 °C, (e) 600 °C and (f) 700 °C.

Manganese oxide particles were positively charged in the ethanol suspensions and moved toward the cathode under applied electric field. The charging mechanism can be attributed to the adsorption of H^+ ions[68].

The SEM pictures of the manganese oxide particles on stainless steel wires and foils can be seen in Figure 5-33 and Figure 5-34. The results suggest the deposition can even be done on substrates with complex shape.

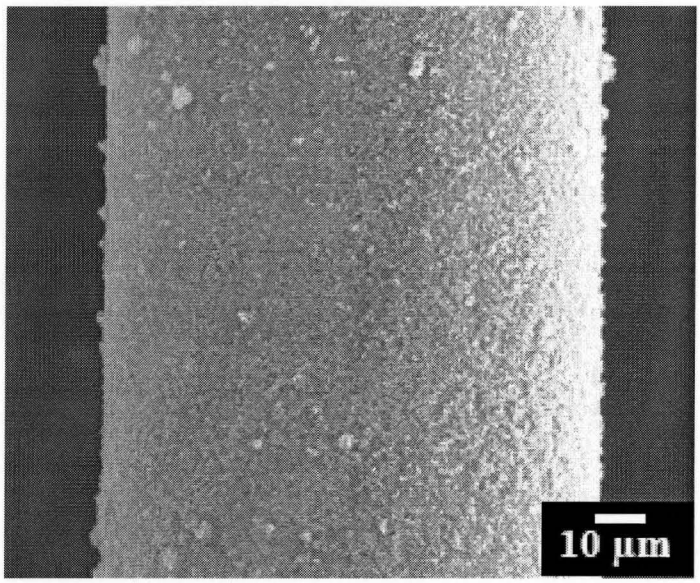

Figure 5-33 SEM micrograph of the MnO_x film on the stainless steel wire substrate prepared by electrophoretic deposition from 1g/L suspension of MnO_x nanoparticles in ethanol.

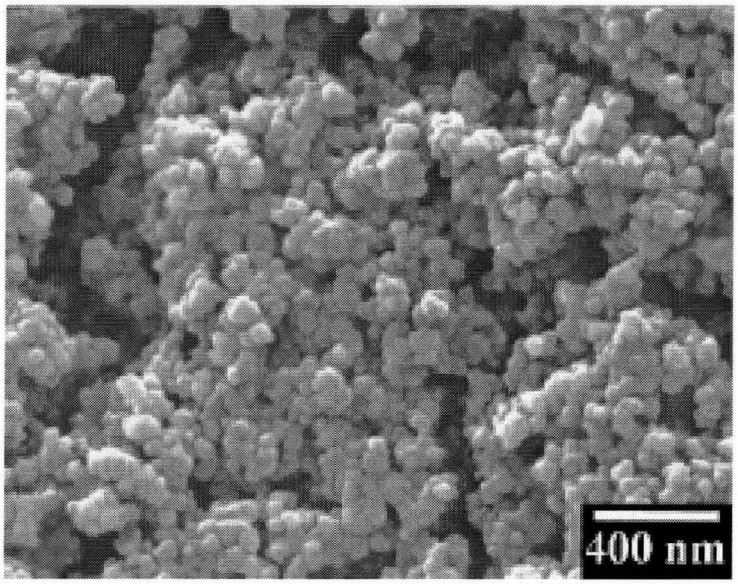

Figure 5-34 SEM picture for MnO_x film prepared by electrophoretic deposition from 1 g/L suspension of MnO_x nanoparticles in ethanol on stainless steel foil.

Similar deposits were obtained on nickel substrates. The thickness of the films was in the range of up to 2 μg/cm^2. The deposits contained agglomerated manganese oxide particles and exhibited porosity.

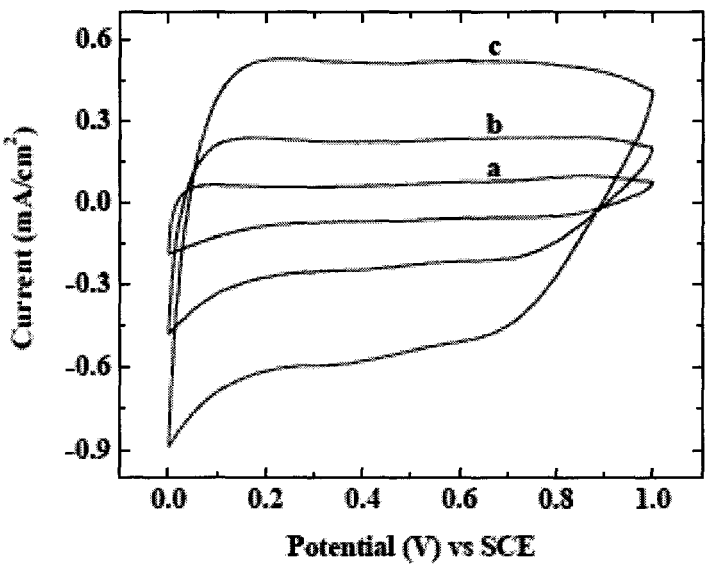

Figure 5-35 Cyclic voltammograms of the 90 μg/cm^2 MnO_x film prepared by EPD, tested in the 0.5 M Na_2SO_4 electrolyte solution at scan rate of (a) 5 mV/s, (b) 20 mV/s and (c) 50 mV/s.

The manganese oxide film demonstrated a capacitive behavior in the potential range of 0.0-1.0 V versus SCE in 0.5 M Na_2SO_4 electrolyte. Figure 5-35 shows CVs at different scan rates. The shape of the CV's deviates from the ideal capacitive behavior, probably due to the large agglomeration of the manganese oxide particles.

The SC of the 90 μg/cm^2 manganese oxide film was found to be 230 F/g at a scan rate of 2 mV/s in 0.5 M Na_2SO_4 electrolyte as seen in Figure 5-36. The highest SC value was 375 F/g when tested in 1.0 M Na_2SO_4 at 2 mV/s. The manganese oxide films prepared by EPD of manganese oxide nanoparticles showed similar capacitive properties

compared with the manganese oxide films deposited by ELD from $KMnO_4$ solutions. Both of the films showed higher SC values at higher electrolyte concentration.

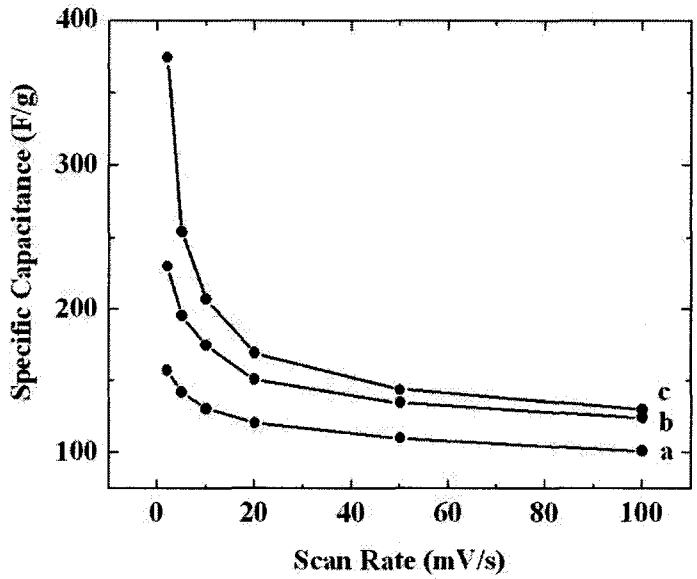

Figure 5-36 Specific capacitance versus scan rate for 90 μg/cm^2 manganese oxide film tested at different scan rates in (a) 0.1 M Na_2SO_4, (b) 0.5 M Na_2SO_4 and (c) 1.0 M Na_2SO_4 electrolyte.

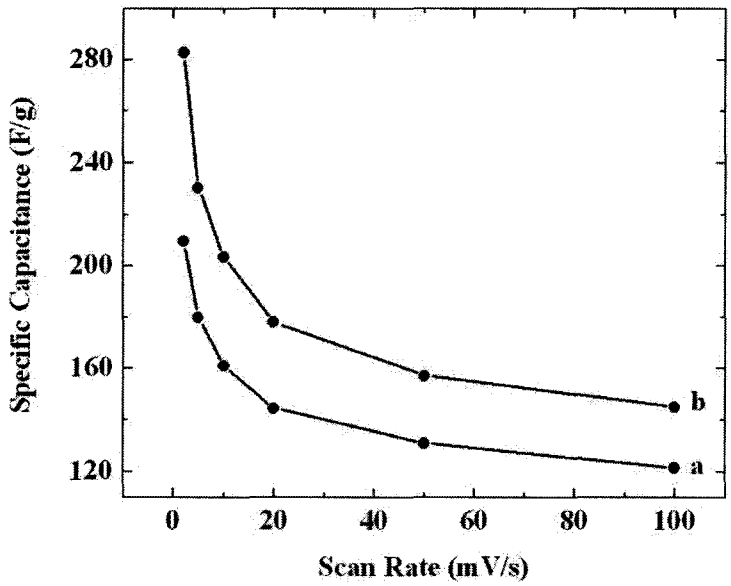

Figure 5-37 Specific capacitance versus scan rate for 90 μg/cm^2 manganese oxide film tested at different scan rates in (a) 0.1 M K_2SO_4, (b) 0.5 M K_2SO_4 electrolyte.

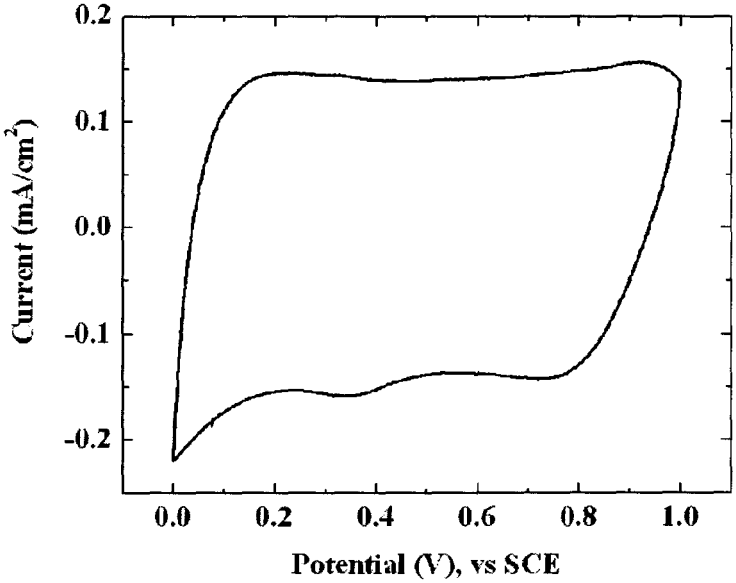

Figure 5-38 Cyclic voltammogram of the 5.92 μg MnO_x film deposited on the quartz crystal prepared by EPD, tested in 0.1 M Na_2SO_4 electrolyte solution at 20 mV/s

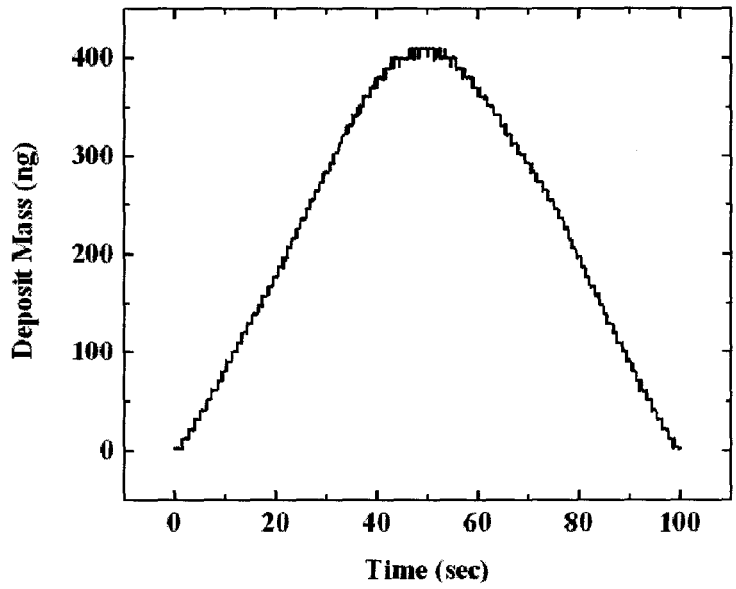

Figure 5-39 Mass change of the 5.92 μg MnO_x film deposited on the quartz crystal during the cyclic voltammetry measurement.

The effect of electrolyte solutions on the manganese oxide films was further investigated with the use of quartz crystal microbalance. 5.92 μg of MnO_x film was

deposited electrophorectially on a quartz crystal with a gold plated area of 0.192 cm^2 as the electrode. Cyclic voltammetry measurement and weight change were performed on the manganese oxide film simultaneously. Figure 5-38 and Figure 5-39 are the CV window of the manganese oxide film at 20 mV/s and its corresponding weight change through out the charge-discharge cycle. When the manganese oxide film was fully charged, a mass increase of 410 ng was observed from the QCM measurement.

According to Pang et al.[52], the charge storage mechanism of the manganese oxide film is believed to be based on the insertion of protons within the near-surface region. Since the electrolyte solution used in the testing is 0.1 M Na_2SO_4 and it only contained H^+ ion and Na^+ ion, the charge/discharge reaction can be described by the following:

$MnO_2 + H^+ + e^- \rightarrow MnOOH$ (5.6)

$MnO_2 + Na^+ + e^- \rightarrow MnOONa$ (5.7)

When the manganese oxide film is fully charged, the theoretical weight gain is 68.1 ng when based on Eq. 5.6, and a weight gain of 1570 ng when based on Eq. 5.7. The experimental result of 410 ng weight gain indicated that the charge storage mechanism of the manganese oxide film is based on the insertion of both H^+ and Na^+ ions within the near-surface region.

5.4. EPD of Manganese Oxide in Aqueous Solutions

5.4.1. EPD of Manganese Oxide in Aqueous Solutions with Sodium Alginate

Manganese oxide powders were obtained by chemical precipitation method using the reduction reaction described by Eqs 5.5.

Analysis of EDS showed that obtained powders included K with a Mn/K atomic ratio of 3.11±0.04. The XRD studies showed amorphous nature of as prepared manganese oxide (Figure 5-32). Crystallization was observed after heat treatment of the powders at 400 °C for 1 hour. The XRD patterns at temperatures in the range from 400 °C to 700 °C showed peaks of a birnessite phase (JCPDS file 87-1497). According to Ma and Ching[105, 106], the birnessite has near MnO_2 stoichiometry. The birnessite formula is generally expressed as $A_xMnO_{2+y}(H_2O)_z$, where A represents as alkali metal cation. The average MS of manganese usually falls between 3.6 to 3.8, which represents a predominance of Mn^{4+} with minor amount of Mn^{3+}. Thermal dehydration can result in the formation of a dehydrated form of birnessite[105, 106].

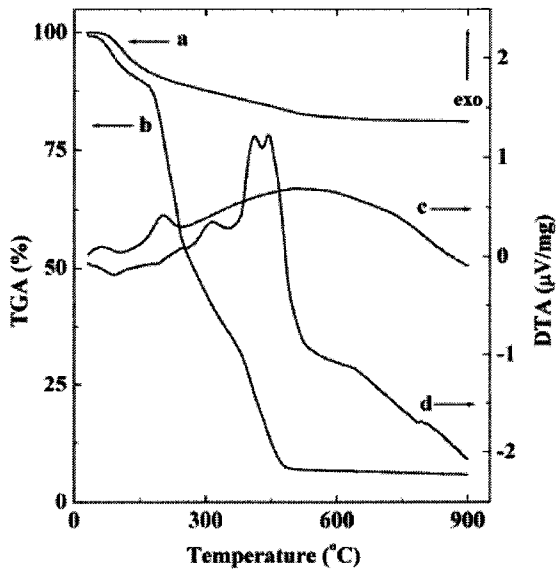

Figure 5-40 TGA and DTA for as prepared manganese oxide powders (a, c) and alginic acid films (b, d) deposited from 1 g/L sodium alginate solution at current density of 1 mA/cm^2.

TGA studies (Figure 5-40) showed weight loss below 500 °C, which can be mainly attributed to dehydration. The total weight loss at 900 °C was 19.0 wt.%. Broad endotherms in DTA data can be related to dehydration in agreement with the corresponding TGA data.

As prepared powders were used for electrophoretic deposition. Aqueous suspensions of manganese oxide particles were unstable and showed rapid sedimentation when ultrasound treatment was interrupted. Electrophoretic deposition experiments have not yielded noticeable deposition from such suspensions at deposition voltages of 3-20 V. In contract, well dispersed and stable suspensions of manganese oxide particles were obtained using sodium alginate (Na-Alg) as an additive. It should be noted that sodium alginate is an anionic polyelectrolyte with carboxyl end groups. The dissociation of sodium alginate can be achieved in basic solutions:

$Na\text{-}Alg \rightarrow Na^{+} + Alg^{-}$ (5.8)

The dissociations results in the formation of anionic Alg- species. It is suggested that adsorption of alginate on the surface of manganese oxide particles enabled electrosteric stabilization of the particles in aqueous solutions and provided electric charge, which is necessary for electrophoretic deposition. It was found that alginate promotes electrophoretic deposition of films from the suspension of manganese oxide particles. The experimental results described below indicate that alginate can be used as a dispersant, charging additive and binder for the electrophoretic deposition of manganese oxide. Experimental conditions were found for the deposition of alginate films and further utilized for the electrophoretic deposition of manganese oxide using alginate additive.

Obtained results indicate that alginate films can be deposited on various conductive substrates such as stainless steel, nickel, platinum and graphite using 0.2-2.0 g/L aqueous solutions of sodium alginate. The pH dependent charge of the alginate macromolecules is important for electrophoretic deposition. It is known that the reduction in solution pH results in decreasing charge of alginate macromolecules and precipitation of alginic acid at pH<3. Low pH can be generated electrochemically at the anode surface using the electrochemical decomposition of water:

$2H_2O \rightarrow O_2 + 4H^{+} + 4e^{-}$ (5.9)

It suggested that electric field provides electrophoretic motion of Alg- species which form alginic acid H-Alg films on the anodic substrates

$Alg^{-} + H^{+} \rightarrow H\text{-}Alg$ (5.10)

Obtained films were removed from the platinum substrates and studied by TGA and DTA. The TGA data in Figure 5-40 showed several steps in weight loss in agreement with the literature data for alginic acid[107]. The weight loss below 160 °C can be attributed to deposit dehydration. The decomposition and burning out of alginic acid resulted in weight loss at higher temperatures. Data of DTA revealed exotherms in the temperature range of 350 to 500 °C, which can be attributed to burning out of alginic acid. The exotherms correspond to the steps in the weight loss observed in the same temperature range.

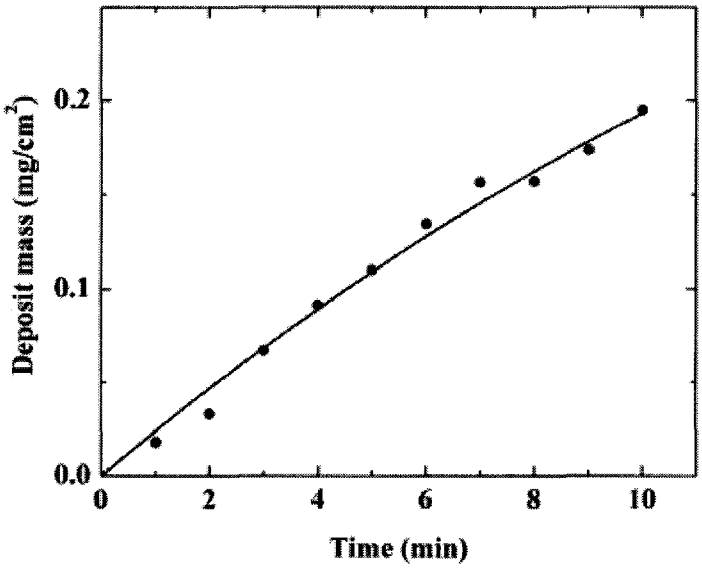

Figure 5-41 Deposit mass versus deposition time for deposits prepared from 1 g/L sodium alginate solutions at current density of 1 mA/cm^2.

Figure 5-41 shows deposit mass versus deposition time for alginic acid films. The deposition yield increased with increasing deposition time at a constant current density, indicating the formation of alginic acid films of different weight.

The addition of manganese oxide particles to the sodium alginate solutions resulted in increasing deposit yield, which indicates co-deposition of the particles and alginic acid. Figure 5-42 shows deposit mass versus manganese oxide particle concentration in suspensions containing 0.5 g/L sodium alginate. The deposit mass increased with increasing concentration of the particles in the suspensions. The increase in deposition time resulted in higher deposition yield. Further increase in particle concentration required larger amount of sodium alginate for particle stabilization in the suspensions.

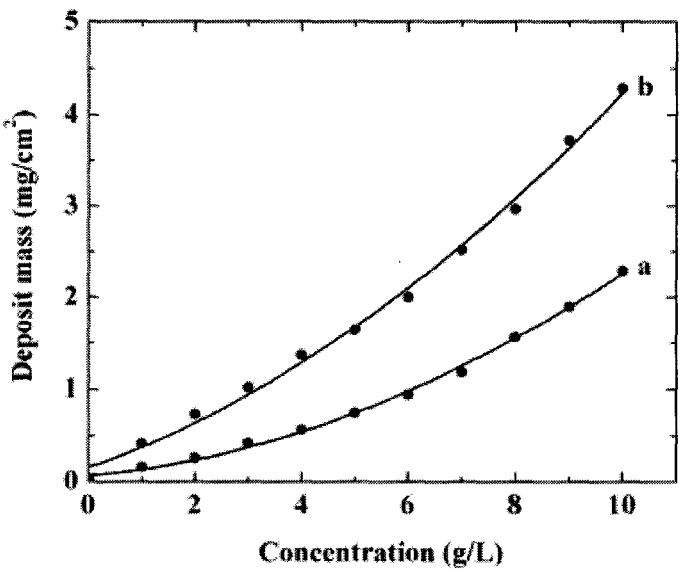

Figure 5-42 Deposit mass versus manganese oxide concentration in 0.5 g/L sodium alginate solutions at deposition voltage of 10 V and deposition time of (a) 2 minutes and (b) 4 minutes.

The experimental data shown in the Figure 5-42 indicates that the increase in deposit yield with particle concentration is non-linear. It is in this regard that Hamaker[108] equation predicts linear increase in the deposit mass M with increasing particle concentration C_S in dilute suspensions:

$$M = \mu E t S C_S \quad \textbf{(5.11)}$$

where μ is particle mobility in an electric field E, t is deposition time, S is the electrode area.

However, theoretical and experimental data reported by Biesheuvel and Verweij[108] showed more than linear increase in the deposition yield with increasing particle concentration, which is attributed to the movement of the deposit-suspension boundary. It was shown that the deposit yield can be described by the equation:

$$M = \mu E t S C_S C_C / (C_C - C_S) \quad \textbf{(5.12)}$$

where C_C is the particle concentration in the deposit. Hamaker equation can be obtained if C_S is appreciably lower than C_C. The experimental results (Figure 5-42) show more than linear increase in the deposit yield with increasing particle concentration. The results are in a qualitative agreement with the theory of electrophoretic deposition and experimental data for other materials reported in the literature[107]. However, it is important to note that the deposits obtained in this work contain not only manganese oxide particles but also alginic acid macromolecules. Indeed, the results of TGA and DTA studies indicate the composite nature of the deposited films.

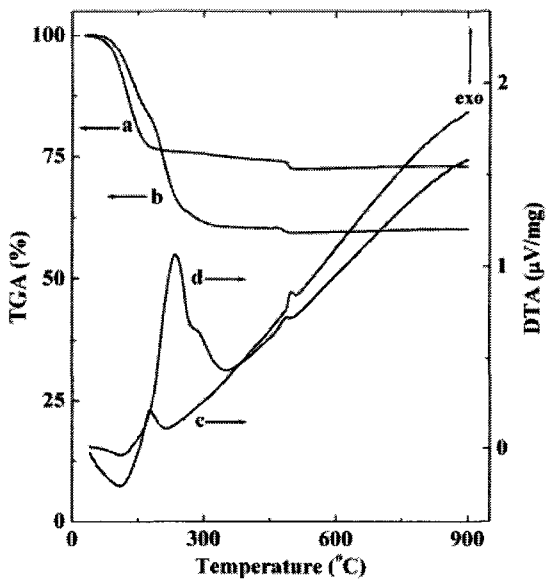

Figure 5-43 Data of TGA and DTA for the films deposited from aqueous suspensions containing 10 g/L MnO_x and 0.5 g/L sodium alginate(a, c) and film prepared from 5 g/L MnO_x and 2 g/L sodium alginate(b, d).

The TGA and DTA data for the films prepared from different suspensions (Figure 5-43) shows several steps in weight loss which can be attributed to deposit dehydration and burning out of alginic acid. The total weight loss for the film prepared from the 10 g/L manganese oxide suspension, containing 0.5 g/L sodium alginate was found to be 27.1 wt.%. This weight loss exceeds the weight loss obtained for pure manganese oxide powders (Figure 5-40). The additional weight loss can be attributed to burning out of alginic acid. Taking into account the TGA data for pure manganese oxide, the alginic acid content in the deposits was found to be ~ 10 wt.%. The deposit prepared from 5 g/L manganese oxide suspension, containing 2 g/L sodium alginate showed weight loss of 39.9 wt.%, indicating alginic acid content of 25.8 wt.%. The corresponding DTA data showed endotherm at 100 °C and exotherms at higher temperatures, which correspond to

the observed steps in weight loss. The exotherms can be attributed to burning out of alginic acid. Similar exotherms were observed for pure alginic acid (Figure 5-40). Obtained results indicate that deposit composition depends on the concentration of manganese oxide particles and sodium alginate in the suspensions used for deposition.

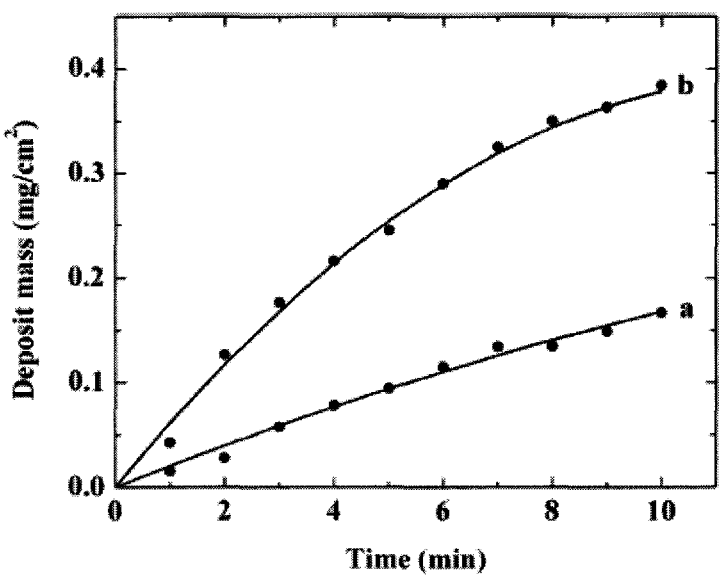

Figure 5-44 Deposit mass versus deposition time for 5 g/L manganese oxide suspension containing 0.5 g/L sodium alginate at current densities of (a) 1 mA/cm^2 and (b) 2 mA/cm^2.

The amount of the deposited material can be varied by the variation of the deposition time at a constant current density or constant voltage. Figure 5-44 shows deposit mass versus deposition time for the 5 g/L sodium alginate. The deposit mass increased with increasing deposition time, indicating the possibility of deposition of films of different weight. The increase in current density enabled higher deposit yield. It is important to note that the concentration of particles in suspensions and deposit yield are comparable with the literature data for electrophoretic deposition of other materials[109, 110, 111, 112]. Therefore, the results of this work indicate that electrophoretic deposition can be

used for the deposition of manganese oxide films at a practically important deposition rate.

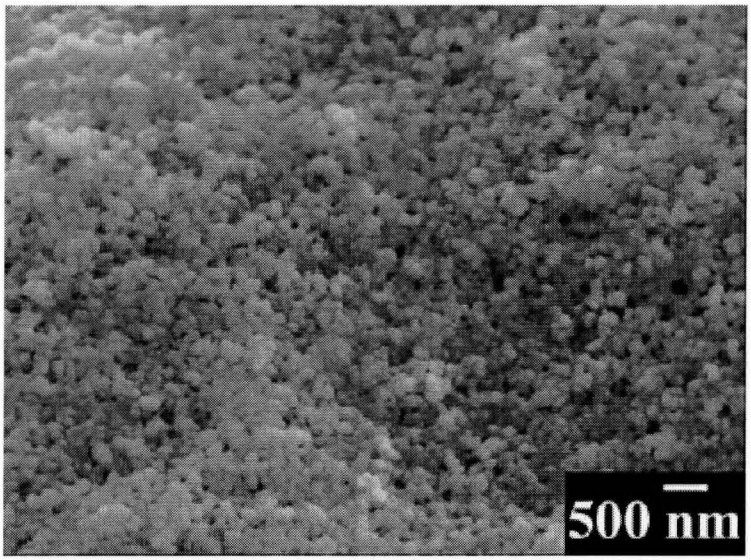

Figure 5-45 SEM image of film prepared from 10 g/L aqueous manganese oxide suspension containing 0.5 g/L sodium alginate at deposition voltage 5 V on stainless steel.

Figure 5-45 shows SEM picture of a deposit on a stainless steel substrate. The SEM pictures of the fracture of the deposits of different thickness are shown in Figure 5-46. The deposit consists of submicrometer particles with average particle size of 50 nm. Studies of SEM showed that films of different thickness in the range 2-100 μm can be obtained by variation in deposition time and voltage. It is important to note that the use of fine particles can result in deposit cracking during drying, which can be prevented by the use of binders. However, for many applications of electrophoretic deposition, the binder content in the deposits must be optimized.

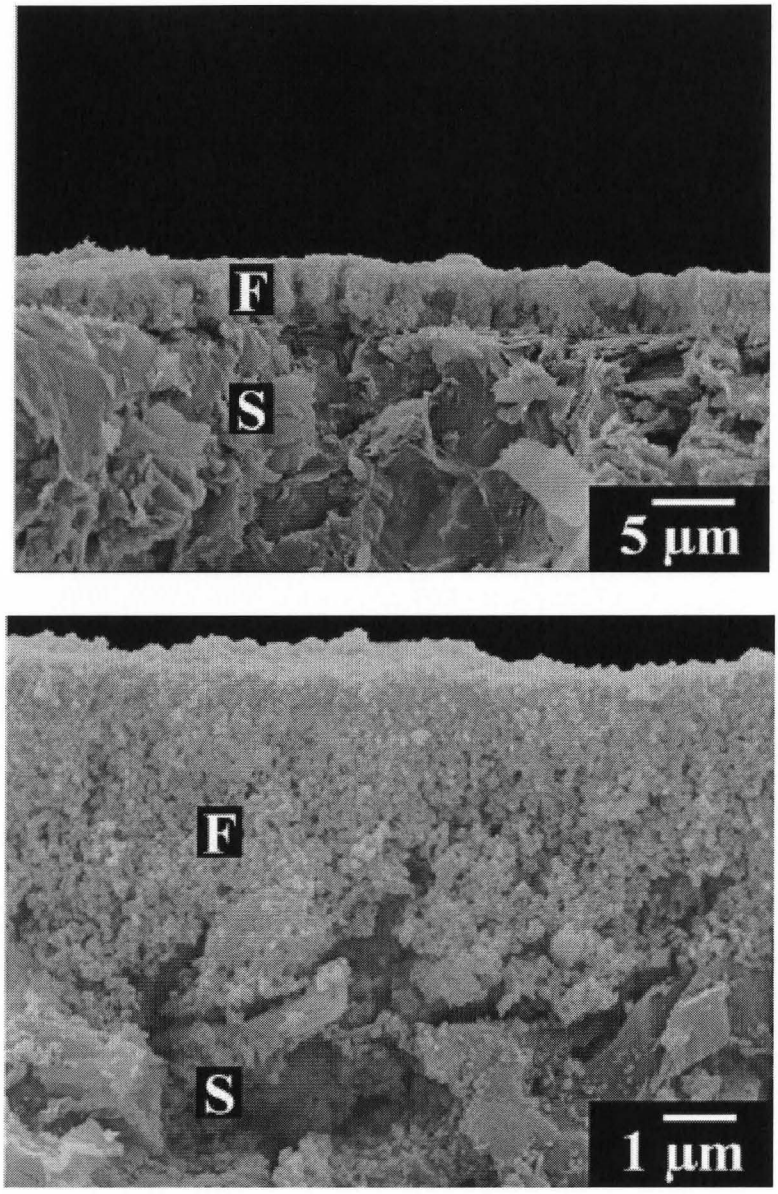

Figure 5-46 SEM image of fractures of film (F) on graphite substrate (S) at different magnifications: films were prepared from 10 g/L manganese oxide suspension containing 0.5 g/L sodium alginate at deposition voltage of 3 V.

The application of manganese oxide films in electrochemical supercapacitors requires the use of fine particles with high surface area. It is known that electrode materials with small particle size and high surface area are beneficial to redox reactions

which underlie the charge storage mechanism. The binder content in the materials is usually in the range of 5-10 wt.%[113]. The increase in binder content can result in increased electrical resistance, which affects the electrochemical properties. The TGA data for the deposit prepared from the 10 g/L manganese oxide suspension containing 0.5 g/L alginate showed binder content of 10 wt.%. Such deposits were used for the investigation of electrochemical properties.

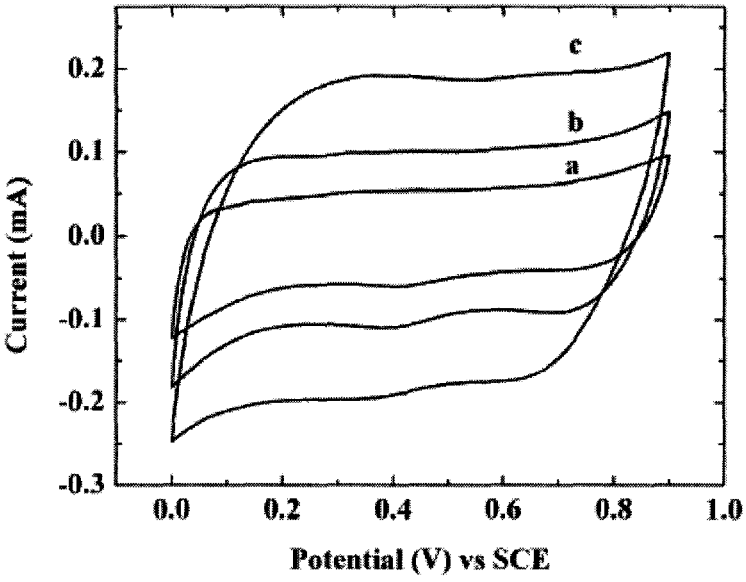

Figure 5-47 Cyclic voltammograms at scan rates of (a) 2 mV/s, (b) 5 mV/s and (c) 10 mV/s for 80 μg/cm^2 film, prepared from 10 g/L manganese oxide suspension containing 0.5 g/L sodium alginate at deposition voltage of 3 V.

Figure 5-47 shows typical CVs in the 0.1 M Na_2SO_4 solutions obtained at different scan rates in the potential range 0.0-0.9 V versus SCE. The manganese oxide electrodes exhibited capacitive like current-potential responses. It is clear from Figure 5-47 that there are no redox peaks in the range between 0.0 and 0.9 V.

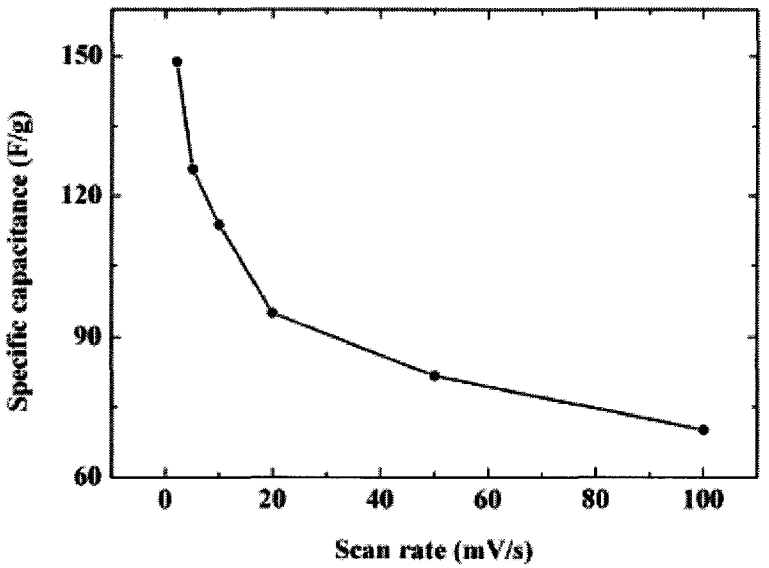

Figure 5-48 SC versus scan rate for 80 μg/cm^2 film, prepared from 10 g/L manganese oxide aqueous suspension containing 0.5 g/L sodium alginate at deposition voltage of 3 V.

The SC of the obtained films was calculated from the CV curves using Eq. 4.2. The results presented in Figure 5-48 indicate that highest SC of 150 F/g was observed at a scan rate of 2 mV/s. The obtained SC of electrophoretically deposited films is comparable with the SC of manganese oxide films of similar weight prepared by other methods[113, 114]. The SC decreased with increasing scan rate. Similar decrease in SC was reported in elsewhere[115]. The decrease in SC is attributed to low conductivity of manganese oxide.

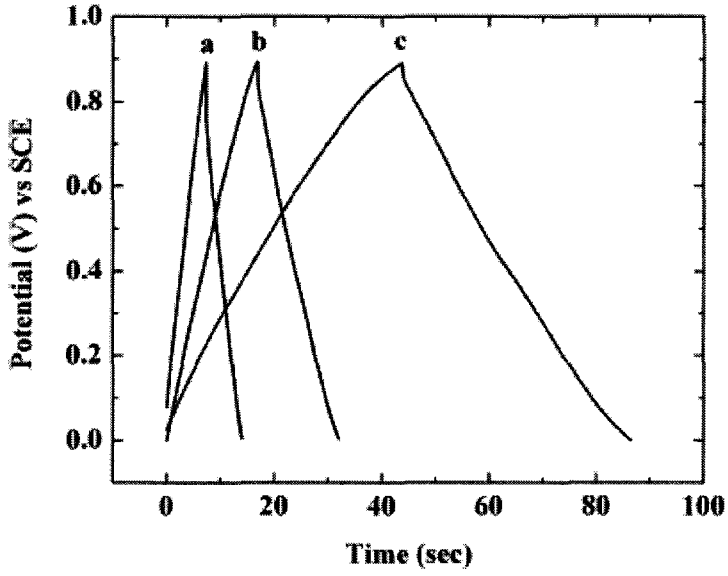

Figure 5-49 Charge and discharge behavior at current densities of (a) 1 mA/cm^2, (b) 0.5 mA/cm^2 and (c) 0.2 mA/cm^2 for 80 μg/cm^2 film, prepared from 10 g/L manganese oxide suspension containing 0.5 g/L sodium alginate at deposition voltage of 3 V.

Figure 5-49 shows charge/discharge behavior of manganese oxide film in the 0.1 M Na_2SO_4 solution. The charge and discharge curves are almost linear and indicate capacitive behavior in agreement with the CV data. The small initial potential drop observed during discharge can be attributed to the low conductivity of the active material.

5.4.2. EPD of Manganese Oxide in Aqueous Solutions with Sodium Alginate and Carbon Nanotubes

The attempt of co-deposition of manganese oxide with carbon nanotubes with cathodic ELD by means of layer structure did not yield satisfactory results. The experiment indicates that more homogenous distribution of carbon nanotubes is necessary to achieve co-deposition. The experiment of EPD of manganese oxide in aqueous solution with carbon nanotubes is the continuation of the previous work, but with the

attempt of incorporating carbon nanotubes into the manganese oxide-alginate matrix to improve the conductivity problem of manganese oxide. This approach offers advantages compared to the ELD methods. Indeed, in the absence of ions, higher stability of carbon nanotubes can be expected in agreement with the DLVO theory.

Sodium alginate is found to be able to dissociate into alginate species in basic solutions. The adsorption of alginate on the surface of both manganese oxide particles and carbon nanotubes in aqueous solutions will provide an electric charge. The charge of the macro-molecules of MnO_x-Alg and CNT-Alg is necessary for the electrophoretic deposition. Alginate acted as both a dispersant, charging additive and binder for the electrophoretic deposition of manganese oxide and carbon nanotubes.

The anodic electrophoretic deposition of CNT films with sodium alginate on stainless steel substrates can also be seen from the SEM pictures.

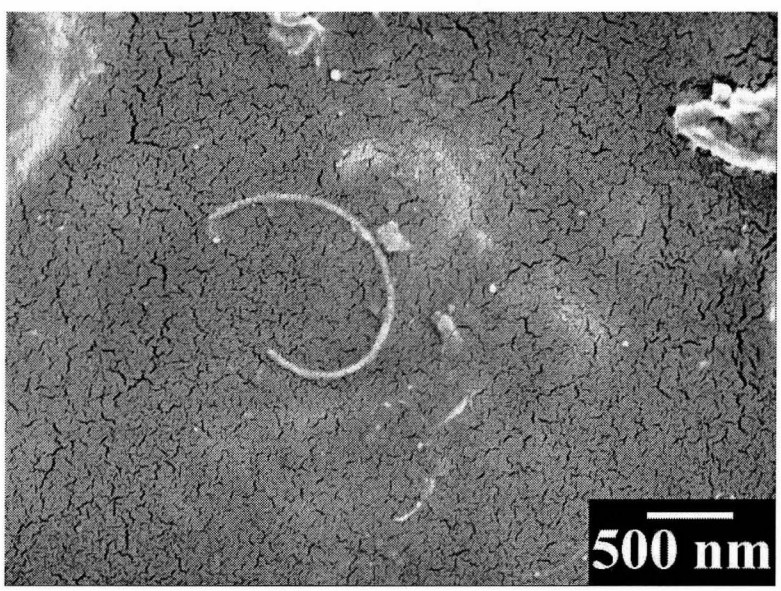

Figure 5-50 SEM picture of the CNT-alginate composite films deposed at 50 V

The introduction of manganese oxide to the suspension containing sodium alginate and CNT was successful. A maximum of 10 g/L of manganese oxide nanoparticles was able to add to the suspension containing 0.2g/L sodium alginate and 0.04 g/L CNT without causing agglomeration. Uniform films were able to be deposited from this suspension.

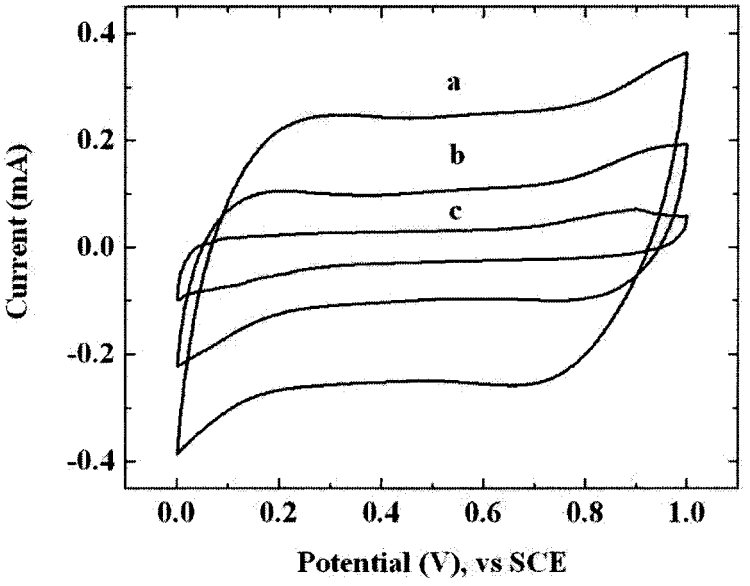

Figure 5-51 Cyclic voltammograms of the 79 μg/cm^2 MnO_x-CNT film deposited electrophorectically and tested at 0.1 M Na_2SO_4 at a scan rate of: (a) 50 mV/s, (b) 20 mV/s and (c) 5 mV/s

Films obtained from the deposition of MnO_x-CNT-Alg suspension are being tested for electrochemical performance. The CV windows of the co-deposited MnO_x-CNT film demonstrate ideal capacitive behavior is shown in Figure 5-51.

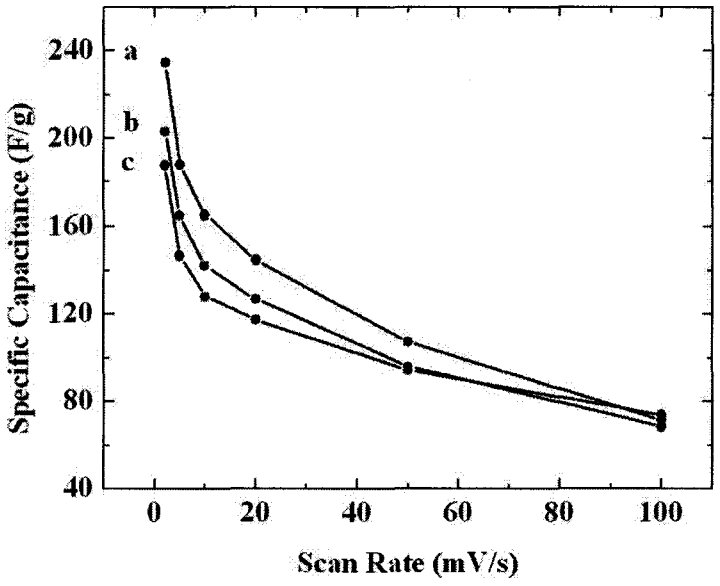

Figure 5-52 Specific capacitance as a function of scan rate of the MnO_x-CNT films deposited electrophorectially with a film weight of (a) 53 μg/cm^2, (b) 80 μg/cm^2 and (c) 112μg/cm^2 in 0.1 M Na_2SO_4 solutions.

EPD of MnO_x-CNT films with different weight have also been deposited from the MnO_x-CNT suspensions and tested for electrochemical performance. The SC values of different films weight is shown in Figure 5-52. The film with the highest specific capacitance value is the 53 μg/cm^2 MnO_x-CNT, and the SC value is 235 F/g. By comparing both the 80 μg/cm^2 MnO_x films deposited electrophorectically, one with CNT as additive, and one without CNT as additive. The film with CNT as additive demonstrated an increase in SC values from 150 F/g to 203 F/g. If one take into account of the existence of 10 wt.% of CNT in the MnO_x-CNT film, the actual SC could be even higher. Although the SC values of 203 F/g is still lower than the highest observed SC values for manganese oxide films, which is 760 F/g observed for very thin film in the range of a few ng/cm^2.

After the addition of the MnO_x nanoparticles into the suspension, the suspension becomes less stable. Agglomeration will start happening 30 minutes after the ultra sound treatment stopped. Therefore, it is an indication of the CNT interacts with the MnO_x-algenate, and further study is needed in improving the stability of the suspension. If the stability of the suspension can be improved further, there can be a further increase in the SC values of the electrode.

6. Conclusions

Cathodic electrosynthesis had been developed for the fabrication of manganese oxide films using Mn^{2+} species for electrochemical supercapacitors. Chitosan had been successfully used during the deposition to improve the film integrity. Electrochemical testing of the electrodes showed good capacitive behaviour with excellent cycling stability. A novel method had been developed for the deposition of multiwall carbon nanotubes with the use of chitosan. The deposits of the multiwall carbon nanotubes films showed preferred orientation of the carbon nanotubes perpendicular to the substrates. Composite electrodes of manganese oxide and carbon nanotubes had been successfully fabricated by cathodic electrodeposition with variable carbon nanotubes content.

Cathodic electrolytic deposition had been successfully developed for the fabrication of manganese oxide using Mn^{7+} species. Different processing parameters such as deposition time and current density were investigated. It was concluded that at high current density, the manganese oxide films showed high porosity and high specific capacitance values. Electrochemical behaviour of the deposits had also been investigated in different electrolytes with different concentrations. It was found that the manganese oxide films showed excellent stability in various sulphate electrolytes and the higher the electrolyte concentration the better the electrochemical performance of the electrodes.

A novel chemical process had been developed for the fabrication of manganese oxide particles with diameter of 20–50 nm. The manganese oxide particles were successfully charged and stabilized in non-aqueous solution with a particle concentration

of 1 g/L. In aqueous suspension, a manganese oxide particle concentration up to 10 g/L was achieved with the use of sodium alginate as dispersant, charging additive and binder. Electrophoretic deposition was achieved through both suspensions and uniform films of manganese oxide were obtained. Electrochemical testing of the films deposited from both aqueous and non-aqueous suspensions showed excellent capacitive behaviour for the use in electrochemical supercapacitors. Charge storage mechanism of the manganese oxide films was investigated with the use of QCM and it was found that the insertion of both H^+ and Na^+ ions were involved in the ion exchange process during charging/discharging.

Stabilization of multiwall carbon nanotubes in the manganese oxide suspensions was achieved through the use of sodium alginate as an additive. Electrophoretic deposition was achieved from the suspensions, containing CNT. The composition of the deposited films can be controlled by controlling the concentration of CNT and manganese oxide in the suspension. The composite electrodes of CNT-MnO_x showed improved electrochemical performance when compared to the electrodes deposited without CNT.

Obtained results indicated that various electrochemical strategies for electrolytic deposition and electrophoretic deposition can be used for the fabrication of manganese dioxide electrodes for electrochemical supercapacitors. Electrolytic deposition resulted in smaller particle size, higher porosity and higher specific capacitance. Electrophoretic deposition offered the advantage of higher deposition rate and higher deposit thickness.

Moreover, electrophoretic deposition enabled co-deposition of manganese oxide and carbon nanotubes, which resulted in improved capacitive behavior of thick films.

7. References

[1] R. Kotz and M. Carlen, *'Principles and Applications of Electrochemical Capacitors'*, Electrochemica Acta, **45** (2000): p2483.
[2] B. E. Conway, *'Transition from "Supercapacitor" to "Battery" Behavior in Electrochemical Energy Storage'*, Journal of the Electrochemical Society, **138** (1991): p1539.
[3] A. G. Pandolfo and A. F. Hollenkamp, *'Carbon Properties and Their Role in Supercapacitors'*, Journal of Power Sources, **157** (2006): p11.
[4] R. J. Brodd, A. Kozawa and K. V. Kordesch, *'Primary Batteries 1951 – 1976'*, Journal of the Electrochemical Society, **125** (1978): p271c.
[5] R. A. Huggins, *'Supercapacitors and Electrochemical Pulse Sources'*, Solid State Ionics, **134** (2000): p179.
[6] A. Nishino, *'Capacitors: Operating Principles, Current Market and Technical Trends'*, Journal of Power Sources, **60** (1996): p137.
[7] P. Rodatz, G. Paganelli, A. Sciarretta and L. Guzzella, *'Optimal Power Management of an Experimental Fuel Cell / Supercapacitor – Powered Hybrid Vehicle'*, Control Engineering Practice, **13** (2005): p41.
[8] P. J. Mahon and C. J. Drummond, *'Essay: Supercapacitors - Nanostructured Materials and Nanoscale Processes Contributing to the Next Mobile Generation'*, Australian Journal of Chemistry, **54** (2001): p473.
[9] H. E. Becker, U.S. Patent 2800616, General Electric, (1957).
[10] B. E. Conway, *'Electrochemical Supercapacitors – Scientific Fundamentals and Technological Applications'*, Kulwer, New York, 1999.
[11] A. K. Shukla, S. Sampath and K. Viayamohanan, *'Electrochemical Supercapacitors: Energy Storage Beyond Batteries'*, Current Science, **79** (2000): p1656.
[12] G. Salitra, A. Soffer, L. Eliad, Y. Cohen and D. Aurbach, *'Carbon Electrodes for Double-Layer Capacitors. I. Relations between Ion and Pore Dimensions '*, Journal of The Electrochemical Society, **147** (2000): p2486.
[13] D. Qu and H. Shi, *'Studies of Activated Carbons Used in Double-Layer Capacitors'*, Journal of Power Sources, **74** (1998): p99.
[14] B. McEnaney, T. D. Burchell (Eds.), *'Carbon Materials for Advanced Technologies, Pergamon'*, 1999, p1.
[15] M. Inagaki and L. R. Radovic, *'Nanocarbons'*, Carbon, **40** (2002), p2263.
[16] H. O. Pierson, *'Handbook of Carbon, Graphite, Diamond an dFullerenes'*, Noyes Publication, NJ, USA, 1993.
[17] R. C. Bansal, J. B. Donnet and F. Stoeckli, *'Active Carbon'*, Marcel Dekker, New York, 1988 (Chapter 2).
[18] K. Kinoshita and X. Chu, *'Proceedings of the Symposium on Electrochemical Capacitors'*, The Electrochemical Society, Pennington, NJ, 1995: p171.
[19] C. A. Leon y Leon and L. R. Radovic, *'Chemistry and Physics of Carbon'*, vol. 24, Marcel Dekker, New York, 1994: p213.
[20] K. Kinoshita, *'Carbon: Electrochemical and Physiochemical Properties'*, Wiley-Interscience, New York, 1988.
[21] P. E. Fanning and M. A. Vannice, *'DRIFTS Study of the Formation of Surface Groups on Carbon by Oxidation'*, Carbon, **31** (1993): p721.
[22] S. Biniak, A. Swiatkowski, M. Pakula and L. R. Radovic (Eds.), *'Chemistry and Physics of Carbon'*, vol. 27, Marcel Dekker, New York, 2001: p125.
[23] B. R. Puri and P. L. Walker (Eds.), *'Chemistry and Physics of Carbon'*, vol. 6, Marcel Dekker, New York, 1970: p191.
[24] D. Qu, *'Studies of the Activated Carbons Used in Double-Layer Supercapacitors'*, Journal of Power Sources, **109** (2002): p403.

[25] R. Taylor, H. Marsh, E. A. Heintz and F. Rodriguez-Reinoso (Eds.), *'Introduction to Carbon Technologies'*, Universidad de Alcante, Secretarido de Publicaciones, 1997: p167.
[26] J. B. Donnet, R. C. Bansal and M. J. Wang, *'Carbon Black Science and Technology'*, 2nd Ed., Marcel Dekker, New York, 1993.
[27] J. P. Zheng and T. R. Jow, *'High Energy and High Power Density Electrochemical Capacitors'*, Journal of Power Sources, **62** (1996): p155.
[28] F. Beck, M. Dolata, E. Grivei and N. Probst, *'Electrochemical Supercapacitors Based on Industrial Carbon Blacks in Aqueous H_2SO_4'*, Journal of Applied Electrochemie, **31** (2001): p845.
[29] R. Richner, S. Muller and A. Wokaum, *'Crafted and Crosslinked Carbon Black as an Electrode Material for Double Layer Capacitors'*, Carbon, **40** (2002): p307.
[30] S. H. Yoon, Y. Korai, I. Mochida, H. Marsh and F. Rodriguez-Reinoso (Eds.), *'Sciences of Carbon Materials'*, Universidad de Alicante, 2000: p287.
[31] K. Otsuka and C. L. Segal, *'Advanced Capacitor World Summit: Building the Technology Applications and New Business Opportunities for High Performance Electrochemical Capacitors'*, Washington, DC, 2003.
[32] C. C. Hu and C. C. Wang, *'Effects of Electrolytes and Electrochemical PreTreatments on the Capacitive Characteristics of Activated Carbon Fabrics for Supercapacitors'*, Journal of Power Sources, **125** (2004): p299.
[33] N. M. Rodriguez, *'A Review of Catalytically Grown Carbon Nanofibers'*, Journal of Materials Research, **8** (1993): p3233.
[34] K. H. An, K. K. Jeon, J. K. Heo, S. C. Lim, D. J. Bae and Y. H. Lee, *'High-Capacitance Supercapacitor Using a Nanocomposite Electrode of Single-Walled Carbon Nanotube and Polypyrrole'*, Journal of the Electrochemical Society, **149** (2002): pA1058.
[35] E. Frackowiak, K. Jurewicz, K. Szostak, S. Delpeux and F. Beguin, *'Nanotubular Materials as Electrodes for Supercapacitors'*, Fuel Processing Technology, **77/78** (2002): p213.
[36] E. Frackowiak and F. Beguin, *'Carbon Materials for the Electrochemical Storage of Energy in Capacitors'*, Carbon, **39** (2001): p937.
[37] C. Merino, P. Soto, E. Vilaplana-Ortego, J. M. Gomez de Salazar, F. Pico and J. M. Rojo, *'Carbon Nanofibres and Activated Carbon Nanofibres as Electrodes in Supercapacitors'*, Carbon, **43** (2005): p551.
[38] Y. H. Lee, K. H. An, S. C. Lim, W. S. Kim, H. J. Jeong, C. H. Doh and S. I. Moon, *'Applications of Carbon Nanotubes to Energy Storage Devices'*, New Diamond Frontier Carbon Technology, **12** (2002): p209.
[39] M. Hugues, G. Z. Chen, M. S. P. Shaffer, D. J. Fray and A. H. Windle, *'Electrochemical Capacitance of a Nanoporous Composite of Carbon Nanotubes and Polypyrrole'*, Chemistry of Materials, **14** (2002): p1610.
[40] B. E. Conway, V. Birss, J. Wojtowicz, H. Angerstein-Kozlowksa and B. E. Conway, Canadian Patent 1196683, *'Reports to Continental Group, Inc., 1975-1980; D. Craig'*, (1985).
[41] S. Trasatti and G. Buzzanca, *'Ruthenium Dioxide: A New Interesting Electrode Material'*, Journal of Electro-analytical Chemistry, **29** (1971): p1.
[42] J. P. Zheng and T. R. Jow, *'A New Charge Storage Mechanism for Electrochemical Capacitors'*, Journal of The Electrochemical Society, **142** (1995): pL6.
[43] J. P. Zheng, P. J. Cygan and T. R. Jow, *'Hydrous Ruthenium Oxide as an Electrode Material for Electrochemical Capacitors'*, Journal of The Electrochemical Society, **142** (1995): p2699.
[44] K. C. Liu and M. A. Anderson, *'Porous Nickel Oxide / Nickel Films for Electrochemical Capacitors'*, Journal of The Electrochemical Society, **143** (1996): p124.
[45] K. W. Nam and K. B. Kim, *'A Study of the Preparation of NiO_x Electrode via Electrochemical Route for Supercapacitor Applications and Their Charge Storage Mechanism'*, Journal of the Electrochemical Society, **149** (2002): pA346.
[46] V. Srinivasan and J. W. Weidner, *'Capacitance Studies of Cobalt Oxide Films Formed via Electrochemical Precipitation'*, Journal of Power Sources, **108** (2005): p15.
[47] C. Lin, J. A. Ritter and B. N. Popov, *'Characterization of Sol-Gel-Derived Cobalt Oxide Xerogels as Electrochemical Capacitors'*, Journal of The Electrochemical Society, **145** (1998): p4097.

[48] F. Sevgl, B. Orel, P. Bukovec, K. Kalcher and M. G. Hutchins, *'Spectroelectrochemical and Structural Properties of Electrochromic Co (Al) – Oxide and Co (Al, Si) – Oxide Films prepared by the Sol-Gel Route'*, Journal of Electroanalytical Chemistry, **418** (1996): p53.
[49] J. B. Goodenough, H. Y. Lee and V. Manivannan, *'Supercapacitors and Batteries'*, Materials Research Society Symposium – Proceedings, **548** (1999): p655.
[50] T. Brousse, M. Toupin, R. Dugas, L. Athouel, O. Crosnier and D. Belanger, *'Crystalline MnO_2 as Possible Alternatives to Amorphous Compounds in Electrochemical Supercapacitors'*, Journal of the Electrochemical Society, **153** (2006): pA2171.
[51] S. C. Pang, M. A. Anderson and T. W. Chapman, *'Novel Electrode Materials for Thin-Film Ultracapacitors: Comparison of Electrochemical properties of Sol-Gel-Derived and Electrodeposited Manganese Dioxide'*, Journal of the Electrochemical Society, **147** (2000): p444.
[52] S. C. Pang and M. A. Anderson, *'Novel Electrode Materials for Electrochemical Capacitors: Part II. Material Characterization of Sol-Gel Derived and Electrodeposited Manganese Dioxide Thin Films'*, Journal of Materials Research, **15** (2000): p2096.
[53] S. F. Chin, S. C. Pang and M. A. Anderson, *'Material and Electrochemical Characterization of Tetrapropylammonium Manganese Oxide Thin Films as Novel Electrode Materials for Electrochemical Capacitors'*, Journal of the Electrochemical Society, **149** (2002): pA379.
[54] J. N. Broughton and M. J. Brett, *'Electrochemical Capacitance in Manganese Thin Films with Chevron Microstructure'*, Electrochemical and Solid-State Letter, **5** (2002): pA279.
[55] B. Djurfors, J. N. Broughton, M. J. Brett and D. G. Ivey, *'Microstructural Characterization of Porous Manganese Thin Films for Electrochemical Supercapacitor Applications'*, Journal of Materials Science, **38** (2003): p4817.
[56] S. Devaraj and N. Munichandraiah, *'High Capacitance of Electrodeposited MnO_2 by the Effect of a Surface-Active Agent'*, Electrochemical and Solid-State Letters, **8** (2005): pA373.
[57] S. L. Kuo and N. L. Wu, *'Investigation of Pseudocapacitive Charge-Storage Reaction of $MnO_2.nH_2O$ Supercapacitors in Aqueous Electrolytes'*, Journal of the Electrochemical Society, 153 (2006): pA1317.
[58] K. S. Ryu, Y. G. Lee, Y. S. Hong, Y. J. Park, X. Wu, K. M. Kim, M. G Kang N. G. Park and S. H. Chang, *'Poly(ethylenedioxythiophene) (PEDOT) as Polymer Electrode in Redox Supercapacitor'*, Electrochemica Acta, **50** (2004): p843.
[59] M. Mastragostino, C. Arbizzani, R. Paraventi and A. Zanelli, *'Polymer Selection and Cell Design for Electric-Vehicle Supercapacitors'*, Journal of the Electrochemical Society, **147** (2000): p407.
[60] V. Gupta and N. Miura, *'High Performance Electrochemical Supercapacitor from Electrochemically Synthesized Nanostructured Polyaniline'*, Materials Letter, **60** (2006): p1466.
[61] K. Jurewicz, S. Delpeux, V Bertagan, F. Beguin and E. Frackowia, *'Supercapacitors from Nanotubes/Polypyrrole Composites'*, Chemical Physics Letter, **347** (2001): p36.
[62] R. J. Brodd, K. R. Bullock, R. A. Leising, R. L Middaugh, J. R. Miller and E. Takeuchi, *'Batteries, 1977 to 2002'*, Journal of the Electrochemical Society, **151** (2004): pK1.
[63] R. N. Reddy and R. G. Reddy, *'Sol-gel MnO_2 as an Electrode Material for Electrochemical Capacitors'*, Journal of Power Sources, **124** (2003): p330.
[64] R. N. Reddy and R. G. Reddy, *'Synthesis and Electrochemical Characterization of Amorphous MnO_2 Electrochemical Capacitor Electrode Material'*, Journal of Power Sources, **132** (2004): p315.
[65] C. H. Chen, E. M. Kelder, P. J. J. M. van der Put and J. Schoonman, *'Thin-Film Components for Lithium-Ion Batteries'*, Proceedings of the Symposium on Exploratory Research and Development of Batteries for Electric and Hybrid Vehicles', (1996): p43.
[66] W. S. Yoon, S. H. Ban, K. K. Lee, K. B. Kim, M. G. Kim and J. M. Lee, *'Electrochemical Characterization of Layered $LiCoO_2$ Films Prepared by Electrostatic Spray Deposition'*, Journal of Power Sources, **97-98** (2001): p282.
[67] K. W. Nam and K. B. Kim, *'Manganese Oxide Film Electrodes Prepared by Electrostatic Spray Deposition fro Electrochemical Capacitors'*, Journal of the Electrochemical Society, **153** (2006): p181.
[68] I. Zhitomirsky, *'Cathodic Electrodeposition of Ceramic and Organoceramic Materials. Fundamental Aspects'*, Advances in Colloid and Interface Science, **97** (2002): p279.

[69] B. V. Derjaguin and L. Landau, *'Theory of the Stability of Strongly Charged Lyophobic Sols and of the Adhesion of Strongly Charged Particles'*, Acta Physicochimica, USSR **14** (1941): p633.
[70] E. J. W. Verwey and J. T. G. Overbeek, *'Theory of the Stability of Lyophobic Colloids'*, Elsevier, Amsterdam, New York, 1948.
[71] I. Zhitomirsky, R. Chaim, L. Gal-Or and H. Bestgen, *'Electrochemical Al_2O_3-Cr_2O_3 Alloy Coatings on Non-Oxide Ceramic Substrates'*, Journal of Materials Science, **32** (1997): p5205.
[72] I. Zhitomirsky, L. Gal-Or, A. Kohn and H. W. Hennicke, *'Electrodeposition of Ceramic Films from Non-Aqueous and Mixed Solutions'*, Journal of Materials Science, **30** (1995): p5307.
[73] I. Zhitomirsky, *'Cathodic Electrosynthesis of Titanium and Ruthenium Oxides'*, Materials Letters, **33** (1998): p305.
[74] I. Zhitomirsky and A. Petric, *'Electrolytic and Electrophoretic Deposition of CeO_2 Films'*, Materials Letter, **40** (1999): p263.
[75] I. Zhitomirsky, *'Electrophoretic Hydroxyapatite Coatings and Fibers'*, Materials Letters, **42** (2000): p262.
[76] I. Zhitomirsky and L. Gal-Or, in: N.B. Dahotre, T. S. Sudarshan (Eds.), *'Intermetallic and Ceramic Coatings'*, Marcel Dekker Inc, New York, 1999, chapter 3.
[77] I. Zhitomirsky, *'Electrophoretic Deposition of Organic-Inorganic Nanocomposites'*, Journal of Material Science, **41** (2006): p8186.
[78] I. Zhitomirsky, *'Ceramic Films Using Cathodic Electrodeposition'*, JOM-e Minerals, Metals and Materials Society, **52** (2000), http://www.tms/org/pubs/journals/JOM/0001/Zhitomirsky/Zhitomirsky-0001.html
[79] R. Damodaran and B. M. Moudgil, *'Electrophoretic Deposition of Calcium Phosphates from Non-Aqueous Media'*, Colloids and Surfaces A: Physicochemical and Engineering Aspects, **80** (1993): p191.
[80] P. F. Grosso, R. E. Rutherford Jr. and D. E. Sargent, *'Electrophoretic Deposition of Luminescent Materials'*, Journal of the Electrochemical Society, **117** (1970): p1456.
[81] K. Mikeska and W. R. Cannon, in: J. A. Mangels, G. L. Messing (Eds.), *'Advances in Ceramics, Forming of Ceramics'*, vol. 9, The American Ceramic Society Inc., Columbus, Ohio, 1984, p164.
[82] Y. Matsumoto, T. Morikawa, H. Adachi and J. Hombo, *'A New Preparation Method of Barium Titanate Perovskite Film Using Electrochemical Reduction'*, Materials Research Bulletin, **27** (1992): p1319.
[83] Y. Matsumoto, H. Adachi, J. Hombo, *'New Preparation Method for PZT films using Electrochemical Reduction'*, Journal of the American Ceramic Society, **76** (1993): p769.
[84] G. H. A. Threse and P. V. Kamath, *'Electrochemical Synthesis of Metal Oxides and Hydroxides'*, Chemistry of Materials, **12** (2000): p1195.
[85] L. Gal-Or, I. Silberman and R. Chaim, *'Electrolytic ZrO_2 Coatings I. Electrochemical Aspects'*, Journal of the Electrochemical Society, **138** (1991): p1939.
[86] Z. R. Ulberg and Y. F. Deinega, *'Electrophoretic Composite Coatings'*, Ellis Horwood, New York, 1992.
[87] A. J. Aldykiewicz Jr, A. J. Davenport and H. S. Isaacs, *'Studies of the Formation of Cerium-Rich Protective Films Using X-Ray Absorption Near-Edge Spectroscopy and Rotating Disk Electrode Methods'*, Journal of the Electrochemical Society, **143** (1996): p147.
[88] J. A. Switzer, *'Electrochemical Synthesis of Ceramic Films and Powders'*, American Ceramic Society Bulletin, **66** (1987): p1521.
[89] R. Chaim, I. Zhitomirsky, L. Gal-Or and H. Bestgen, *'Electrochemical Al_2O_3-ZrO_2 Composite Coatings on Non-Oxide Ceramic Substrates'*, Journal of Materials Science, **32** (1997): p389.
[90] I. Zhitomirsky, *'Electrolytic Deposition of Oxide Films in the Presence of Hydrogen Peroxide'*, Journal of the European Ceramic Society, **19** (1999): p2581.
[91] R. S. Jayashree and P. V. Kamath, *'Factors Governing the Electrochemical Synthesis of α-Nickel (II) Hydroxide'*, Journal of Applied Electrochemistry, **29** (1999): p449.
[92] I. Zhitomirsky, *'New Developments in Electrolytic Deposition of Ceramic Films'*, American Ceramic Society Bulletin, **79** (2000): p57.
[93] D. Velegol, J. D. Feick and L. R. Collins, *'Electrophoresis of Spherical Particles with a Random Distribution of Zeta Potential or Surface Charge'*, Journal of Colloid and Interface Science, **230** (2000): p114.

[94] P. Sarkar, P. S. Nicholson, *'Electrophoretic Deposition (EPD): Mechanisms, Kinetics and Application to Ceramics'*, Journal of the American Ceramic Society, **79** (1996): p1987.
[95] D. De and P. S. Nicholson, *'Role of Ionic Depletion in Deposition During Electrophoretic Deposition'*, Journal of the American Ceramic Society, **82** (1999): p3031.
[96] G. Z. Sauerbrey, *'The Use of Quartz Oscillators for Weighting Thin Layers and for Microweighting'*, Z. Phys., **155** (1959): p206.
[97] J. W. Murray, L. S. Balistrieri and B. Paul, *'The Oxidation State of Manganese in Marine Sediments and Ferromanganese Nodules'*, Geochimica Cosmochimca Acta, **48** (1984): p1237.
[98] J. Moon, M. Awano, H. Takagi and Y. Fujishiro, *'Synthesis of Nanocrystalline Manganese Oxide Powders: Influence of Hydrogen Peroxide on Particle Characteristics'*, Journal of Materials Research, **14** (1999): p4594.
[99] X. Pang, I. Zhitomirsky, *'Electrodeposition of Composite Hydroxyapatite-Chitosan Films'*, Materials Chemistry and Physics, **94** (2005): p245.
[100] C. Y. Lee, H. M. Tsai, H. J. Chuang, S. Y. Li, P. Lin and T. Y. Tseng, *'Characteristics and Electrochemical Performance of Supercapacitors with Manganese Oxide-Carbon Nanotube Nanocomposite Electrodes'*, Journal of the Electrochemical Society, **152** (2005): pA716.
[101] J. K. Chang and W. Tsai, *'Material Characterization and Electrochemical Performance of Hydrous Manganese Oxide Electrodes for Use in Electrochemical Pseudocapacitors'*, Journal of the Electrochemical Society, **150** (2003): pA1333.
[102] K. R. Prasad and N. Miura, *'Electrochemically Synthesized MnO_2-Based Mixed Oxides for High Performance Redox Supercapacitors'*, Electrochemistry Communications, **6** (2004): p1004.
[103] M. Pourbaix, *'Atlas of Electrochemical Equilibria in Aqueous Solutions. 2d English ed.'*, 1974, Houston, Tex.: National Association of Corrosion Engineers.
[104] J. Wei, N. Nagarajan and I. Zhitomirsky, *'Manganese Oxide Films for Electrochemical Supercapacitors'*, Journal of Materials Processing Technology, **186** (2007): p356.
[105] Y. Ma, J. Luo and S. L. Suib, *'Syntheses of Birnessites Using Alcohol as Reducing Reagents: Effects of Synthesis Parameters on the Formation of Birnessites'*, Chemistry of Materials, **11** (1999): p1972.
[106] S. Ching, D. J. Petrovay, M. L. Jorgensen and S. L. Suib, *'Sol-Gel Synthesis of Layered Birnessite-Type Manganese Oxides'*, Inorganic Chemistry, **36** (1997): p883.
[107] M. P. Segato and E. T. G. Cavalheiro, *'Thermal Analysis of Ammonium, Mono-, Di-, and Triethanolammonium Alginates'*, Journal of Thermal Analysis and Calorimetry, **87** (2007): p737.
[108] P. M. Biesheuvel and H. Verweij, *'Theory of Cast Formation in Electrophoretic Deposition'*, Journal of the American Ceramic Society, **82** (1999): p1451.
[109] O. van der Biest and L. J. Vandeperre, *'Electrophoretic Deposition of Materials'*, Annual Review Materials Science, **29** (1999): p327.
[110] E. Tada and G. S. Frankel, *'Effects of Particulate Silica Coatings on Localized Corrosion Behaviour of AlSi 304SS Under Atmospheric Corrosion Conditions'*, Journal of the Electrochemical Society, **154** (2007): pC318.
[111] B. Ferrari and R. Moreno, *'Zirconia Thick Films Deposited on Nickel by Aqueous Electrophoretic Deposition'*, Journal of the Electrochemical Society, **147** (2000): p2987.
[112] A. R. Boccaccini and I. Zhitomirsky, *'Application of Electrophoretic and Electrolytic Deposition Techniques in Ceramics Processing'*, Current Opinion in Solid State & Materials Science., **6** (2002): p251.
[113] S. Devaraj and N. Munichandraiah, *'Electrochemical Supercapacitors Studies of Nanostructured α-MnO_2 Synthesized by Microemulsion Method and the Effect of Annealing'*, Journal of the Electrochemical Society, **154** (2007): pA80.
[114] J. N. Broughton and M. J. Brett, *'Variations in MnO_2 Electrodeposition for Electrochemical Capacitors'*, Electrochimica Acta, **50** (2005): p4814.
[115] J. K. Chang and W. T. Tsai, *'Material Characterization and Electrochemical Performance of Hydrous Manganese Oxide electrodes for Use in Electrochemical Pseudocapacitors'*, Journal of the Electrochemical Society, **150** (2003): pA1333.